NACA TN 3604

NATIONAL ADVISORY COMMITTEE FOR AERONAUTICS

TECHNICAL NOTE 3604

LOW-SPEED YAWED-ROLLING CHARACTERISTICS AND OTHER ELASTIC PROPERTIES OF A PAIR OF 26-INCH-DIAMETER, 12-PLY-RATING, TYPE VII AIRCRAFT TIRES

By Walter B. Horne, Robert F. Smiley,
and Bertrand H. Stephenson

Langley Aeronautical Laboratory
Langley Field, Va.

Washington
May 1956

NATIONAL ADVISORY COMMITTEE FOR AERONAUTICS

TECHNICAL NOTE 3604

LOW-SPEED YAWED-ROLLING CHARACTERISTICS AND OTHER ELASTIC PROPERTIES OF A PAIR OF 26-INCH-DIAMETER, 12-PLY-RATING, TYPE VII AIRCRAFT TIRES

By Walter B. Horne, Robert F. Smiley,
and Bertrand H. Stephenson

SUMMARY

The low-speed (up to 2 miles per hour) cornering characteristics of two 26 × 6.6, type VII, 12-ply-rating tires under straight-yawed rolling were determined over a range of inflation pressures and yaw angles for two vertical loads, one load approximately equal to the rated vertical load and the other load approximately equal to twice the rated vertical load for these tires. The cornering characteristics of one tire rolling along circular paths of different radii were investigated for one condition of vertical load and inflation pressure. Static tests were also performed to determine the vertical, lateral, torsional, and fore-and-aft elastic characteristics of the tires. Several vibration tests were also performed to determine the dynamic lateral elastic characteristics of the tires. The quantities measured included lateral or cornering force, drag force, torsional moment or self-alining torque, pneumatic caster, vertical tire deflection, lateral tire deflection, wheel torsion or yaw angle, rolling radius, and relaxation length. Some supplementary tests which included measurements of tire footprint area and the variation of unloaded tire radius with inflation pressure were made.

During straight-yawed rolling the normal force generally increased with increasing yaw angle within the test range. The variation of normal force with yaw angle was considerably different for the two vertical loads tested. The pneumatic caster was at a maximum at small yaw angles and tended to decrease in value with increasing yaw angle. The sliding-drag coefficient of friction tended to decrease in magnitude with increasing bearing pressure. The coefficient of turning for turning radii of approximately 5, 10, and 15 feet was found to be between 3×10^{-6} and 4×10^{-6} $lb^{-1}\text{-}in.^{-2}$ at a vertical load of 9,000 pounds and a tire inflation pressure of 134 pounds per square inch.

INTRODUCTION

In order to cope with airplane landing and taxiing problems such as landings with yaw, wheel shimmy, and ground handling, those engaged in landing-gear design must have reliable data on many elastic properties of airplane tires under such conditions. Until recently, the experimental data on such tire elastic properties, most of which are summarized and discussed in reference 1, were limited in both scope and quantity. Recently, a program was initiated by the National Advisory Committee for Aeronautics to alleviate this lack of experimental data by determining experimental values of some essential tire parameters for a range of tire sizes under static, kinematic (low-speed steady-state), and dynamic (transient and high-speed) conditions. Some static force-deflection tests of the program have been completed and the results were reported in reference 2. The low-speed yawed-rolling and some other elastic characteristics of two 56-inch-diameter, 24-ply-rating aircraft tires were reported in reference 3. The present paper presents results from parts of the kinematic and static test programs for two 26-inch-diameter, 26 × 6.6, type VII, 12-ply-rating tires.

Most of the investigation consisted of towing the tire specimens along a straight path in a yawed condition. The angle-of-yaw range covered was from 0° to 24.5° and the inflation-pressure range, from about 100 pounds per square inch to 225 pounds per square inch. The two vertical-loading conditions investigated were 9,000 and 17,100 pounds for each tire. The 9,000-pound vertical-load condition represented approximately the rated-load condition for this type of tire as specified by reference 4, whereas the 17,100-pound vertical-load condition represented approximately twice the vertical load for the rated condition. Although this latter condition normally represents a severely overloaded condition, such a condition can exist for some airplane types at take-off or during unusually severe landing impacts. For each yawed-straight-rolling run, the towing speed was held constant and did not exceed 2 miles per hour. The quantities measured included vertical tire deflection, side force, drag force, self-alining torque, pneumatic caster, rolling radius, and relaxation length. Relaxation-length measurements were also determined for the case of zero yaw for a standing tire.

Additional rolling tests were made for the case of a tire rolling at varying degrees of yaw (0° to $\pm 7^\circ$) along paths of circular curvature with radii of about 5, 10, and 15 feet at one vertical-load condition (9,000 pounds for each tire) and one inflation pressure (134 lb/sq in.).

Drag tests were conducted with the wheels locked to obtain measurements in the fore-and-aft direction of the maximum and sliding coefficients of friction and the stiffness of the tires for both wet- and dry-concrete conditions.

Tests were performed on the standing tires to determine the static vertical-, lateral-, and torsional-elasticity characteristics. Some supplementary tests were also performed to determine dynamic lateral-elasticity characteristics, to measure tire footprint area, and to determine the variation of the free tire radius with tire inflation pressure.

SYMBOLS

A_g	gross footprint area, sq in.
A_n	net footprint area, sq in.
b	overall tire-ground contact width, in.
d	outside diameter of free tire, in.
F	force, lb
F_R	resultant force, $\sqrt{F_x^2 + F_y^2}$, lb
F_x	instantaneous drag or fore-and-aft force (ground force parallel to direction of motion), lb
F_y	instantaneous cornering force (ground force perpendicular to direction of motion), lb
F_z	vertical load on tire, lb
F_ψ	normal force (ground force perpendicular to wheel plane, $F_y \cos \psi + F_x \sin \psi$), lb
f	frequency, cps
2h	overall tire-ground contact length, in.
K_x	fore-and-aft spring constant, lb/in.
K_α	torsional spring constant, lb-in./deg
K_λ	lateral or side spring constant, lb/in.
L	relaxation length, in.

L_s static relaxation length, in.

L_y yawed-rolling relaxation length, in.

M_z torsional moment or self-alining torque, lb-in.

N cornering power (rate of change of cornering force with yaw angle for small yaw angles on a rolling tire, $dF_{y,r,e}/d\psi$ or $dF_{\psi,r,e}/d\psi$ for ψ approaching 0), lb/deg

p tire inflation pressure, lb/sq in.

p_b minimum rated bursting pressure of tire, lb/sq in.

p_o tire inflation pressure at zero vertical load ($F_z = 0$), lb/sq in.

p_g average gross footprint pressure, F_z/A_g, lb/sq in.

p_n average tire-ground bearing pressure, F_z/A_n, lb/sq in.

q pneumatic caster, $M_{z,r,e}/F_{\psi,r,e}$, in.

r outside radius of free tire, $\frac{\text{Tire circumference}}{2\pi}$, in.

r_e rolling radius, $\frac{v}{\omega}\cos\psi$, in.

s peripheral distance around tire, in.

t time, sec

v rolling velocity, in./sec

w maximum tire width, in.

x displacement in direction of motion, in. or ft

δ vertical tire deflection due to combined vertical and yaw loads, in.

δ_o vertical tire deflection due to vertical load only, in.

η_1 energy-dissipation parameter for static lateral-elasticity tests

η_2 reduction in oscillation amplitude per cycle

η_3 energy-dissipation parameter for dynamic lateral-elasticity tests, $\frac{2(1 - \eta_2)}{(1 + \eta_2)}$

λ lateral distortion of tire equator, in.

λ_o lateral distortion of tire equator at center of contact, in.

$\mu_{x,m}$ maximum drag coefficient of friction, $F_{x,n,m}/F_z$

$\mu_{x,s}$ sliding-drag coefficient of friction, $F_{x,n,s}/F_z$

μ_ψ yawed-rolling coefficient of friction, $F_{R,r,e,m}/F_z$

ρ turning radius, ft

ψ torsion or yaw angle, deg

ω wheel angular velocity, radians/sec

Subscripts:

e equilibrium or steady-state rolling condition

m maximum

n nonrolling condition

r rolling condition

s sliding condition

Bars over symbols denote the average values of the quantities involved for tires A and B.

APPARATUS

Test Vehicle

The basic test vehicle consists of the fuselage and wing center section of a cargo airplane which was towed tail first by a tractor truck at an attitude such that the original airplane shock struts were nearly vertical. The original yokes and torque links of the landing-gear struts along with the wheel assemblies were replaced by steel wheel housings which held the tires and wheels tested. These steel wheel housings were connected together by means of an instrumented truss. Holes located in the wheel housing at angular intervals of $3\frac{1}{2}^{\circ}$ permitted the wheel frames to be rotated through a yaw-angle range from 0° to 24.5° toe out. (It might be noted that a small initial misalinement of the wheels of approximately 0.3°, which was noted in ref. 3, was eliminated for the present investigation.) A sketch of the basic test vehicle is shown in figure 1. A more detailed description of this test vehicle is given in reference 3 and applies in general to the present investigation.

The weight of the test vehicle acting on the tires for the light-weight condition tested was approximately 9,000 pounds for each tire. For the heavy-weight condition tested, a concrete weight can (weighing approximately 8,000 pounds) was attached to each wing stub. (See fig. 2.) This weight increased the load on each tire to approximately 17,100 pounds. The maximum towing force required was approximately 4,000 pounds for each tire.

Instrumentation

The test vehicle was equipped with instruments for measuring side force, torsional moment (self-alining torque for the yawed-rolling case), drag, vertical tire deflection, horizontal translation, and wheel rotation. Measurements of these quantities were recorded simultaneously on a 14-channel recording oscillograph mounted in the test vehicle. This oscillograph was equipped with a 0.01-second timer. This instrumentation is discussed in more detail in reference 3.

Tires

General description.- The tires tested in this investigation were a pair of 26-inch-diameter, 26 × 6.6, type VII, 12-ply-rating rib tread tires which were made by the same manufacturer. The specifications for these tires given in table I were either obtained from reference 4 or by direct measurements. Figure 3 shows inflated and deflated half cross sections for the two test tires. These cross sections were obtained from

plaster casts taken when the tires were in a new and unused condition at the beginning of the tests. There appears to be no appreciable difference between the profiles for the two tires.

Tire wear.- During the course of the present investigation, there was an appreciable progressive change in the cross-sectional shape of the tires due to skidding and working of the tires. Therefore, the chronological order in which the test data were collected may be of some importance in the interpretation of the data. This chronological order is indicated in this paper by a series letter which is assigned to all test data. Specifically, the tests in chronological order are A, B, C, and D.

The change in tire-tread pattern due to tire wear throughout the test is illustrated in figure 4. At the beginning of the tests both tires had a rectangular cross-sectional tread pattern (fig. 4(a)) and this pattern was substantially preserved throughout series A (fig. 4(b)). During test series B the sides of the treads in direct contact with the ground began to wear away and this wearing away produced the tread shape shown in figure 4(c), which was taken at the beginning of test series C. During test series C this wear increased substantially as is shown in figure 4(d) for tire B at the end of test series C. For test series D, for which only tire A was tested, the small projecting edges remaining on the tread at the conclusion of test series C (shown in fig. 4(d)) were cut off before beginning the tests. (See fig. 4(e).)

It should be noted that, when the tires were removed from the test vehicle at the conclusion of the tests, tire B was found to have suffered several apparently deep cuts around its outboard sidewall in the proximity of the wheel rim. These cuts were evidently made by the outboard side of the wheel rim cutting into the tire during one of the runs of test series C at the larger yaw angle where large vertical and lateral tire deflections were experienced. In order to investigate the importance of these cuts, the section of the tire having the deepest cut was removed and inspected. A photograph of this section is presented as figure 4(f). From this cross section it appeared that this cut penetrated completely through only one ply of the casing and therefore probably did not appreciably affect the tire characteristics. It was found after close examination that tire A had not experienced this type of damage.

Free tire radius.- Radius-pressure hysteresis loops associated with increasing and decreasing pressure are shown in figure 5 for tires A and B. The elapsed time from the start is shown for a few of the measurements presented. The variation in tire radius due to hysteresis for a given pressure is seen to be practically negligible (less than 0.1 inch) in the operating pressure range for these tires for this relatively slow rate of change of pressure (roughly, 3 hours for most of the cycle). Also shown in this figure are several radius measurements which were made after the tires had been left unloaded at constant pressure for at least 24 hours in order to reach an equilibrium condition.

Test Surface

All yawed-straight-rolling and drag tests were conducted by towing the test vehicle along the center of a 9-inch-thick reinforced-concrete taxi strip. This taxi strip had a slight crown so that the tires on the test vehicle were subject to a slight tilt relative to the surface. However, this tilt was less than 1°. The texture of the taxi strip, a boarded concrete surface, as determined from plaster casts, is shown in figure 6 for three random positions on the strip. All other tests, with the exception of the static torsional-elasticity and the yawed-curvilinear-rolling tests, were conducted on a much smoother, level, reinforced-concrete surface. The test surfaces for the exceptions were smooth steel plates.

TEST PROCEDURE AND EXPERIMENTAL RESULTS

The present investigation of tire characteristics is divided into the following parts: yawed-straight-rolling tests, yawed-curvilinear-rolling tests, relaxation-length tests, locked-wheel drag tests, static vertical-elasticity tests, static lateral-elasticity tests, dynamic lateral-elasticity tests, static torsional-elasticity tests, and supplementary measurements.

Yawed-Straight-Rolling Tests

For each run of the yawed-straight-rolling tests, the test vehicle was moved into towing position on the dry, clean, concrete taxi strip and the wheel housings were rotated and locked at the particular yaw angle desired. The tires were adjusted to the test inflation pressure and were then jacked clear of the ground to remove any residual stresses remaining from the previous runs or resulting from the changing of the yaw angles of the wheels. The jacks were then removed and the initial vertical tire deflections noted. For most of the runs, the vehicle was then towed straight ahead from this initial essentially unstressed condition for a distance of approximately 40 feet at an approximately constant speed. Although the speed remained approximately constant throughout any particular run, it varied from run to run within a speed range from approximately 0.7 to 2 miles per hour. Figure 7 shows one of the tires during a run at 24.5° yaw. For several runs, which are noted in table II, the vehicle was backed up before starting the straight-ahead rolling portion of the run in order to put an initial negative lateral stress in the tires. This initial stressing was applied before starting these particular runs for the purpose of obtaining sufficiently large changes in lateral force during the early stages of these runs to enable determination of the yawed-rolling relaxation length. (If the vehicle was not thus backed up, it usually turned out that the lateral-force test data

obtained during the early stages of the yawed runs were not sufficiently accurate for this relaxation-length determination.) A comparison of the variation of lateral force with distance rolled for these two types of towing conditions is shown in figure 8 for the light-weight towing condition for a yaw angle of 3.5° and a tire inflation pressure of approximately 163 pounds per square inch.

All test runs at 0°, 3.5°, 7°, 10.5°, 14°, 17.5°, 21°, and 24.5° were made with both wheels symmetrically yawed with respect to the longitudinal axis of the test vehicle. Although these particular yaw angles were the only angles easily attainable on the test vehicle, some test runs at 1.75° were made by setting the wheels unsymmetrically yawed with respect to the longitudinal axis of the test vehicle (that is, one wheel was set at 0° and the other at 3.5° yaw). When towed ahead in this unsymmetrically yawed condition, the test vehicle first veers off to the side because of the unsymmetrical forces. After a short run, however, the vehicle runs smoothly with the longitudinal axis of the test vehicle yawed with respect to the direction of motion such that both wheels have the same final intermediate yaw angle of 1.75° with respect to the direction of motion.

The following measurements were recorded continuously from the start of the run: side force, torsional moment or self-alining torque, drag force, vertical tire deflection, wheel rotation, and vehicle translation in the direction of motion.

Table II contains all test data obtained during the final steady-state stage of each yawed-rolling run. (It should be noted that the run numbers listed in this table and in all other tables and figures do not indicate the chronological order in which the respective runs were made. These run numbers are listed only for convenience in referring to the test data.) Data are presented for three different test series (A to C) which represent either different vertical loadings or different tire wear. The variation of normal force $\bar{F}_{\psi,r,e}$, self-alining torque $\bar{M}_{z,r,e}$, and pneumatic caster $\bar{q}$ with yaw angle are shown in figures 9 and 10 for all vertical loads and inflation pressures. Sample rolling-radius data are plotted in figure 11 as functions of yaw angle, tire inflation pressure, and vertical tire deflection.

The buildup of cornering force with horizontal distance rolled during the initial stages of the yawed-straight-rolling runs is illustrated in figure 12 for several test inflation pressures for the vertical-load conditions investigated. Inasmuch as for most runs there was a slight initial residual force or preload in the tires, the original test curves did not pass exactly through the origin. In order to take this fact into consideration, the test curves shown in this figure have been horizontally shifted (if necessary) so that the extrapolation of each curve is made to pass through the origin.

Yawed-Curvilinear-Rolling Tests

In the yawed-curvilinear-rolling tests, the right wheel frame of the test vehicle was anchored to the floor by tie-down fittings in order to make it as immovable as possible. (See fig. 13(a).) A steel plate, approximately 5 feet wide, welded to a steel I-beam, was placed under the tire (tire A) in the left wheel frame. (See fig. 13(b).) This steel plate was pulled out from under the tire, by means of hydraulic rams, along circular-arc paths whose radii were determined by the pivot-point location on the steel I-beam. (See fig. 13(b).) Thus, this test setup simulates the rolling of the tire in a circular path on a steel surface. The test vehicle was restrained from rotating about the right wheel frame as the plate was pulled out from under the tire by means of the tie-down fittings connected to the left wheel frame which are shown in figure 13(b). Figure 13(c) shows an overall view of the test setup.

All test runs at nominal yaw angles of 0°, $3\frac{1}{2}^\circ$, and 7° were made by pinning the instrumented truss to the left wheel frame as was done for the yawed-straight-rolling tests. Intermediate nominal yaw angles of 1.75° and 5.25° were obtained by clamping the truss to the left wheel frame with the aid of heavy-duty clamps. The actual yaw angles differed slightly from the nominal angles because of misalinement of the test vehicle with respect to the pivot point.

Before each run the left wheel housing was rotated and pinned or clamped at the particular nominal yaw angle desired. The left tire (tire A) was then adjusted to the test inflation pressure and jacked clear of the ground to remove any residual stresses remaining from the previous runs or from the changing of the wheel yaw angle. The jack was then removed and the actual yaw angle and vertical tire deflection were measured. Then, the plate was pulled out from under the tire through a distance of approximately 4 feet. Measurements of side force and self-alining torque were recorded continuously during the run. The rolling speed was approximately 6 inches per minute (0.006 mile per hour).

The data obtained from the yawed-curvilinear-rolling tests are presented in figure 14. This figure shows the variation of cornering force and self-alining torque with yaw angle and turning radius for tire A at the test condition of F_Z = 9,000 pounds and p = 134 pounds per square inch.

Relaxation-Length Tests

Two types of relaxation lengths were determined in this investigation, namely, static relaxation length L_S and yawed-rolling relaxation

length L_y. The definitions for these relaxation lengths are given in reference 3. The methods used to determine these relaxation lengths are as follows:

Static relaxation length L_s.- The standing tires were given initial lateral deflections by pulling outward, by means of hydraulic rams, plates placed underneath the tires. The lateral distortion of each tire tread nearest the center of the tire relative to the wheel center plane was then measured for several points around the tire circumference between the footprint edge and a point 180° from the center of contact.

Yawed-rolling relaxation length L_y.- The basic data for the yawed-rolling relaxation lengths were obtained from the initial (force buildup) phase of the 1.75°, 3.5°, and 7° yawed-straight-rolling tests. This constant was evaluated in this paper for only these angles since skidding appeared to be too significant at larger angles.

Relaxation-length data.- Samples of the test data obtained from the two methods used to determine the relaxation length of the tire specimens are shown in figure 15. This figure shows experimental data for two runs, plotted both in linear and semilogarithmic coordinates, together with empirical exponential curves which were obtained by fitting straight lines to these data on the semilogarithmic plots. The corresponding relaxation length for each set of data is, by definition, the denominator of the power of e in the equation of the exponential curve fitted to the data. (For example, the relaxation length for the data in figure 15(b) is 5.4 inches.) The values of relaxation length obtained in this manner from the test runs are listed in table III for the static-relaxation-length tests and in table II for the yawed-rolling relaxation-length tests. These tables list only relaxation-length measurements for some of the light-loading conditions tested (test series A and B). For the heavy-loading condition (test series C), no static-relaxation-length data are presented since for this condition the tire treads, which were used as references for lateral-deflection measurements, had been so irregularly worn by previous testing that it was impractical to obtain sufficiently accurate measurements. For the yawed-rolling relaxation length for the heavy-loading condition, no relaxation-length data are presented either for the reason that the corresponding force-buildup data did not appear sufficiently accurate to warrant relaxation-length determinations or, in other cases, for the reason that the experimental force-buildup data could not be accurately fitted by exponential curves.

Locked-Wheel Drag Tests

The method used to determine tire stiffness and sliding drag in the fore-and-aft direction on dry concrete was as follows: With the wheels positioned at 0° yaw and locked to prevent rotation, the test vehicle

was pulled forward by hydraulic rams (see ref. 3) at a speed less than 10 inches per minute (0.009 mile per hour). A continuous record was taken of drag force and horizontal displacement during each run. In addition, several runs were made with the concrete surface in a wet condition. For these particular runs, the tires were jacked clear of the taxi-strip immediately before a run and the concrete surface below each tire was wetted thoroughly with water by means of a garden hose. The jacks were then removed and the run commenced as just described for the dry-concrete runs. Throughout each wet-concrete run, a stream of water was directed onto the concrete surface in front of each tire so that the tires would always remain in contact with wet concrete for the duration of the run.

During these tests, the weight of the test vehicle remained constant; however, the vertical load on the tires decreased slightly with increasing drag force as a consequence of the moment produced by the drag force. This change in vertical load was taken into account in the computation of friction coefficients. (It was not taken into account in the other tests since the effect was small for those conditions.)

Most of the experimental data obtained from the locked-wheel drag tests are presented in table IV. Also, typical data are shown in figure 16 for the buildup of fore-and-aft force with horizontal distance pulled for several runs.

Static Vertical-Elasticity Tests

The following procedure was used in the static vertical-elasticity tests: The vertical load on each tire was increased by increments from zero load cumulatively up to a maximum vertical-load value and was then reduced by increments to zero. The vertical tire deflection was noted for each value of vertical load. The unloaded tire inflation pressure p_0 and loaded inflation pressure p were also measured. This procedure was followed for all test inflation pressures.

Most of the static vertical-elasticity data obtained are presented in figure 17. This figure shows the variation of vertical load with vertical tire deflection for the two tire specimens for the test inflation pressures. Additional data, obtained mostly from the yawed-rolling tests (table II) are presented in figure 18. This figure shows the variation of average vertical tire deflection with average tire inflation pressure for the two vertical loads tested ($\bar{F}_Z \approx 9{,}000$ pounds and $\bar{F}_Z = 17{,}100$ pounds). It is noted that in figure 18 the average tire deflections for the locked-wheel drag and footprint-area tests are usually about 0.3 inch smaller than the corresponding deflections for the rest of the tests. This difference probably is a result of the fact that during these tests it was not convenient to rotate the wheels about their axles between runs. Consequently, during the relatively long duration of these

tests (approximately one week for the locked-wheel drag tests), because of creep under the constant vertical loading of approximately 9,000 pounds for each tire, the tires developed a flat spot at the part of the tire nearest the ground. This flat-spot effect will be referred to later in connection with the determination of ground bearing pressure.

Static Lateral-Elasticity Tests

In the static lateral-elasticity tests, the test vehicle was pulled sideways at the wheel axles, first in one direction and then in the other, by means of hydraulic rams through several cycles at a rate between 25 seconds and 60 seconds per cycle. The vertical tire deflection and loaded tire inflation pressure were measured on each tire before each run. During the run, continuous measurements of side force and side tire deflection were recorded on the oscillograph. This procedure was followed for several test inflation pressures at both the 9,000-pound (series A) and the 17,100-pound (series C) vertical-load conditions.

The basic static lateral-elasticity test data are presented in figures 19 and 20 and table V. Figure 19 shows the variation of side force with side tire deflection for several test inflation pressures at an average vertical loading of 9,000 pounds for each tire (test series A). Figure 20 shows this variation at an average vertical loading of 17,100 pounds for each tire (test series C). (It is noted that for run 149 in fig. 20 the test data are relatively irregular. This irregularity is believed to be the result of a shifting in some part of the test setup during the course of this run rather than the result of an actual irregularity in the tire stiffness.) Table V contains a list of all test conditions together with some tire lateral stiffness and hysteresis parameters (to be discussed later) derived from the data in figures 19 and 20.

Dynamic Lateral-Elasticity Tests

In the dynamic lateral-elasticity tests, the test vehicle was pulled sideways at the wheel axle approximately 0.5 inch by means of a hydraulic ram. This ram was connected to the wheel axle by a steel cable which was severed completely by an axe stroke at the start of the run. The subsequent lateral oscillations of the test vehicle at the wheel axle were measured by a linear slide wire and were recorded continuously during the run on the oscillograph. The vertical tire deflection and loaded tire inflation pressure were measured for each tire before each run. This procedure was followed for several test inflation pressures at both the 9,000-pound (series A) and 17,100-pound (series C) vertical-load test conditions.

From each of the dynamic lateral-elasticity tests, a time history of the airplane lateral deflection which is similar to the record shown in figure 21 was obtained. As can be seen from this record this oscillation is approximately an exponentially decaying sinusoidal oscillation. The corresponding frequency f and decrease in amplitude per cycle η_2 obtained for each test run are given in table VI.

Static Torsional-Elasticity Tests

The test procedure for the static torsional-elasticity tests was as follows: Steel turntables were placed beneath the wheels of the test vehicle. These turntables were connected to a hydraulic ram in such a manner that, when the ram was retracted, each turntable-tire combination would rotate through an angle proportional to the ram retraction.

The vertical tire deflection and loaded tire pressure were measured before each run. Continuous measurements of torsional moment and turntable angular displacement were recorded during each run on the oscillograph. This procedure was followed for several test inflation pressures at both the 9,000-pound (series A) and 17,100-pound (series C) vertical-load test conditions.

The basic static torsional-elasticity test data are shown in figures 22 and 23. Figure 22 shows the variation of torsional moment with torsion angle for several test inflation pressures at a vertical loading of 9,000 pounds for each tire (test series A). Figure 23 shows this variation at a vertical loading of 17,100 pounds for each tire (test series C). Table VII contains a list of all test conditions together with tire torsional stiffness parameters obtained from figures 22 and 23.

Supplementary Measurements

In addition to the tests just described, some tire-contact or footprint-area measurements were made for the tire specimens at several inflation pressures and vertical tire deflections. These measurements were obtained from the imprint left on a piece of heavy paper placed between a chalked portion of the tires and a smooth concrete hangar floor. Several typical imprints are shown in figure 24. The tire footprint data obtained from the tire imprints are presented in table VIII.

PRECISION OF DATA

The instruments used in the tests and the methods of reducing data are believed to yield results which are, on the average, accurate within the following limits:

Vertical load on tire, F_Z, percent	±3
Cornering force, F_Y, percent	±3
Force perpendicular to wheel frame (normal force) or lateral force, F_ψ, percent	±3
Drag force, F_X, lb	±300
Self-alining torque or torsional moment, M_Z, lb-in.	±3,000
Tire inflation pressure, p_o or p, lb/sq in.	±3
Free radius, r, in.	±0.02
Rolling radius, r_e, in.	±0.2
Horizontal translation, x, percent	±3
Vertical tire deflection, δ_o or δ, in.	±0.2
Lateral tire deflection, λ_o or λ, in.	±0.02
Yaw angle or torsion angle for all tests except yawed-curvilinear-rolling tests, deg	±0.1
Yaw angle for yawed-curvilinear-rolling tests, deg	±0.5

DISCUSSION OF PARAMETERS

Normal Force $F_{\psi,r,e}$

The variation of steady-state normal force with yaw angle, obtained from the test data in table II, is shown in figure 9 for an approximately rated vertical-load condition ($\bar{F}_Z \approx 9{,}000$ pounds, test series A and B), in figure 10 for an approximately twice rated vertical-load condition ($\bar{F}_Z = 17{,}100$ pounds, series C), and in figure 25 for both vertical loadings at two tire inflation pressures. The following observations can be drawn from the data shown in these figures. The normal force generally increased with increasing yaw angle within the test range. It should be noted that the shape of the normal-force curves differed for the two vertical loads tested as is shown in figure 25. At the approximately rated vertical-load condition ($\bar{F}_Z \approx 9{,}000$ pounds), the slopes of the normal-force curves tend to decrease with increasing yaw angle; this result is in agreement with the results reported in reference 3 for two 56-inch-diameter tires for comparable loading conditions. At the heavy approximately twice rated vertical-load condition ($\bar{F}_Z = 17{,}100$ pounds), it can be seen that the slopes of the normal-force curves tend to increase with increasing yaw angle up to yaw angles of 16° to 18° and the slopes tend to decrease with further increase in yaw angle. No comparison can be made for the heavy-load condition between the 26-inch-diameter tires and the 56-inch-diameter tires of reference 3 since the 56-inch-diameter tires were not tested at vertical loads greater than the rated load.

Cornering Force $F_{y,r,e}$

The steady-state cornering force follows substantially the same trends that were described for the normal force, as is shown in figure 26 for two typical loading conditions.

Initial Rate of Cornering-Force Buildup $\left(\frac{d\bar{F}_{y,r}}{d\bar{x}}\right)_{\bar{x}\rightarrow 0}$

The variation of the initial rate of cornering-force buildup with distance rolled as a function of yaw angle and tire inflation pressure for small yaw angles (obtained from the data in table II) is shown in figure 27 for test series A and B ($\bar{F}_Z \approx 9{,}000$ pounds). (This parameter may be of some use in testing the reliability of some tire-motion theories.) For test series C ($\bar{F}_Z = 17{,}100$ pounds), the initial force-buildup data were not sufficiently accurate to obtain this quantity. For constant tire inflation pressure, the initial rate of buildup is seen to increase approximately linearly with increasing yaw angle. For constant yaw angles, the initial rate of buildup appears to increase with increasing inflation pressure at least up to 183 pounds per square inch; for larger pressures the trend is uncertain.

Cornering Power N

The variation of cornering power with vertical tire deflection and inflation pressure for the two vertical loads tested is shown in figures 28(a) and 28(b), respectively. These data, which are derived from the initial slope of the curves for the variation of normal force with yaw angle given in figures 9 and 10, indicate that, for constant vertical tire deflection, the cornering power increases with increasing inflation pressure and that, for constant inflation pressure, the cornering power decreases with increasing vertical tire deflection.

In order to compare the present test results for the 26-inch tire with the results of previous tests on other tires of the same general type (type VII, see ref. 4), cornering-force data from the present tests are compared in figure 29 with data for a 56-inch-diameter tire from reference 3 and for 32- and 44-inch-diameter tires from reference 5. These data are presented in the form of a plot of the ratio $\frac{\bar{N}}{(\bar{p} + 0.11\bar{p}_b)\bar{w}^2}$ against $\bar{\delta}_o/\bar{r}$, where $\bar{p}_b$ is the tire minimum rated bursting pressure as taken from reference 4. (The form of these ratios is based on the results of an unpublished study of tire characteristics.) From figure 29 it appears that

for the 26-inch and 56-inch tires the indicated cornering-power parameter $\frac{\bar{N}}{(\bar{p} + 0.11\bar{p}_b)\bar{w}^2}$ is substantially the same for these two tires, although, of course, this conclusion is not certain since the two sets of data do not overlap very much. In regard to the 32- and 44-inch-tire data from reference 5, these data are seen to be in fair agreement with the data for the 26- and 56-inch tire, but the data point for the 44-inch tire appears somewhat higher than most of the other data points. At least part of this apparent discrepancy may easily be due to the fact that the value of tire width w used to calculate the cornering-power parameter for this test tire (and also for the 32-inch tire) were not given in reference 5 but had to be estimated from the nominal tire size with the aid of the corresponding tire specifications in reference 4. These tire specifications, however, permit a rather large tolerance for the tire-width dimension. For example, for the 44-inch tire the specifications require that $w = 13.20 \pm 0.30$ inches; this tolerance could lead to an error of approximately ±5 percent in the determination of the cornering-power parameter $\frac{\bar{N}}{(\bar{p} + 0.11\bar{p}_b)\bar{w}^2}$.

Effect of Path Curvature on Cornering Force

The variation of cornering force with yaw angle for a tire rolling along circular paths of approximately 5, 10, and 15 feet radii is shown in figure 14. This variation of cornering force with yaw angle appears to be essentially linear throughout the yaw-angle range investigated. It should be noted, however, that the cornering-force curves are offset from the origin by different amounts depending upon the magnitude of the turning radius ρ. This offset of cornering force at the origin (0° yaw) due to circular rolling appears to be inversely proportional to the turning radius, as would be expected from theoretical considerations (ref. 6). The effect of circular rolling on cornering power appears to be small since the slopes of the curves for the variation of cornering force with yaw angle given in figure 14 appear to be substantially equal for the three turning radii investigated. The value of cornering power for tire A obtained from this test (237 lb/deg) is in relatively close agreement with the average cornering power for tires A and B (265 lb/deg) obtained from the yawed-straight-rolling test for the same conditions of vertical load and tire inflation pressure; thus, the cornering characteristics of the two test tires were substantially alike.

Self-Alining Torque $\bar{M}_{z,r,e}$

The variation of self-alining torque with yaw angle is shown in figures 9 and 10 for the two vertical loadings investigated. The self-alining torque generally increased with increasing yaw angle for small yaw angles and decreased with increasing yaw angle at large yaw angles. For constant vertical load, the data indicate that increasing the tire inflation pressure tends to reduce the magnitude of the self-alining torque at most yaw angles. In the case of constant inflation pressure, illustrated in figure 25, increasing the vertical load tends to increase the self-alining torque.

Maximum Self-Alining Torque $\bar{M}_{z,r,e,m}$

The variation of maximum self-alining torque with tire inflation pressure is shown in figure 30 for the two test conditions investigated. For constant vertical loading over the range of inflation pressures investigated, increasing the inflation pressure tends to decrease the maximum self-alining torque. For constant inflation pressure, the maximum self-alining torque increases with increasing vertical load.

Pneumatic Caster $\bar{q} = \dfrac{\bar{M}_{z,r,e}}{\bar{F}_{\psi,r,e}}$

The variation of pneumatic caster with yaw angle for all test conditions is shown in figures 9 and 10. These figures show that the pneumatic caster is at a maximum at small yaw angles and generally decreases with increasing yaw angle for the test range covered (up to 24.5° yaw angle). For the case of constant inflation pressure, illustrated in figure 25, the pneumatic caster is seen to increase with increasing vertical load.

Drag Force $\bar{F}_{x,r,e}$

The variation of drag force with yaw angle for all test conditions is shown in figure 31. The data show that the effect of inflation pressure on drag force for the two vertical loadings investigated is apparently small. In order to show trends more clearly, the ratio of drag force to cornering force $\bar{F}_{x,r,e}/\bar{F}_{y,r,e}$ is plotted against yaw angle for all test conditions in figure 32. If the total horizontal ground force under yawed rolling were normal to the wheel plane, the drag force $\bar{F}_{x,r,e}$ would be equal to the cornering force $\bar{F}_{y,r,e}$ multiplied by the tangent of the yaw angle or $\bar{F}_{x,r,e}/\bar{F}_{y,r,e} = \tan \psi$. Tan ψ is represented in this figure

by the heavy solid lines. Since the data do not usually fall along this line, it appears that some force parallel to the wheel plane exists for most of the yaw-angle range investigated.

Yawed-Rolling Coefficient of Friction $\bar{\mu}_{\psi,r} = \bar{F}_{R,r,e,m}/\bar{F}_z$

The variation of yawed-rolling coefficient of friction with average bearing pressure or ground pressure is shown in figure 33. (See square symbols in this figure.) These data were derived from data given in table II and in figures 18 and 34 (to be discussed later). It should be noted, however, that only a few values of yawed-rolling friction coefficient were obtained because of the limitations of the test setup and that the values shown were derived mostly from extrapolated maximum values of the faired curves given in figure 9. These facts tend to decrease the reliability of the yawed-rolling friction-coefficient data to some extent. The limited data obtained are in fair agreement with similar test results reported in reference 3 for two 56-inch tires, as is shown in figure 35, where a comparison of friction coefficients for these two 56-inch tires (data obtained from ref. 3) with present test results is given. (Compare circle and diamond symbols in fig. 35.) From this comparison it appears that the yawed-rolling coefficients of friction are somewhat smaller for the 26-inch tires; however, since the data for the 26-inch tires are partly extrapolated, this conclusion is subject to some question.

Sliding-Drag (Fore-and-Aft) Coefficient of Friction $\bar{\mu}_{x,s} = \bar{F}_{x,s}/\bar{F}_z$

The variation of sliding-drag coefficient of friction with average bearing pressure for both dry and wet concrete for the one vertical loading tested ($\bar{F}_z \approx 9{,}000$ pounds) is shown in figure 33. (See circle symbols.) These data were derived from data given in table IV and figure 34. The sliding-drag coefficient of friction for the dry-concrete condition appears to decrease in magnitude with increasing bearing pressure. The friction coefficients found for the limited number of tests made with the concrete in a wet condition indicate a slight reduction in magnitude for the sliding-drag coefficients of friction over that for the dry-concrete condition. Also shown in figure 33 for comparison purposes are the limited number of yawed-rolling coefficient-of-friction values obtained from the yawed-rolling tests. (See square symbols.) A comparison of these data indicate somewhat higher values for sliding-drag coefficients of friction than for the corresponding yawed-rolling coefficients of friction.

A comparison of sliding-drag and yawed-rolling coefficients of friction obtained from tests on two 56-inch tires (ref. 3) with present test results is shown in figure 35. The friction coefficients for both sets of tires are seen to be in fairly good agreement and show the same general trends.

Maximum Drag Coefficient of Friction $\bar{\mu}_{x,m} = \bar{F}_{x,m}/\bar{F}_z$

The maximum drag force $\bar{F}_{x,m}$ at incipient slip is generally slightly larger in magnitude than the drag force $F_{x,s}$ required for steady sliding of the locked wheels and tires, as is shown in figure 16 for several typical runs. A comparison of maximum and sliding-drag coefficients of friction is presented in figure 36. Most of the data shown in this figure indicate that the maximum drag coefficient of friction is approximately 3 percent greater in magnitude than the sliding-drag coefficient of friction.

Fore-and-Aft Spring Constant $\bar{K}_x$

The variation of fore-and-aft spring constant with tire inflation pressure, obtained from data in table IV for the one vertical loading investigated ($\bar{F}_z \approx 9{,}000$ pounds), is shown in figure 37. These data are derived from the initial slope of the curves for the variation of the fore-and-aft (drag) force $\bar{F}_x$ with horizontal displacement $\bar{x}$. Samples of these curves for three test inflation pressures are presented in figure 16. For the one vertical loading tested, figure 37 indicates that the fore-and-aft spring constant increases slightly with increasing inflation pressure for the pressure range investigated.

Lateral Spring Constant $\bar{K}_\lambda$

The variation of static lateral spring constant with tire inflation pressure for the two vertical loadings tested, obtained from the slope of the straight-line portions of the curves in figures 19 and 20, is shown in the upper part of figure 38 together with the corresponding dynamic data. The static data are also given in table V whereas the corresponding dynamic data are given in table VI and are discussed in the appendix. If the static data are considered first, the lateral spring constant is seen to increase with increasing inflation pressure at constant vertical loading and to decrease with increasing vertical load at constant inflation pressure at least within the range tested. The dynamic spring-constant data, which are not entirely trustworthy (see the appendix), are in good agreement with the static test data for the light-loading condition tested ($\bar{F}_z = 9{,}000$ pounds) but are in poor agreement with the static

test data at the heavy-loading condition ($\bar{F}_z$ = 17,100 pounds). This disagreement at the heavy-loading condition is probably due in part to the fact that the procedure for determining the dynamic spring constants from the test data is of somewhat dubious merit for the heavy-loading conditions because of the influence of rocking motions of the airplane during these particular tests. (See the appendix.)

Lateral Hysteresis Damping Parameters η_1 and η_3

In order to obtain a quantitative measure of the lateral hysteresis damping, the following considerations were used. During each half cycle of a lateral hysteresis loop, a certain energy E_A is dissipated in hysteresis damping, and at the maximum amplitude of the half cycle a certain maximum amount of energy E_B is stored in the tire. These two energy quantities are indicated in the hysteresis-loop sketch of figure 39 by the respective shaded areas A and B. The ratio $\eta_1 = \frac{E_A}{E_B} = \frac{\text{Area A}}{\text{Area B}}$, which is the ratio of energy dissipated per half cycle of a hysteresis loop to the maximum energy stored during this half cycle, was selected as a quantitative measure of the hysteresis damping and was evaluated for the hysteresis loops in figures 19 and 20. The resulting values of η_1 are listed in table V and are plotted in the lower part of figure 38 as a function of tire inflation pressure. Also shown in figure 38 is the variation of the corresponding dynamic hysteresis parameter η_3 which is based on similar considerations for the dynamic case which are discussed in the appendix. These data for η_3 are listed in table VI. The damping for the dynamic case appears to be considerably greater than that for the static case. Although this difference might be expected from a qualitative point of view, since the interpretation of the dynamic test data used to determine η_3 may be based on oversimplified concepts, the quantitative differences between these two sets of data should not necessarily be viewed as being highly reliable.

Torsional Spring Constant K_α

The variation of static torsional spring constant $K_{\alpha,n}$ with tire inflation pressure for the two vertical loadings tested is shown in figure 40. The values of static spring constant shown in figure 40, which are listed in table VII, were obtained from the approximately straight-line portions of the "decreasing moment" portions of the curves in figures 22 and 23. (The initial slopes of these curves were not used for this purpose since these initial slopes are often more representative

of the tire-hysteresis properties than of the tire spring constants.) From figure 40 it appears that the static torsional spring constants for the two test tires are in fair agreement with each other. For constant vertical loading the static torsional spring constant appears to be largely independent of pressure, and for constant pressure it appears to increase with increasing vertical load.

Also shown in figure 40 are some torsional spring constants $K_{\alpha,r}$ which were obtained from the initial slopes of the self-alining torque curves of figure 10 - $\bar{K}_{\alpha,r} = \left(\frac{d\bar{M}_{z,r,e}}{d\bar{\psi}}\right)_{\bar{\psi}\rightarrow 0}$. These spring constants $\bar{K}_{\alpha,r}$ obtained from the rolling tests are seen to be generally smaller than the corresponding static spring constants $K_{\alpha,n}$.

Footprint Area A_g or A_n

The variation of gross footprint area A_g, net footprint area A_n, and the ratio of net footprint area to gross footprint area A_n/A_g with vertical tire deflection for the test tires, obtained from data in table VIII, is shown in figure 34. Both A_g and A_n appear to increase nonlinearly with increasing vertical tire deflection for the vertical-tire-deflection range covered. The ratio of net footprint area to gross footprint area appears to increase slightly with increasing vertical tire deflection and averages approximately 75 percent of the gross footprint area. This ratio will, of course, change for tires having tread designs different from the ones tested.

Footprint Length 2h and Width b

The variation of footprint length 2h and width b with vertical tire deflection, obtained from data in table VIII, is shown in figure 41. These data indicate that both the footprint length and width increase nonlinearly with increasing vertical tire deflection. Also shown in this figure as solid lines are the lengths of chords of circles having diameters equal to the free diameter d and maximum width w, respectively, of the tire at its rated inflation pressure and located at a distance $r - \delta_o$ from the center of the circles. A comparison of these quantities indicates that the experimental values of footprint width are approximately equal to the corresponding chord lengths, whereas experimental values of footprint length are usually smaller than the corresponding chord lengths for the vertical-tire-deflection range investigated.

Average Bearing Pressure $\bar{p}_n = \overline{F_z/A_n}$ and Average Gross Footprint Pressure $\bar{p}_g = \overline{F_z/A_g}$

The variation of average bearing pressure and average gross footprint pressure with tire inflation pressure is given in figure 42. Although this variation could have been directly obtained from table VIII for a few test points, in order to obtain a greater range of deflection, the data shown in figure 42 are derived from mean values of the curves given in figure 17 for the variation of vertical load with vertical tire deflection and from the faired curves given in figure 34 for the variation of footprint area with vertical tire deflection.

It should be noted that these data in figure 42 can be somewhat in error because the data in figures 17 and 34, on which figure 42 is based, were not obtained under completely similar conditions. Specifically, the footprint-area data of figure 34, as was previously noted, were obtained at a time when a flat spot was present on the tire, whereas no flat spot was present for the data presented in figure 17. As was previously mentioned in connection with figure 18, the difference in vertical tire deflection for these two conditions is approximately 0.3 inch. The heavy solid line represents $\bar{p}_n = \bar{p}_g = \bar{p}$. Comparison of this line with the data for the average bearing pressure $\bar{p}_n$ indicates that the average bearing pressure is usually approximately 25 pounds per square inch greater than the inflation pressure for the inflation-pressure range covered. The average gross footprint pressure p_g, however, for the inflation-pressure range covered is always less than the inflation pressure, and the difference between inflation pressure and average gross footprint pressure increases with increasing inflation pressure.

Relaxation Length L

The variation of the two types of relaxation length with tire inflation pressure is shown in figure 43 for test series A and B. (No relaxation lengths were determined for test series C.) The scatter of the test data is seen to be so large that it obscures any effects of inflation pressure on the relaxation length which might exist. However, the yawed-rolling relaxation lengths L_y do appear to be slightly smaller than the corresponding static relaxation lengths L_s as was previously observed in reference 3 for two 56-inch-diameter tires.

Coefficient of Turning R

In a study of wheel shimmy, Bourcier de Carbon has utilized a tire coefficient called the coefficient of turning R (see ref. 7), which is defined as follows: Consider the condition where a tire is rolled ahead while exposed to a constant torsional moment $M_{z,r}$ and zero lateral force $F_{y,r}$. For this condition a tire rolls in a circular path of radius ρ. The coefficient of turning R has been defined by Bourcier de Carbon as

$$R = \frac{1}{\rho M_{z,r}} \tag{1}$$

Approximate values of R obtained for the present test tire A were calculated from this equation by using the faired curves shown in figure 14 for the three radii tested. The resulting values of R for the test conditions of $F_z = 9{,}000$ pounds, $p \approx 134$ pounds per square inch, and $\delta_o \approx 2.3$ inches are listed in the following table:

ρ, ft	R, lb^{-1}-$in.^{-2}$
4.71	3.8×10^{-6}
9.83	3.1
14.70	3.3

From this table it appears that the coefficient of turning is somewhere between 3×10^{-6} lb^{-1}-$in.^{-2}$ and 4×10^{-6} lb^{-1}-$in.^{-2}$ for these test conditions.

It may also be of some interest to note that this coefficient of turning R may be expressed in terms of some other usually more easily measured tire properties by making use of the results of an unpublished comparison of the tire-motion theory of Von Schlippe and Dietrich (ref. 6) with the theory of Bourcier de Carbon (ref. 7). From this comparison the correlation relation

$$R = \frac{\pi(L + h)}{90K_{\alpha}h(2L + h)} \tag{2}$$

is obtained. Calculations of the coefficient of turning according to this equation for the same conditions as for the aforementioned tests were made by using the values $h = 6.5$ inches (see fig. 41), $L = 8 \pm 3$ inches (see fig. 43), $K_\alpha = \bar{K}_{\alpha,r} = 1{,}100$ lb-in./deg (see fig. 40), and $K_\alpha = K_{\alpha,r} = 845$ lb-in./deg (from the slope of the faired moment curves in fig. 14). From these calculations the value of R obtained for $K_\alpha = 1{,}100$ lb-in./deg is $R = (3.2 \pm 0.2)\ 10^{-6}$ lb^{-1}-$in.^{-2}$ and for $K_\alpha = 845$ lb-in./deg is $R = (4.2 \pm 0.3)\ 10^{-6}$ lb^{-1}-$in.^{-2}$. These two values for R, calculated from equation (2), are seen to be in fair agreement with the values of R, shown in the preceding table, which were calculated from equation (1); thus, the validity of the correlation relation of equation (2) is at least approximately confirmed. It should be noted that excellent agreement between the sets of values of R calculated from these two equations could hardly be expected since neither the experimental values of $M_{Z,r}$ used with equation (1) nor the experimental values of K_α used with equation (2) are extremely accurate. Although the value of relaxation length L used with equation (2) is also not accurately known (see fig. 43), its accuracy is not usually important since, for not too small values of h, the calculation of R according to this equation is relatively insensitive even to large errors in the relaxation length.

Rolling Radius r_e

The variation of rolling radius with yaw angle, obtained from data in table II, for two typical test conditions is shown in figure 11(a). The rolling radii for both test tires appear to be in relatively good agreement and remain more or less constant in magnitude with increasing yaw angle for the angle-of-yaw range covered (0° to 24.5°). The variation of rolling radius with inflation pressure for the two vertical loadings investigated is shown in figure 11(b). The data presented in figure 11(b) were obtained from table II and are for angles of yaw of 1.75° and 3.5°. In order to show more clearly the trends of these data, the effect of inflation pressure has been isolated in figure 11(c) where rolling radius is plotted against vertical tire deflection for several constant inflation pressures. Figure 11(c) shows that, for constant inflation pressure, the rolling radius decreases with increasing vertical tire deflection and, for constant vertical tire deflection, the rolling radius increases slightly with increasing inflation pressure. Similar variations were observed in reference 3 for two 56-inch-diameter tires.

CONCLUSIONS

Tow tests were made primarily to determine the low-speed yawed-straight-rolling characteristics of two 26 × 6.6, type VII, 12-ply-rating airplane tires at two vertical loads which were approximately equal to the rated vertical load and twice the rated vertical load for these tires. The results of these tests indicated the following primary conclusions:

1. The normal force generally increased with increasing angle of yaw within the test range. The variation of normal force with angle of yaw was considerably different for the two vertical loads tested.

2. The cornering power, under constant inflation pressure, decreased with increasing vertical tire deflection for the two vertical loads investigated. For the case of constant vertical tire deflection, increasing the vertical load increased the cornering power.

3. The self-alining torque generally increased with increasing angle of yaw for small angles of yaw and decreased with increasing angle of yaw at large angles of yaw.

4. The pneumatic caster was at a maximum at small angles of yaw and generally decreased with increasing angle of yaw for the test range covered.

5. The sliding-drag coefficient of friction decreased with increasing bearing pressure; and at comparable bearing pressures, both the sliding-drag and yawed-rolling coefficients of friction followed approximately the same trends and magnitudes that were reported for two 56-inch-diameter tires in NACA Technical Note 3235.

6. The coefficient of turning (Christian Bourcier de Carbon's constant R) for one tire rolling along a path of circular curvature was determined for several turning radii (approximately 5, 10, and 15 feet). The coefficient was found to be between 3×10^{-6} lb^{-1}-$in.^{2}$ to 4×10^{-6} lb^{-1}-$in.^{-2}$ at a vertical load of 9,000 pounds and a tire inflation of 134 pounds per square inch.

Langley Aeronautical Laboratory,
National Advisory Committee for Aeronautics,
Langley Field, Va., October 27, 1955.

APPENDIX

INTERPRETATION OF RESULTS OF DYNAMIC LATERAL-ELASTICITY TESTS

In order to interpret the frequency and amplitude-decrease tests, results of the dynamic lateral-elasticity tests in terms of tire lateral spring constants and hysteresis losses, the following considerations were made.

As a first approximation it was assumed that during these tests the test vehicle experienced only purely lateral oscillations against the spring restraints of the two test tires in such a way that the behavior of the test system could be considered to be somewhat similar to the free oscillations of a simple mass oscillating with a linear spring and viscous damping. Such a system is illustrated in the following sketch:

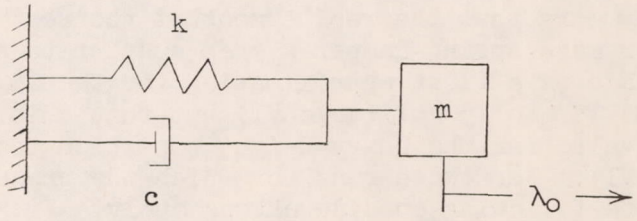

The spring constant k for the simplified system corresponding to the test system is taken as the sum of the spring constants for the two test tires ($k = 2\bar{K}_\lambda$); the damper constant c is related to the hysteresis damping of the system and the mass m is taken as the mass of the test vehicle. This analogy between the actual test system and a simple mass oscillator is, of course, not a perfect analogy for the following reasons: First, it assumes that the only restraints on the lateral motion of the test vehicle were supplied by the two test tires. Actually, however, the test vehicle was also partly restrained from lateral motion by the airplane tail support by which the test vehicle was attached to the towing truck. The airplane tail, however, was attached to the towing truck in such a manner that the tail support caused only a small lateral restraint; apparently, the lateral stiffness of this support was less than one-tenth the

combined lateral stiffness of the two test tires. A second limitation on the validity of the analogy arises from the fact that the center of gravity of the test vehicle is not exactly at the same longitudinal station of the test vehicle as the two test tires. This offset, which is about 3.3 feet for the light-weight condition tested ($\bar{F}_Z$ = 9,000 pounds) and about 2.0 feet for the heavy-weight condition ($\bar{F}_Z$ = 17,100 pounds), is not believed to be large enough to be of great importance. A third limitation arises from the neglect of the possible effects of flexibility of the reinforced landing-gear struts. Finally and apparently the most important limitation on the validity of the analogy arises from the fact that its validity requires that the test vehicle shall experience only pure lateral oscillations without rolling or rocking motions. At the light-weight condition tested, both visual observation of the tests and examination of the test records indicated that the test vehicle did perform largely purely lateral oscillations without rolling. For the heavy-weight condition for most of the runs, however, it was apparent from visual observations that significant rolling motions were occurring. (Apparently, the natural rolling frequency of the test vehicle for the light-weight condition was about 4 cycles per second.)

In view of the preceding considerations, particularly with respect to rolling, it appears that the replacement of the test system by an equivalent linear mass-spring-damper system subject to pure lateral motion might be acceptable as a first approximation for the light-weight condition tested (runs 150 to 156 of table VI) but that this analogy is of highly doubtful value for the heavy-weight condition tested (runs 157 to 161 of table VI). For those runs for which the preceding analogy may be reasonable, the following considerations apply.

The differential equation for a single-degree-of-freedom linear mass-spring-damper system undergoing free vibrations is

$$m\ddot{\lambda}_o + c\dot{\lambda}_o + k\lambda_o = 0 \tag{A1}$$

and its solution is

$$\lambda_o = \varphi_1 e^{-\frac{c}{2m}t} \cos\left(\sqrt{\frac{k}{m} - \frac{c^2}{4m^2}}\, t + \varphi_2\right) \tag{A2}$$

where φ_1 and φ_2 are constants. The frequency f of the oscillation is

$$f = \frac{1}{2\pi}\sqrt{\frac{k}{m} - \frac{c^2}{4m}} \tag{A3}$$

The equivalent values of c for the present test results are sufficiently small so that equation (A3) can be reduced to the simpler relation

$$f = \frac{1}{2\pi}\sqrt{\frac{k}{m}} \tag{A4}$$

and substitution of $k = 2\bar{K}_\lambda$ into equation (A4) gives

$$\bar{K}_\lambda = 2\pi^2 m f^2 \tag{A5}$$

(The values of $\bar{K}_\lambda$ listed in table VI were calculated from the experimental values of f given in the table with the aid of equation (A5). The values of total vehicle mass used were approximately 619 slugs for test series A and 1,143 slugs for test series C.)

In order to interpret the damping of the oscillation, consider the following sketch of an exponentially damped oscillation:

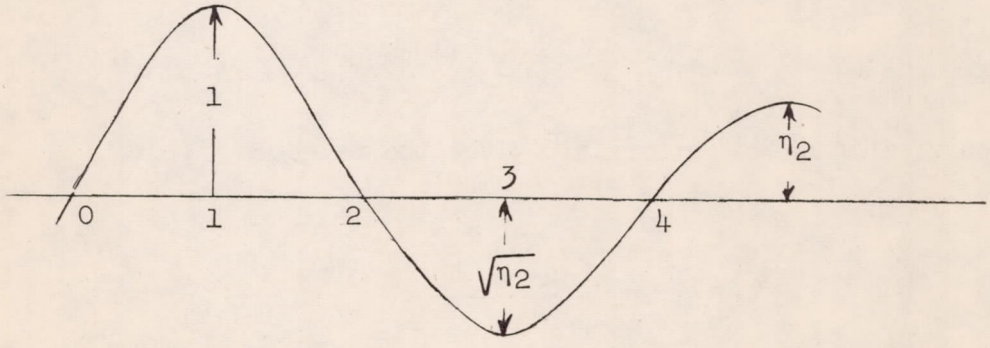

If the amplitude of the oscillation at the first positive peak (point 1 of the sketch) is designated as unity and that of the peak one cycle later as η_2, the magnitude of the first negative peak, for an exponential decay, will be approximately $\sqrt{\eta_2}$. Consider now the energy loss in going through a half cycle of oscillation, from point 1 to point 3 in the previous sketch. The energy E_1 of the system at point 1 (with unit deflection) will be approximately the same as the energy stored in a linear spring of stiffness k and unit deflection, which is $E_1 = \frac{1}{2} k(1)^2$; and, similarly, for point 3 the energy is $E_3 = \frac{1}{2} k\left(\sqrt{\eta_2}\right)^2 = \frac{1}{2} k\eta_2$. In accordance with the discussion of static hysteresis, it is assumed here that the energy dissipated in the half cycle from points 0 to 2, designated as ΔE_{02}, is a fraction η_3 (corresponding to η_1 for the static case) of the maximum stored energy for that half cycle E_1 or $\Delta E_{02} = \eta_3 \frac{1}{2} k(1)^2$. Thus, for the quarter cycle from points 1 to 2, $\Delta E_{12} = \frac{1}{2} \Delta E_{02} = \frac{1}{2} \eta_3 \frac{1}{2} k(1)^2$ and, similarly, from points 2 to 3, $\Delta E_{23} = \frac{1}{2} \eta_3 \frac{1}{2} k\left(\sqrt{\eta_2}\right)^2$. Then, using the relation

$$E_3 = E_1 - \Delta E_{12} - \Delta E_{23}$$

substituting the various value of E, and dividing through by $\frac{1}{2} k$ gives

$$\eta_2 = 1 - \frac{1}{2} \eta_3 - \frac{1}{2} \eta_3 \eta_2$$

Solution of this equation for η_3 gives the relation

$$\eta_3 = \frac{2(1 - \eta_2)}{1 + \eta_2} \tag{A6}$$

(The values of η_3 listed in table VI were calculated from the experimental values of η_2 given in the table with the aid of equation (A6).)

REFERENCES

1. Hadekel, R.: The Mechanical Characteristics of Pneumatic Tyres. S & T Memo. No. 5/50, British Ministry of Supply, TPA 3/TIB, Mar. 1950.

2. Horne, Walter B.: Static Force-Deflection Characteristics of Six Aircraft Tires Under Combined Loading. NACA TN 2926, 1953.

3. Horne, Walter B., Stephenson, Bertrand H., and Smiley, Robert F.: Low-Speed Yawed-Rolling and Some Other Elastic Characteristics of Two 56-Inch-Diameter, 24-Ply-Rating Aircraft Tires. NACA TN 3235, 1954.

4. Anon: Military Specification - Casings; Aircraft Pneumatic Tire. Military Specification, MIL-C-5041, Sept. 16, 1949; Amendment-2, Feb. 8, 1951.

5. Evans, R. D.: Cornering Power of Airplane Tires. The Goodyear Tire & Rubber Co., Oct. 17, 1946.

6. Von Schlippe, B., and Dietrich, R.: Zur Mechanik des Luftreifens. (The Mechanics of Pneumatic Tires.) Junkers Flugzeug- und Motorenwerke, A.-G. (Dessau). (Translation available from ASTIA as ATI 105296.)

7. Bourcier de Carbon, Christian: Analytical Study of Shimmy of Airplane Wheels. NACA TM 1337, 1952.

TABLE I.- TIRE SPECIFICATIONS

Specifications	Military specification (ref. 4)	Start of test, tires in new and unused conditions	
		Tire A	Tire B
Tire:			
Type[a]	VII	------	-----
Ply rating	12	------	-----
Static load, lb	8,000	------	-----
Inflation pressure, lb/sq in.	160	------	-----
Burst pressure, lb/sq in.	640 (minimum)	------	-----
Moment of static unbalance, oz-in.	17 (maximum)	------	-----
Diameter, deflated, in.	----------	24.5	24.5
Diameter, inflated, in.	25.00 (minimum)	------	------
	25.75 (maximum)	25.6	25.4
Maximum width, deflated, in.	----------	5.9	5.8
Maximum width, inflated, in.	6.38 (minimum)	------	------
	6.65 (maximum)	6.5	6.5
Bead width, in.	1.50 (maximum)	1.15	1.20
Minimum wall thickness, in.	----------	[b]0.4	[b]0.4
Wall thickness at tread center line (including tread), in.	----------	0.7	0.7
Depth of tread at tread center line, in.	0.21 (minimum)	0.2	0.2
Casing weight, lb	31 (maximum)	[c]24.0	[b]23.0
Tread pattern	Rib	Rib	Rib
Moment of inertia about wheel axle (deflated), lb-ft-sec^2	----------	[b]0.57	[b]0.57
Moment of inertia about wheel axle (inflated to 160 lb/sq in.), lb-ft-sec^2	----------	[b]0.59	------
Inner tube:			
Thickness, in.		0.09	0.09
Weight, lb		[d]4.0	4.5
Wheel:			
Rim diameter, in.		16.0	16.0
Weight, lb		24.3	24.8
Moment of inertia about wheel axle, lb-ft-sec^2		0.17	0.17

[a]Type VII is an extra high pressure tire.

[b]End of test, tires in worn condition.

[c]Casing weight was 22.9 at end of test.

[d]Inner-tube weight increases to 5.0 lb when inflated to 160 lb/sq in.

TABLE II.- YAW TEST DATA

(a) Series A: $\bar{F}_z$ = 9,000 lb; $(F_z)_{tire\ A}$ = 9,000 lb; $(F_z)_{tire\ B}$ = 9,000 lb

Run	Average values											Tire A				Tire B			
	$\bar{p}$, lb/sq in.	$\bar{\delta}_o$, in.	$\bar{\delta}$, in.	$\bar{\psi}$, deg	$\bar{F}_{y,r,e}$, lb	$\bar{F}_{x,r,e}$, lb	$\bar{F}_{\psi,r,e}$, lb	$\bar{M}_{z,r,e}$, lb-in.	$\bar{q}$, in.	$\bar{l}_y$, in.	$\frac{d\bar{F}_{y,r}}{dx}$, lb/in.	p, lb/sq in.	δ_o, in.	δ, in.	r_e, in.	p, lb/sq in.	δ_o, in.	δ, in.	r_e, in.
1	103	3.0	3.0	1.75	270	100	270	3,100	11.48	(a)	30	103	3.0	3.2	11.6	103	2.9	2.9	11.6
2	104	3.0	3.0	3.5	650	100	650	4,400	6.77	(a)	50	104	2.9	2.9	11.6	104	3.0	3.1	11.7
3	124	2.5	2.6	1.75	300	0	300	3,200	10.67	(a)	(a)	124	2.5	2.5	11.8	124	2.5	2.6	11.8
4	123	2.6	2.6	3.5	830	100	830	3,200	3.86	(a)	70	123	2.6	2.4	(a)	123	2.6	2.6	11.8
5	142	2.4	2.3	1.75	560	100	560	(a)	(a)	(a)	(b)	142	2.5	2.2	(a)	142	2.3	2.3	12.0
6	142	2.3	2.4	1.75	470	100	470	2,100	4.47	(a)	(b)	142	2.3	2.4	11.9	142	2.3	2.4	11.9
7	142	2.3	2.3	1.75	550	100	550	2,300	4.18	(a)	70	142	2.2	2.2	11.9	142	2.3	2.3	12.0
8	142	2.3	2.3	3.5	1,130	100	1,130	(a)	(a)	(a)	(b)	142	2.3	2.3	(a)	142	2.3	2.3	12.1
9	142	2.3	2.3	3.5	940	200	950	4,700	4.95	5.2	(b)	142	2.3	2.4	(a)	142	2.4	2.3	11.9
10	144	2.3	2.3	3.5	890	100	890	3,300	3.71	(a)	90	144	2.3	2.3	(a)	144	2.3	2.3	12.0
11	147	2.4	2.4	7.0	2,190	400	2,220	(a)	(a)	(a)	(b)	147	2.3	2.4	11.9	147	2.5	2.5	12.0
12	142	2.3	2.3	7.0	2,060	400	2,090	6,400	3.06	8.9	(b)	142	2.2	2.2	12.2	142	2.3	2.3	12.0
13	146	2.2	2.4	10.5	3,080	600	3,140	10,200	3.25	(c)	(b)	145	2.2	2.4	11.9	147	2.2	2.5	12.0
14	162	2.1	2.2	1.75	510	100	510	(a)	(a)	(a)	(b)	162	2.1	2.2	11.9	162	2.2	2.1	12.0
15	164	2.1	2.1	1.75	480	100	480	1,400	2.92	(a)	(b)	164	2.1	2.1	(a)	164	2.1	2.1	12.1
16	163	2.0	1.9	1.75	530	100	530	1,800	3.40	(a)	(a)	163	1.9	1.8	12.0	163	2.0	1.9	12.1
17	162	2.1	2.1	3.5	1,140	100	1,140	2,900	2.54	5.1	(b)	162	2.2	2.2	11.9	162	2.1	2.1	12.0
18	163	2.1	2.1	3.5	1,060	100	1,060	3,300	3.11	(a)	100	163	2.2	2.1	(a)	164	2.0	2.1	12.1
19	162	2.1	2.1	7.0	2,100	400	2,130	6,400	3.00	5.3	(b)	161	2.2	2.2	(a)	162	2.0	2.1	12.1
20	163	2.1	2.1	7.0	2,400	200	2,410	5,400	2.24	(a)	200	163	2.1	2.0	(a)	164	2.1	2.2	12.1
21	182	1.9	1.9	1.75	650	100	650	3,100	4.77	(a)	(b)	181	1.9	1.8	12.1	182	1.9	2.0	12.1
22	182	2.0	2.0	1.75	640	0	640	1,500	2.34	(a)	(b)	182	2.0	2.0	12.1	181	2.0	2.0	12.1
23	184	(a)	(a)	1.75	660	100	660	3,200	4.85	(a)	(a)	184	(a)	(a)	12.1	184	1.9	2.0	12.3
24	183	1.9	2.0	3.5	1,410	200	1,420	3,800	2.68	6.6	(b)	183	2.0	2.1	12.0	183	1.9	2.0	12.2
25	182	2.0	2.0	3.5	1,330	100	1,330	3,700	2.78	(a)	150	182	1.9	1.9	(a)	183	2.2	2.1	12.2
26	182	2.0	2.1	7.0	2,550	400	2,580	(a)	(a)	(a)	(b)	182	2.0	2.1	12.1	182	2.0	2.0	12.2
27	182	2.0	1.9	7.0	2,380	400	2,410	7,300	3.03	7.7	(b)	182	2.1	1.9	(a)	182	1.9	1.9	12.2
28	183	1.9	1.9	7.0	2,460	300	2,480	7,200	2.90	(a)	290	183	1.9	1.9	(a)	183	2.0	2.0	12.2
29	201	1.3	1.3	1.75	780	100	780	1,600	2.05	6.9	(b)	201	1.3	1.3	(a)	201	1.2	1.4	12.2
30	205	1.8	1.8	1.75	710	100	710	2,400	3.38	(a)	70	205	1.8	1.7	12.3	205	1.8	1.9	12.2
31	202	1.4	1.4	3.5	1,300	200	1,310	4,200	3.21	6.4	(b)	202	1.4	1.4	(a)	202	1.4	1.3	12.3
32	202	1.8	1.8	3.5	1,340	100	1,340	3,400	2.54	(a)	100	202	1.8	1.8	12.2	202	1.8	1.8	12.2
33	202	1.4	1.2	7.0	2,600	(a)	2,630	6,700	2.60	5.4	(b)	201	1.4	1.2	(a)	202	1.3	1.2	12.3
34	202	1.5	1.4	7.0	2,300	600	2,360	6,100	2.58	4.8	(b)	202	1.5	1.4	(a)	202	1.4	1.4	12.3
35	199	1.9	1.9	7.0	2,630	400	2,660	5,300	1.99	(a)	320	199	1.9	2.1	(a)	198	1.8	1.8	12.1
36	202	1.4	1.6	10.5	3,480	(a)	3,550	8,600	2.42	(c)	(b)	202	1.5	1.7	12.2	202	1.3	1.5	12.2
37	202	1.6	1.7	14.0	4,330	(a)	4,470	8,400	1.88	(c)	(b)	202	1.7	1.8	12.1	202	1.5	1.5	12.2
38	202	1.5	1.7	17.5	4,420	(a)	4,670	5,300	1.13	(c)	(b)	202	1.6	1.7	12.0	202	1.3	1.7	12.2
39	202	1.5	1.7	21.0	4,490	(a)	4,870	6,900	1.42	(c)	(b)	202	1.4	1.6	(a)	202	1.6	1.7	12.1
40	202	1.6	1.8	24.5	4,950	(a)	5,460	2,200	0.40	(c)	(b)	202	1.6	1.8	(a)	202	1.7	1.8	12.2

[a]Value could not be accurately determined.

[b]Test vehicle backed up before start of run.

[c]Value not determined.

TABLE II.- YAW TEST DATA - Continued

(b) Series B: $\bar{F}_z$ = 9,100 lb; $(F_z)_{tire\ A}$ = 9,200 lb; $(F_z)_{tire\ B}$ = 9,000 lb

Run	Average values											Tire A				Tire B			
	p, lb/sq in.	δ_o, in.	$\bar{\delta}$, in.	$\bar{\psi}$, deg	$\bar{F}_{y,r,e}$, lb	$\bar{F}_{x,r,e}$, lb	$\bar{F}_{\psi,r,e}$, lb	$\bar{M}_{z,r,e}$, lb-in.	$\bar{q}$, in.	$\bar{L}_y$, in.	$\frac{d\bar{F}_{y,r}}{dx}$, lb/in.	p, lb/sq in.	δ_o, in.	δ, in.	r_e, in.	p, lb/sq in.	δ_o, in.	δ, in.	r_e, in.
41	102	2.9	3.0	7.0	1,360	500	1,410	8,500	6.03	(a)	140	102	3.0	2.9	11.6	102	2.9	3.1	11.6
42	122	2.7	2.8	7.0	1,660	400	1,700	7,500	4.41	11.2	120	122	2.8	2.8	11.7	123	2.7	2.8	11.6
43	125	2.7	2.9	10.5	2,520	600	2,590	9,100	3.51	(b)	(b)	125	2.5	2.6	(b)	125	2.9	3.1	(b)
44	123	2.9	3.1	14.0	3,200	900	3,320	9,000	2.71	(b)	(b)	124	2.9	3.0	(b)	123	3.0	3.3	(b)
45	145	2.5	2.7	7.0	2,000	300	2,020	6,500	3.22	7.9	(a)	145	2.7	2.9	11.8	145	2.4	2.5	11.8
46	144	2.5	2.6	10.5	2,820	700	2,900	8,600	2.97	(b)	(b)	144	2.5	2.5	(b)	144	2.5	2.7	(b)
47	142	2.3	2.6	14.0	3,740	1,100	3,900	7,500	1.92	(b)	(b)	142	2.2	2.5	(b)	142	2.5	2.6	(b)
48	142	2.4	2.8	17.5	4,140	1,400	4,370	7,700	1.76	(b)	(b)	142	2.4	2.6	(b)	142	2.5	3.0	(b)
49	140	2.4	2.8	17.5	4,230	1,600	4,520	6,400	1.42	(b)	(b)	140	2.6	3.0	(b)	140	2.3	2.6	(b)
50	142	2.4	2.9	21.0	4,650	1,800	4,990	6,500	1.30	(b)	(b)	142	2.3	2.7	(b)	142	2.5	3.0	(b)
51	142	2.5	(a)	24.5	5,260	2,400	5,780	5,300	0.92	(b)	(b)	142	2.6	3.2	(b)	142	2.5	(a)	(b)
52	163	2.2	2.4	7.0	2,120	400	2,150	6,100	2.84	(a)	(a)	163	2.2	2.5	(a)	164	2.2	2.3	12.0
53	162	2.4	2.6	10.5	3,060	700	3,140	7,300	2.32	(b)	(b)	162	2.4	2.7	(b)	162	2.4	2.5	(b)
54	164	2.1	2.4	14.0	4,220	1,300	4,410	7,700	1.75	(b)	(b)	163	2.1	2.3	(b)	165	2.2	2.5	(b)
55	163	2.2	2.5	17.5	4,640	1,500	4,880	(a)	(a)	(b)	(b)	163	2.2	2.5	(b)	163	2.2	2.4	(b)
56	165	2.1	2.5	21.0	4,680	1,700	4,980	4,400	0.88	(b)	(b)	165	2.1	2.4	(b)	165	2.2	2.6	(b)
57	168	2.2	2.6	21.0	5,310	2,000	5,670	6,900	1.22	(b)	(b)	169	2.2	2.7	(b)	167	2.2	2.4	(b)
58	162	2.2	2.7	24.5	5,320	2,400	5,840	4,100	0.70	(b)	(b)	162	2.4	2.8	(b)	162	2.1	2.6	(b)
59	183	1.8	1.8	7.0	2,720	400	2,750	5,900	2.15	8.9	(a)	180	2.0	1.9	(a)	186	1.7	1.7	12.0
60	177	2.0	2.2	10.5	3,750	700	3,810	(a)	(a)	(b)	(b)	178	2.1	2.3	(b)	177	1.9	2.1	(b)
61	183	2.0	2.2	14.0	4,280	1,100	4,420	5,400	1.22	(b)	(b)	183	1.8	2.0	(b)	183	2.2	2.4	(b)
62	183	1.9	2.2	17.5	5,110	1,500	5,320	7,800	1.47	(b)	(b)	183	1.8	2.0	(b)	183	2.0	2.3	(b)
63	182	2.2	2.6	21.0	4,790	1,600	5,050	3,500	0.69	(b)	(b)	182	2.3	2.6	(b)	182	2.2	2.6	(b)
64	204	1.9	2.2	14.0	4,690	900	4,770	5,700	1.19	(b)	(b)	204	2.0	2.3	(b)	205	1.9	2.2	(b)
65	205	1.9	2.1	17.5	5,020	1,500	5,240	5,700	1.09	(b)	(b)	205	1.8	1.9	(b)	205	2.0	2.2	(b)
66	226	1.6	(a)	1.75	910	200	920	2,000	2.17	(a)	90	227	1.7	(a)	12.3	225	1.6	(a)	12.2
67	228	1.6	1.7	1.75	790	100	790	2,900	3.67	(a)	(a)	230	1.7	1.9	12.2	227	1.6	1.5	12.2
68	227	1.8	2.0	3.5	1,470	100	1,470	6,100	4.15	8.7	(a)	227	1.9	2.1	12.2	227	1.7	1.9	12.2
69	225	1.7	(a)	7.0	(a)	(a)	(a)	(a)	(a)	(a)	(a)	224	1.7	(a)	12.2	227	1.8	(a)	12.2
70	226	1.7	(a)	7.0	(a)	300	(a)	(a)	(a)	(a)	(a)	225	1.7	(a)	12.1	227	1.8	(a)	12.2
71	227	1.7	1.9	7.0	2,920	400	2,950	5,800	1.97	7.8	240	230	1.6	1.8	(a)	225	1.8	2.0	(a)
72	226	1.8	1.9	10.5	4,040	600	4,080	6,000	1.47	(b)	(b)	226	1.8	2.0	(b)	227	1.8	1.7	(b)
73	227	1.8	1.9	14.0	4,870	1,200	5,020	5,100	1.02	(b)	(b)	227	1.8	1.9	(b)	227	1.8	2.0	(b)
74	227	1.8	(a)	14.0	4,530	1,100	4,660	6,400	1.37	(b)	(b)	227	1.8	(a)	(b)	227	1.8	(a)	(b)
75	225	1.9	2.1	17.5	5,050	1,400	5,240	5,300	1.01	(b)	(b)	223	1.8	2.2	(b)	227	2.0	2.0	(b)
76	225	1.8	2.0	21.0	4,970	1,700	5,250	3,600	0.69	(b)	(b)	224	1.8	2.0	(b)	227	1.9	1.8	(b)
77	226	1.9	2.1	21.0	5,610	2,000	5,950	2,700	0.45	(b)	(b)	227	1.8	2.0	(b)	225	2.0	2.2	(b)
78	227	2.0	2.2	24.5	5,180	1,900	5,500	2,900	0.53	(b)	(b)	227	2.1	2.3	(b)	227	2.0	2.2	(b)

[a]Value could not be accurately determined.

[b]Value not determined.

TABLE II.- YAW TEST DATA - Concluded

(c) Series C: $\bar{F}_Z$ = 17,100 lb; $(F_Z)_{tire\ A}$ = 16,900 lb; $(F_Z)_{tire\ B}$ = 17,200 lb

Run	Average values									Tire A				Tire B			
	$\bar{p}$, lb/sq in.	$\bar{\delta}_o$, in.	$\bar{\delta}$, in.	$\bar{\psi}$, deg	$\bar{F}_{y,r,e}$, lb	$\bar{F}_{x,r,e}$, lb	$\bar{F}_{\psi,r,e}$, lb	$\bar{M}_{z,r,e}$, lb-in.	$\bar{q}$, in.	p, lb/sq in.	δ_o, in.	δ, in.	r_e, in.	p, lb/sq in.	δ_o, in.	δ, in.	r_e, in.
79	163	3.9	3.9	1.75	290	500	310	3,800	12.26	163	3.9	4.0	11.4	163	3.9	3.7	11.3
80	165	3.8	3.8	3.5	490	600	530	5,300	10.00	165	3.9	4.0	11.5	165	3.7	3.7	11.0
81	163	3.8	3.9	7.0	1,250	800	1,340	10,500	7.84	163	3.9	4.0	11.4	163	3.8	3.9	11.3
82	163	3.8	4.1	10.5	2,230	1,300	2,430	10,700	4.40	163	3.8	4.2	11.5	164	3.8	4.0	11.5
83	163	3.7	4.2	14.0	3,130	1,900	3,500	(a)	(a)	163	3.7	4.2	11.5	164	3.8	4.1	11.5
84	181	3.5	3.6	1.75	300	400	310	1,900	6.13	180	3.6	3.7	11.7	182	3.5	3.5	11.7
85	183	3.6	3.6	3.5	670	400	690	2,700	3.91	183	3.6	3.6	11.6	184	3.6	3.6	11.4
86	184	(a)	(a)	3.5	810	400	830	6,100	7.35	184	(a)	(a)	(a)	184	(a)	(a)	11.7
87	184	3.5	3.7	7.0	2,020	800	2,100	9,600	4.57	184	3.5	3.5	11.7	185	3.5	3.9	11.7
88	185	3.4	3.6	10.5	2,840	1,300	3,030	9,800	3.23	185	3.6	3.6	11.6	186	3.3	3.6	11.7
89	183	3.5	3.7	10.5	2,720	1,000	2,860	12,900	4.51	184	3.4	3.7	(a)	182	3.6	3.8	11.7
90	184	3.4	3.8	14.0	3,970	1,900	4,310	(a)	(a)	184	3.5	3.9	11.7	184	3.4	3.8	11.7
91	184	3.5	4.1	17.5	5,070	2,700	5,650	13,800	2.44	184	3.5	4.1	11.6	184	3.5	4.1	(a)
92	202	3.3	3.3	1.75	560	200	570	4,500	7.89	202	3.4	3.4	11.7	203	3.3	3.2	11.8
93	204	3.2	3.3	3.5	880	400	900	3,900	4.33	204	3.2	3.2	11.7	205	3.3	3.4	11.7
94	202	3.1	3.1	3.5	1,170	300	1,190	5,700	4.79	202	3.2	3.2	(a)	203	3.1	3.1	11.8
95	202	(a)	(a)	7.0	2,360	700	2,430	9,500	3.91	202	(a)	(a)	11.8	202	(a)	(a)	11.7
96	201	3.2	3.4	7.0	1,960	500	2,010	7,800	3.88	199	3.2	3.4	11.8	203	3.2	3.4	11.8
97	204	3.2	3.5	10.5	3,370	1,200	3,530	10,500	2.97	205	3.2	3.7	11.8	204	3.3	3.3	11.8
98	206	3.1	3.5	14.0	4,950	2,000	5,290	(a)	(a)	206	3.2	3.6	11.8	206	3.1	3.5	11.8
99	204	3.1	3.7	17.5	5,800	2,500	6,280	(a)	(a)	204	3.2	3.7	11.8	204	3.1	3.7	11.8
100	202	3.3	4.0	17.5	5,310	2,500	5,820	13,300	2.29	201	3.3	4.1	11.8	203	3.4	3.9	(a)
101	206	3.1	3.9	21.0	7,060	3,400	7,810	(a)	(a)	206	3.2	3.9	(a)	206	3.1	3.9	11.8
102	204	3.1	(a)	24.5	7,790	3,700	8,620	4,800	0.56	204	3.1	4.0	11.6	205	3.1	(a)	11.6
103	223	3.1	3.1	1.75	490	200	500	1,600	3.20	221	3.1	3.1	11.8	226	3.1	3.0	11.8
104	225	3.0	3.1	3.5	1,130	400	1,150	3,700	3.22	224	3.1	3.2	11.9	227	2.9	3.1	11.8
105	226	2.9	3.6	7.0	2,470	800	2,550	12,900	5.06	226	3.0	3.7	11.9	226	2.9	3.6	11.8
106	225	3.0	3.3	10.5	3,790	1,200	3,950	8,900	2.25	227	3.0	3.3	11.9	224	3.0	3.3	11.6
107	226	2.9	3.3	14.0	5,370	1,700	5,620	(a)	(a)	228	3.0	3.3	12.0	224	2.9	3.3	11.9
108	226	3.0	3.5	17.5	6,830	2,400	7,240	11,300	1.56	226	3.0	3.5	11.9	227	3.0	3.5	11.9
109	228	(a)	(a)	21.0	7,500	3,100	8,110	(a)	(a)	228	(a)	(a)	(a)	228	(a)	(a)	(a)
110	224	2.9	3.7	24.5	7,860	3,900	8,770	(a)	(a)	224	3.0	3.9	11.7	225	2.9	3.6	11.7
111	236	2.9	3.8	24.5	8,190	4,200	9,190	4,800	0.52	236	2.9	3.5	(a)	236	3.0	4.2	(a)

[a]Value could not be accurately determined.

TABLE III.- STATIC-RELAXATION-LENGTH DATA

[Test series A]

Run	Tire A					Tire B				
	p_o, lb/sq in.	p, lb/sq in.	F_z, lb	δ_o, in.	L_s, in.	p_o, lb/sq in.	p, lb/sq in.	F_z, lb	δ_o, in.	L_s, in.
112	158	165	9,000	2.1	(a)	158	165	9,000	1.8	9.8
113	(b)	180	9,000	(a)	7.1	(b)	180	9,000	1.8	9.4
114	(b)	180	9,000	1.6	(a)	(b)	182	9,000	1.7	7.7
115	(b)	196	9,000	(a)	9.5	194	200	9,000	(a)	8.2

[a]Value could not be accurately determined.

[b]Value not available.

TABLE IV.- LOCKED-WHEEL DRAG TEST DATA

[Between test series A and B: $\bar{F}_z$ = 9,090 lb for $\bar{F}_x$ = 0; $\bar{F}_z \approx$ 8,930 lb for all values of $\bar{F}_x$ in this table]

Run	Average values							Remarks
	$\bar{p}$, lb/sq in.	$\bar{\delta}_o$, in.	$\bar{F}_{x,n,m}$, lb	$\bar{F}_{x,n,s}$, lb	$\bar{\mu}_{x,m}$,	$\bar{\mu}_{x,s}$,	$\bar{K}_x$, lb/in.	
116	103	2.7	6,710	6,580	0.75	0.74	5,570	Dry concrete
117	103	2.7	6,540	6,540	.73	.73	5,460	
118	103	2.6	6,570	6,480	.74	.73	5,230	
119	102	2.8	6,320	6,130	.71	.69	4,930	Wet concrete
120	123	2.3	6,510	6,430	.73	.72	4,920	Dry concrete
121	122	2.3	6,470	6,410	.72	.72	4,930	
122	123	2.3	6,430	6,190	.72	.69	4,930	Wet concrete
123	142	2.0	6,490	6,260	.73	.70	5,330	Dry concrete
124	141	2.0	6,460	6,250	.72	.70	5,060	
125	143	2.0	6,390	6,170	.72	.69	5,070	Wet concrete
126	159	1.9	6,290	6,130	.70	.69	5,180	Dry concrete
127	163	1.8	6,320	6,160	.71	.69	5,820	
128	162	1.8	6,280	5,980	.70	.67	4,930	Wet concrete
129	180	1.7	6,100	6,070	.68	.68	5,650	Dry concrete
130	180	1.7	6,160	6,070	.69	.68	5,860	
131	184	1.7	6,320	6,030	.71	.67	5,660	
132	181	1.7	6,160	6,000	.69	.67	5,960	Wet concrete
133	205	1.6	6,050	5,800	.68	.65	5,280	Dry concrete
134	207	1.6	6,140	5,860	.69	.66	5,210	
135	203	1.5	6,130	5,620	.69	.63	(a)	Wet concrete
136	232	1.5	6,240	5,600	.70	.63	6,310	Dry concrete
137	232	1.4	6,090	5,660	.68	.63	6,280	
138	229	1.5	6,230	5,720	.70	.64	5,660	
139	222	1.6	6,300	5,950	.71	.67	(a)	
140	228	1.5	6,050	5,350	.68	.60	5,800	Wet concrete

[a]Value could not be accurately determined.

TABLE V.- STATIC LATERAL-ELASTICITY TEST DATA

Run	Test series	Average values				
		$\bar{F}_z$, lb	$\bar{p}$, lb/sq in.	$\bar{\delta}_o$, in.	$\bar{K}_\lambda$, lb/in.	η_1
141	A	9,000	142	2.0	2,050	0.48
142	A	9,000	142	2.2	1,850	.56
143	A	9,000	162	1.8	2,200	.36
144	A	9,000	182	1.9	2,430	.37
145	A	9,000	202	1.7	2,450	.36
146	C	17,100	161	3.6	1,350	(a)
147	C	17,100	185	3.3	1,800	.66
148	C	17,100	199	(a)	2,010	.48
149	C	17,100	227	2.9	2,520	(a)

[a]Value could not be accurately determined.

TABLE VI.- DYNAMIC LATERAL-ELASTICITY TEST DATA

Run	Test series	Average values						
		$\bar{F}_z$, lb	$\bar{p}$, lb/sq in.	$\bar{\delta}_o$, in.	$\bar{f}$, cps	η_2	$\bar{K}_\lambda$, lb/in.	η_3
150	A	9,000	142	2.0	1.37	0.45	1,910	0.76
151	A	9,000	162	1.8	1.54	.48	2,420	.70
152	A	9,000	162	1.8	1.45	.48	2,140	.70
153	A	9,000	182	1.8	1.54	.53	2,420	.61
154	A	9,000	182	1.8	1.51	.52	2,320	.63
155	A	9,000	202	1.7	1.59	.52	2,580	.63
156	A	9,000	202	1.7	1.59	.55	2,580	.58
157	C	17,100	162	3.8	1.45	(a)	3,950	(a)
158	C	17,100	182	3.4	1.23	(a)	2,840	(a)
159	C	17,100	182	3.4	1.32	(a)	3,280	(a)
160	C	17,100	202	3.2	1.25	(a)	2,940	(a)
161	C	17,100	222	3.1	1.23	.64	2,840	.44

[a]Value could not be accurately determined.

TABLE VII.- STATIC TORSIONAL-ELASTICITY TEST DATA

Run	Test series	Tire A				Tire B			
		$\bar{F}_z$, lb	p, lb/sq in.	δ_o, in.	$K_{\alpha,n}$, lb-in./deg	$\bar{F}_z$, lb	p, lb/sq in.	δ_o, in.	$K_{\alpha,n}$, lb-in./deg
162	A	9,000	122	2.3	1,400	9,000	122	2.4	1,560
163	A	9,000	125	2.4	1,320	9,000	127	2.4	1,480
164	A	9,000	142	2.0	1,400	9,000	142	2.0	1,430
165	A	9,000	162	1.8	1,250	9,000	162	1.9	1,500
166	A	9,000	162	1.8	1,660	9,000	162	1.9	(a)
167	A	9,000	162	1.9	1,480	9,000	162	1.9	1,280
168	A	9,000	162	1.9	1,300	9,000	162	1.9	1,190
169	A	9,000	184	1.8	1,670	9,000	184	1.8	1,510
170	A	9,000	182	1.8	1,470	9,000	182	1.8	1,180
171	A	9,000	202	1.7	1,410	9,000	199	1.8	1,340
172	A	9,000	202	1.7	1,640	9,000	197	1.8	1,410
173	C	16,900	160	3.8	(a)	17,200	161	3.7	2,450
174	C	16,900	183	3.5	2,790	17,200	183	3.3	1,970
175	C	16,900	203	3.1	2,960	17,200	204	3.1	2,570
176	C	16,900	228	3.0	2,780	17,200	227	3.0	1,790

[a]Value could not be accurately determined.

TABLE VIII.- TIRE FOOTPRINT DATA

[Runs 177 to 192 were obtained before test series A; runs 193 to 194 were obtained after test series C]

Run	p_o, lb/sq in.	p, lb/sq in.	F_z, lb	δ_o, in.	A_g, $in.^2$	A_n, $in.^2$	b, in.	2h, in.
Tire A								
177	(a)	111	9,000	2.35	69.1	51.9	5.7	13.1
178	(a)	142	9,000	2.08	62.3	47.6	5.7	12.3
179	(a)	207	9,000	1.62	49.5	36.7	5.7	10.6
Tire B								
180	(a)	103	9,000	2.55	75.0	56.6	5.9	13.6
181	(a)	123	9,000	2.22	69.1	52.2	5.9	12.8
182	(a)	143	9,000	1.94	62.5	47.9	5.9	12.1
183	159	(a)	(a)	.15	6.2	3.4	1.9	3.5
184	159	(a)	(a)	.30	9.0	5.1	2.2	4.6
185	159	(a)	(a)	.52	13.7	9.0	2.9	5.6
186	159	(a)	(a)	.87	24.7	16.9	4.1	7.5
187	159	(a)	(a)	1.20	35.7	25.7	4.9	9.0
188	159	(a)	(a)	1.36	41.3	30.5	5.3	9.6
189	(a)	167	9,000	1.90	58.0	44.2	5.8	11.6
190	(a)	167	9,000	1.78	57.0	43.6	5.8	11.3
191	(a)	187	9,000	1.64	53.2	40.2	5.8	10.8
192	(a)	209	9,000	1.42	49.2	37.4	5.8	10.4
193	(a)	162	17,200	3.60	93.3	80.5	6.8	14.8
194	(a)	182	17,200	3.40	88.8	75.2	6.5	14.4

[a]Value not available.

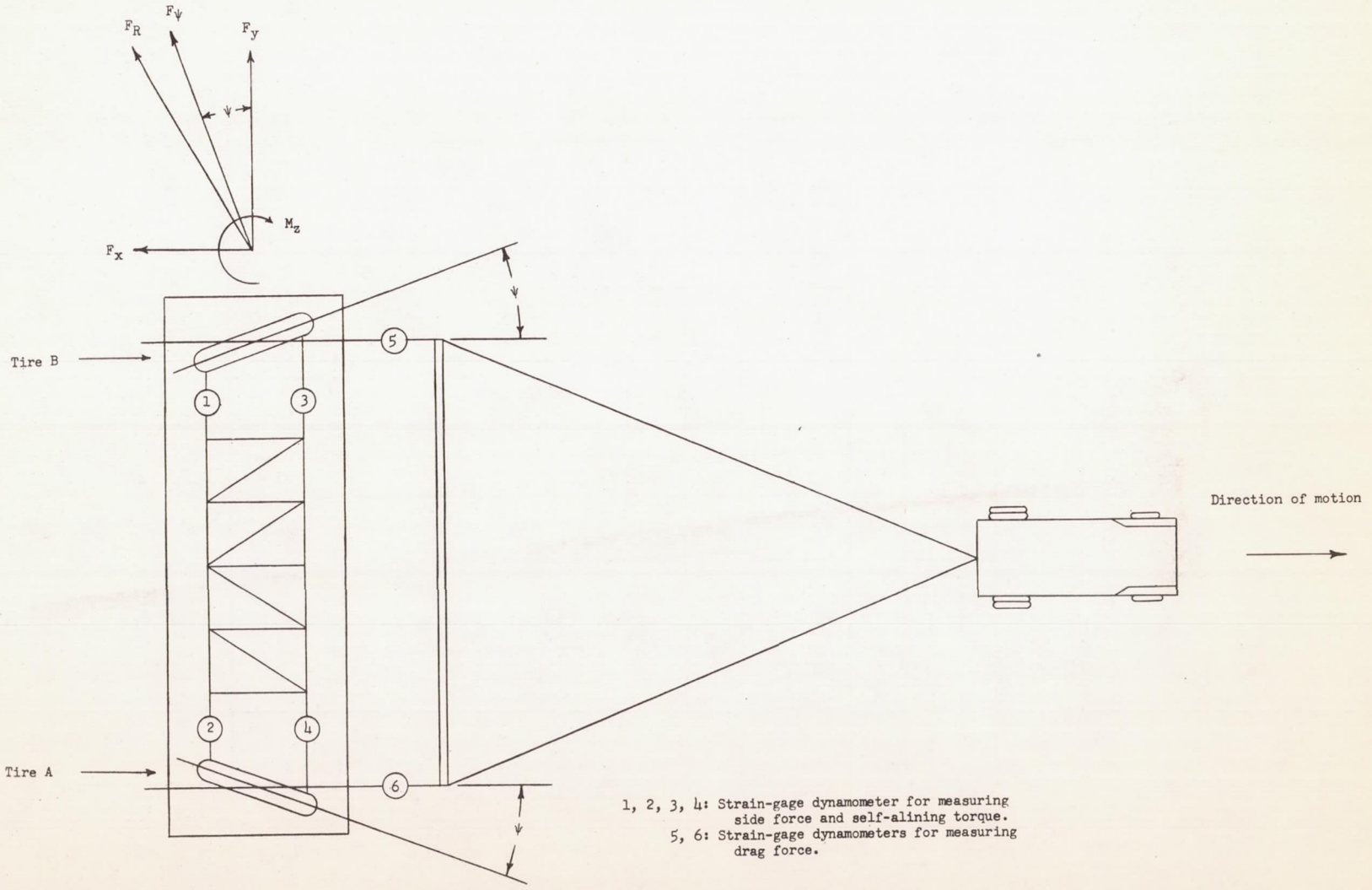

Figure 1.- Sketch of test vehicle.

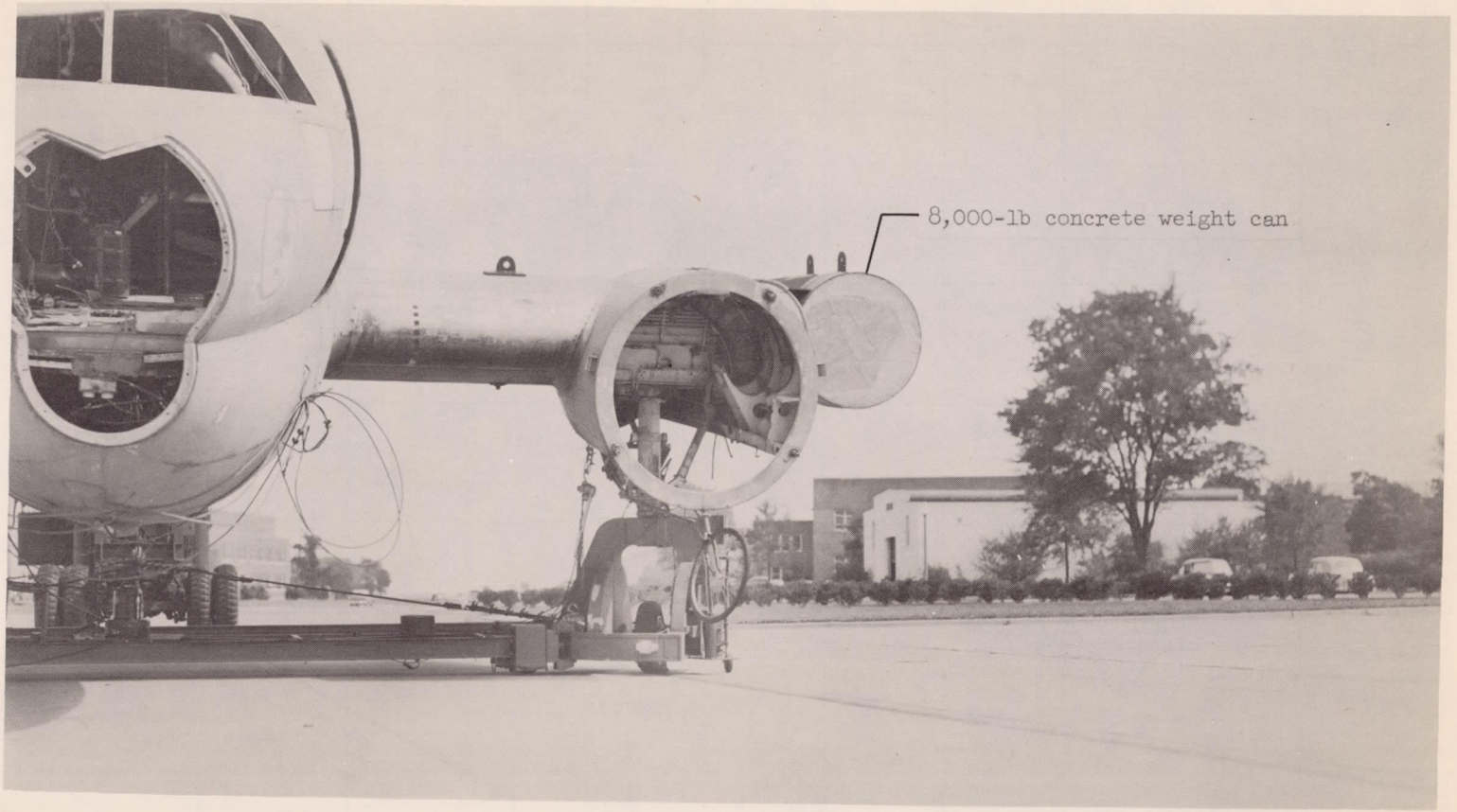

L-86021.1

Figure 2.- View of test vehicle at heavy-weight condition.

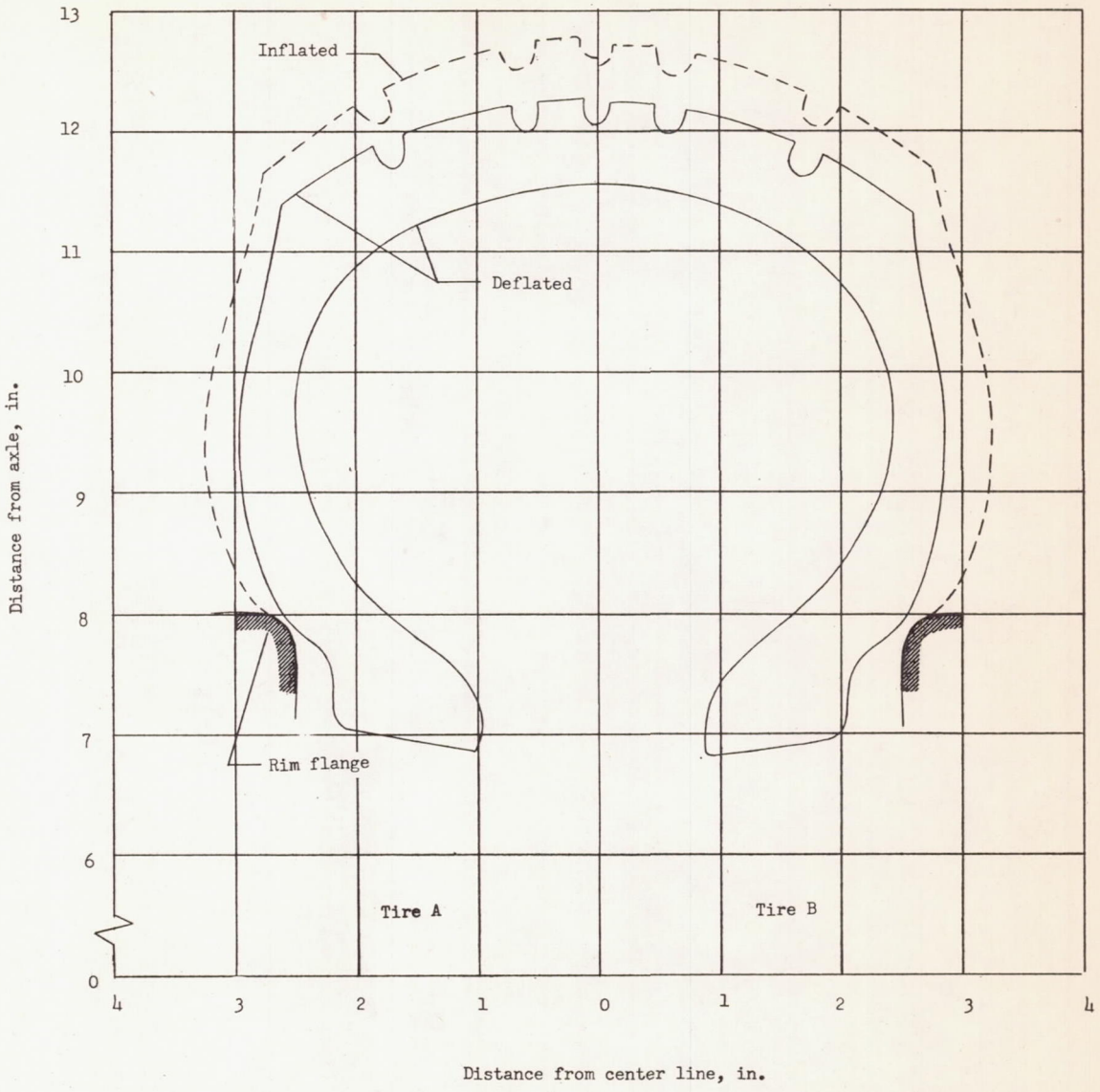

Figure 3.- Tire profiles.

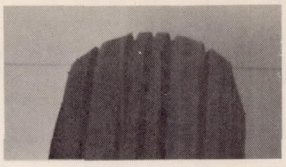

(a) Tread shape of tire A and B at beginning of test series A.

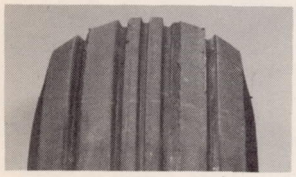

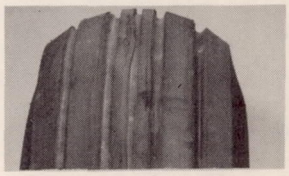

(b) At conclusion of test series A.

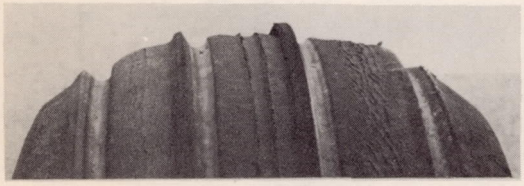

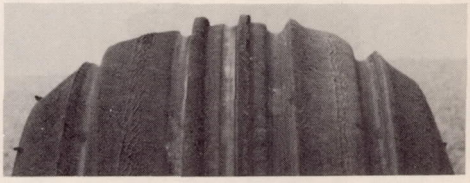

(c) At conclusion of test series B.

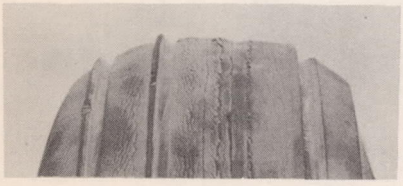

L-90525

(d) At conclusion of test series C.

Tire B

(e) Test series D.

Tire A

Figure 4.- Tire wear.

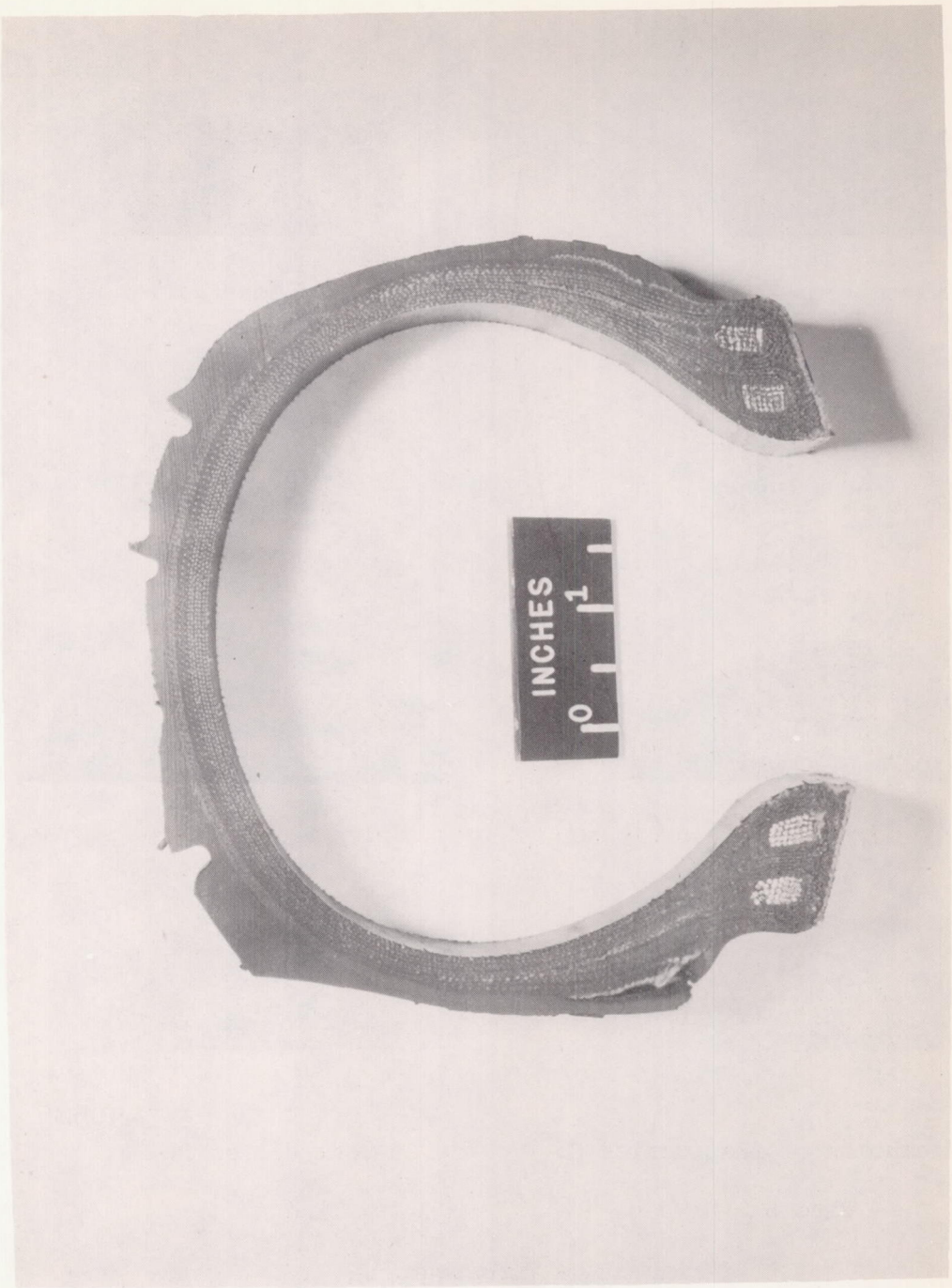

L-90722

(f) Cross section of tire B.

Figure 4.- Concluded.

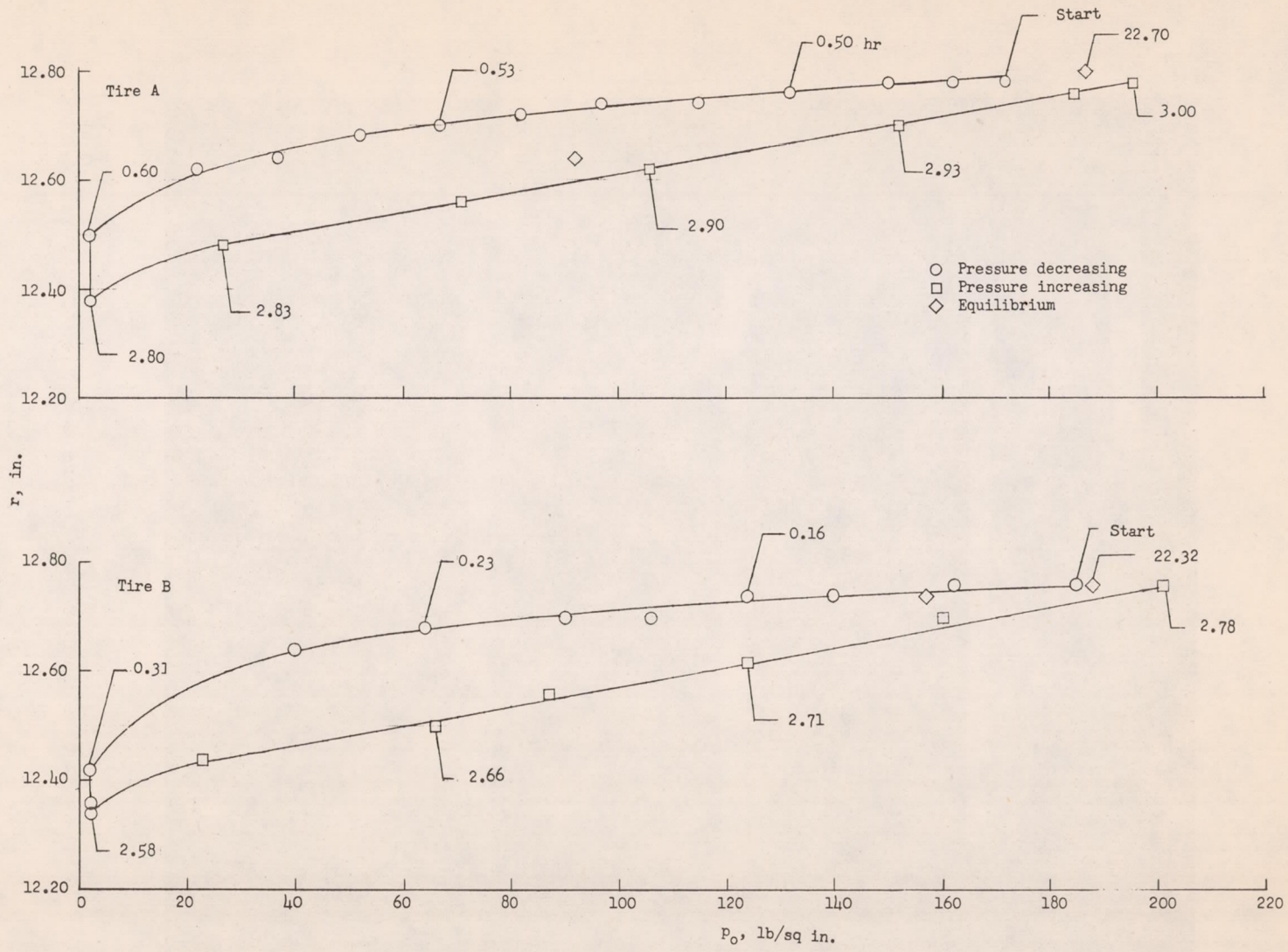

Figure 5.- Radius-pressure hysteresis loop for tires A and B (unloaded).

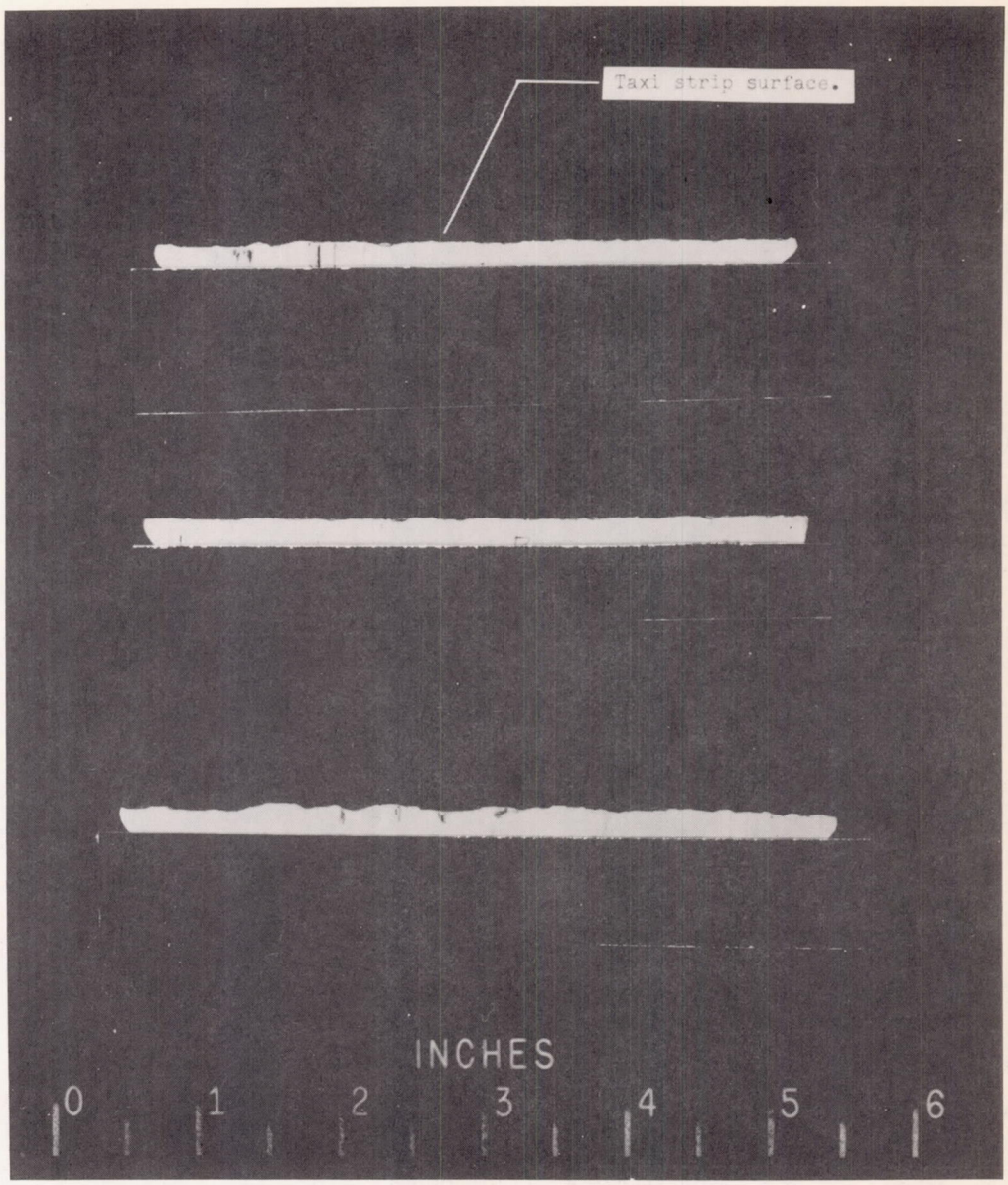

L-84422.1

Figure 6.- Representative samples of concrete-taxi-strip surface roughness.

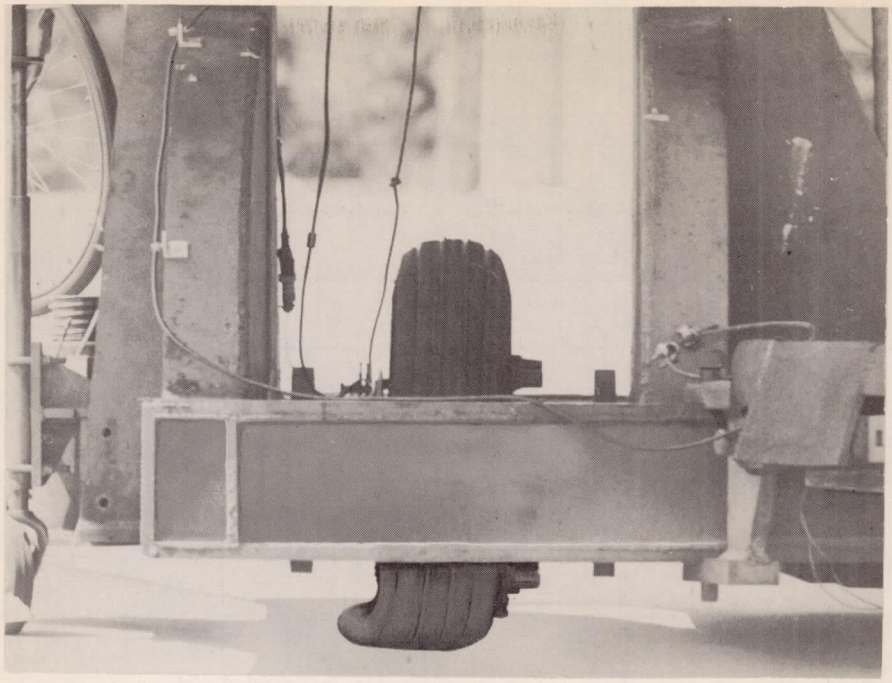

(a) Front view.

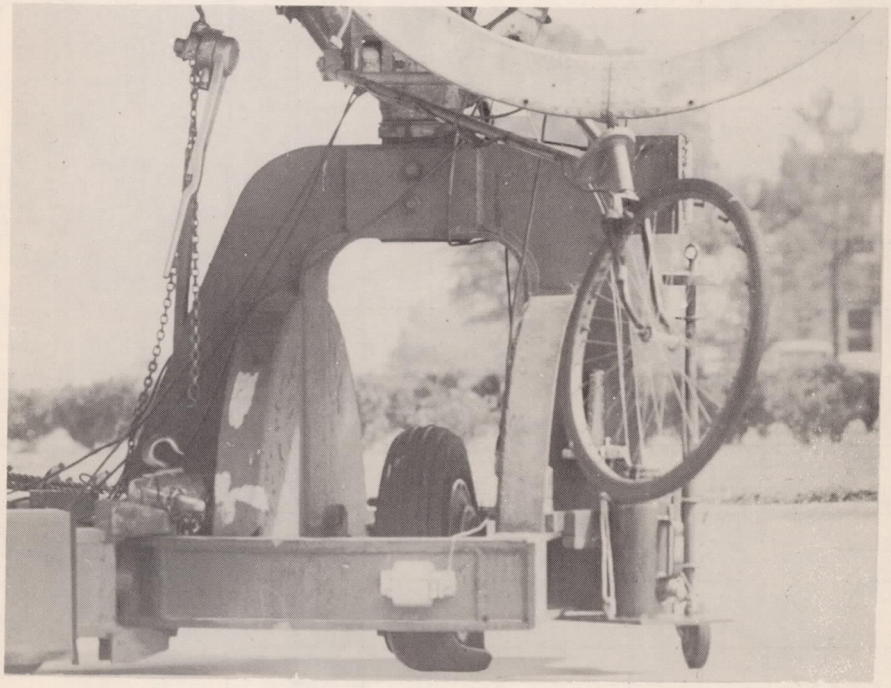

(b) Rear view.

L-90526

Figure 7.- Tire A under yawed rolling at $\psi = 24.5^{\circ}$.

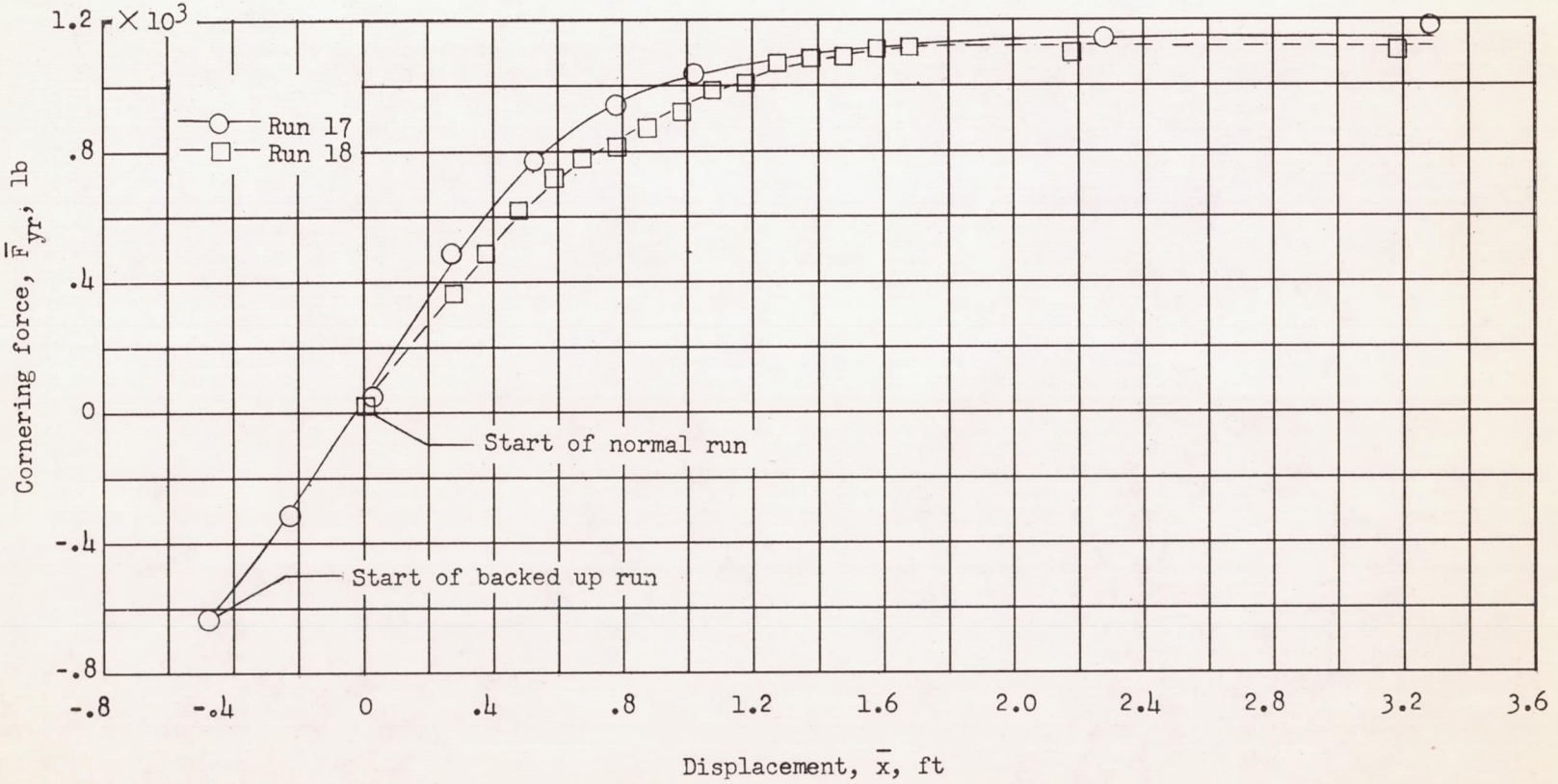

Figure 8.- Comparison of buildup of cornering force with distance rolled for a normal run and for a run where the test vehicle was backed up before starting. Test series A: $\bar{F}_Z$ = 9,000 pounds; $\bar{p} \approx 163$ pounds per square inch; $\bar{\delta}_o \approx 2.1$ inches.

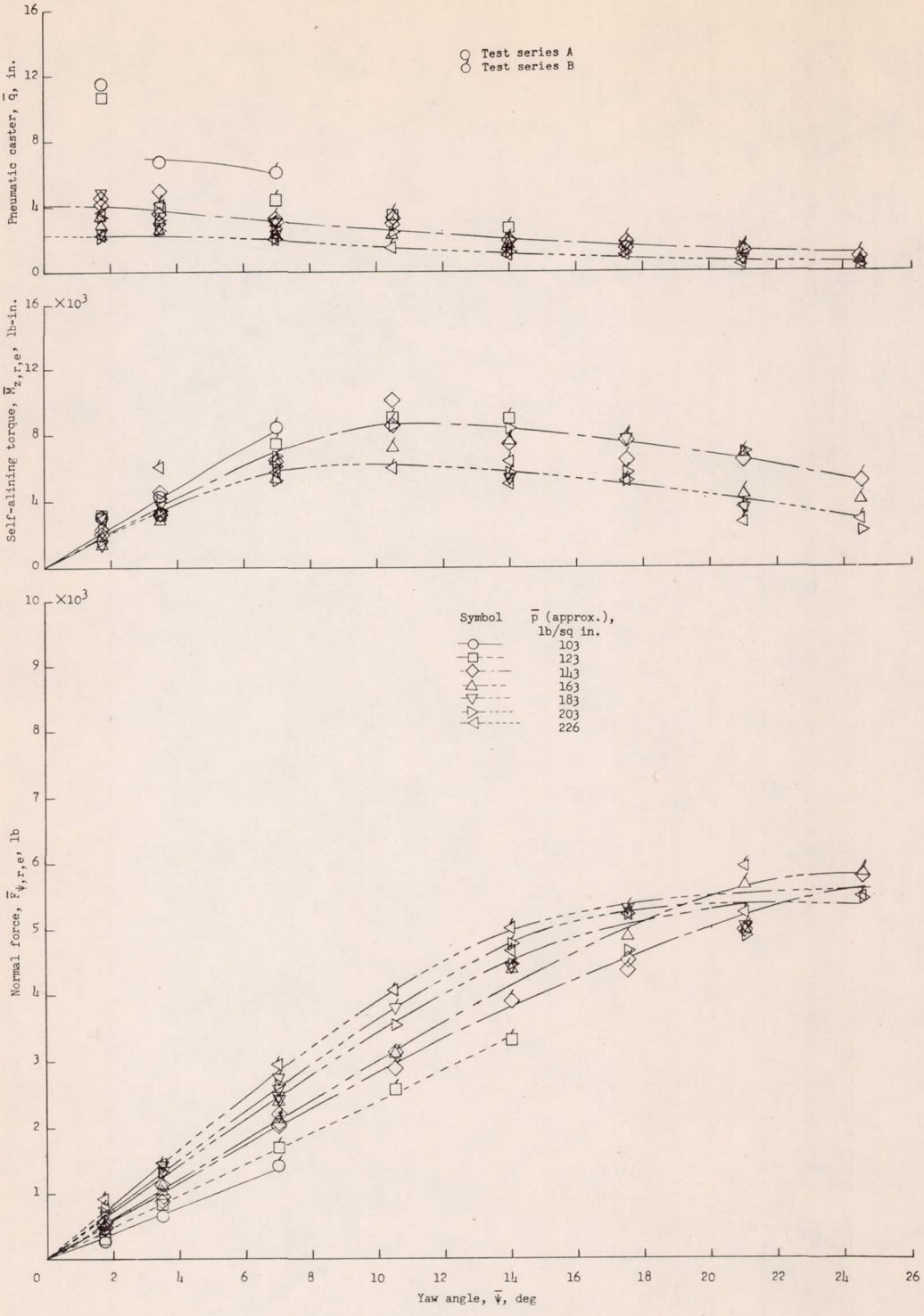

Figure 9.- Variation of normal force, self-alining torque, and pneumatic caster with yaw angle for the different inflation pressures investigated at $\bar{F}_Z$ = 9,000 pounds. Test series A and B.

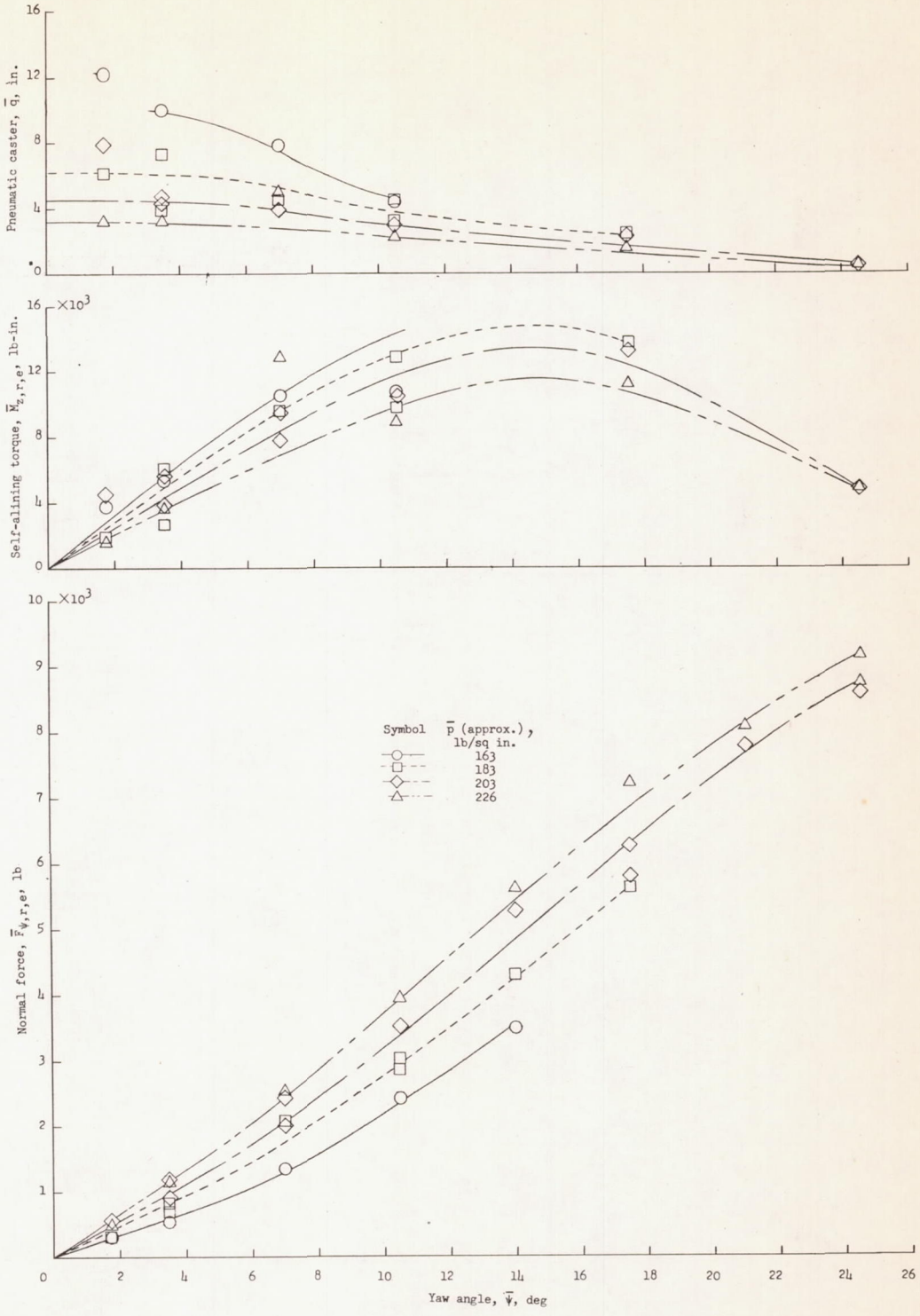

Figure 10.- Variation of normal force, self-alining torque and pneumatic caster with yaw angle for the different inflation pressures investigated at $\bar{F}_Z$ = 17,000 pounds. Test series C.

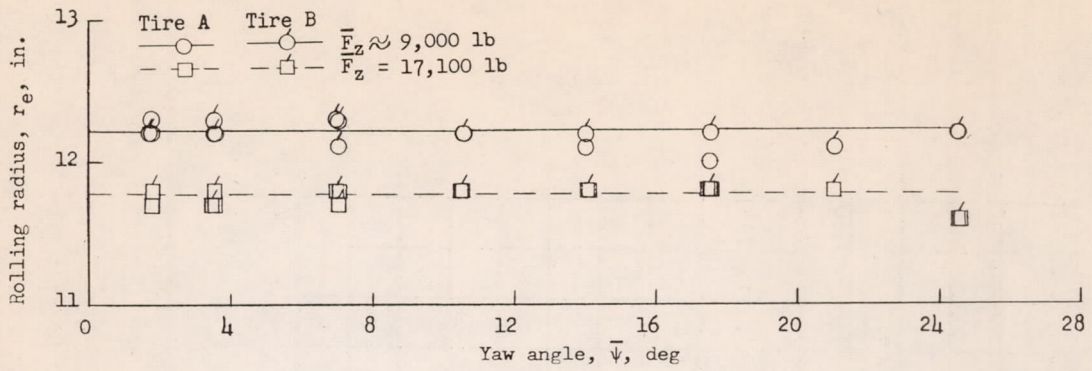

(a) Variation of rolling radius with yaw angle for $\bar{p} \approx 203$ pounds per square inch.

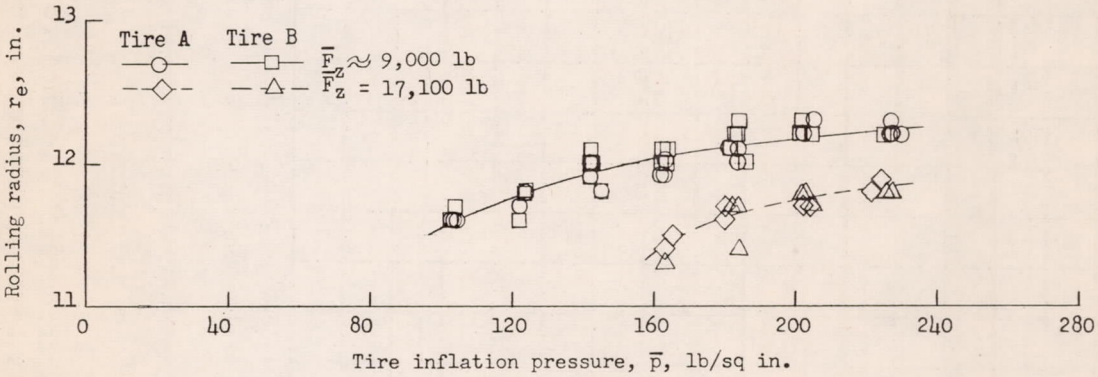

(b) Variation of rolling radius with inflation pressure for $\bar{\psi} = 1.75^\circ$ and 3.5°.

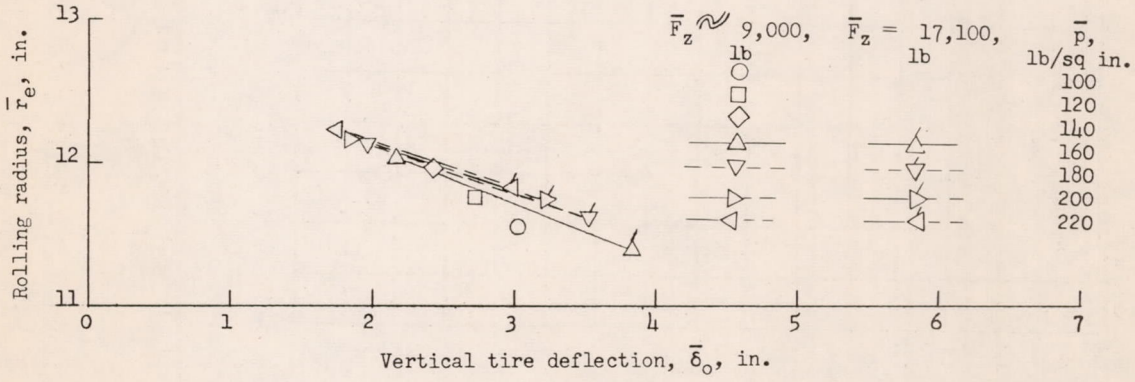

(c) Variation of rolling radius with vertical tire deflection for several constant inflation pressures. (Data obtained from faired curves in figures 11(b) and 17.)

Figure 11.- Variation of rolling radius with yaw angle, inflation pressure, and vertical tire deflection.

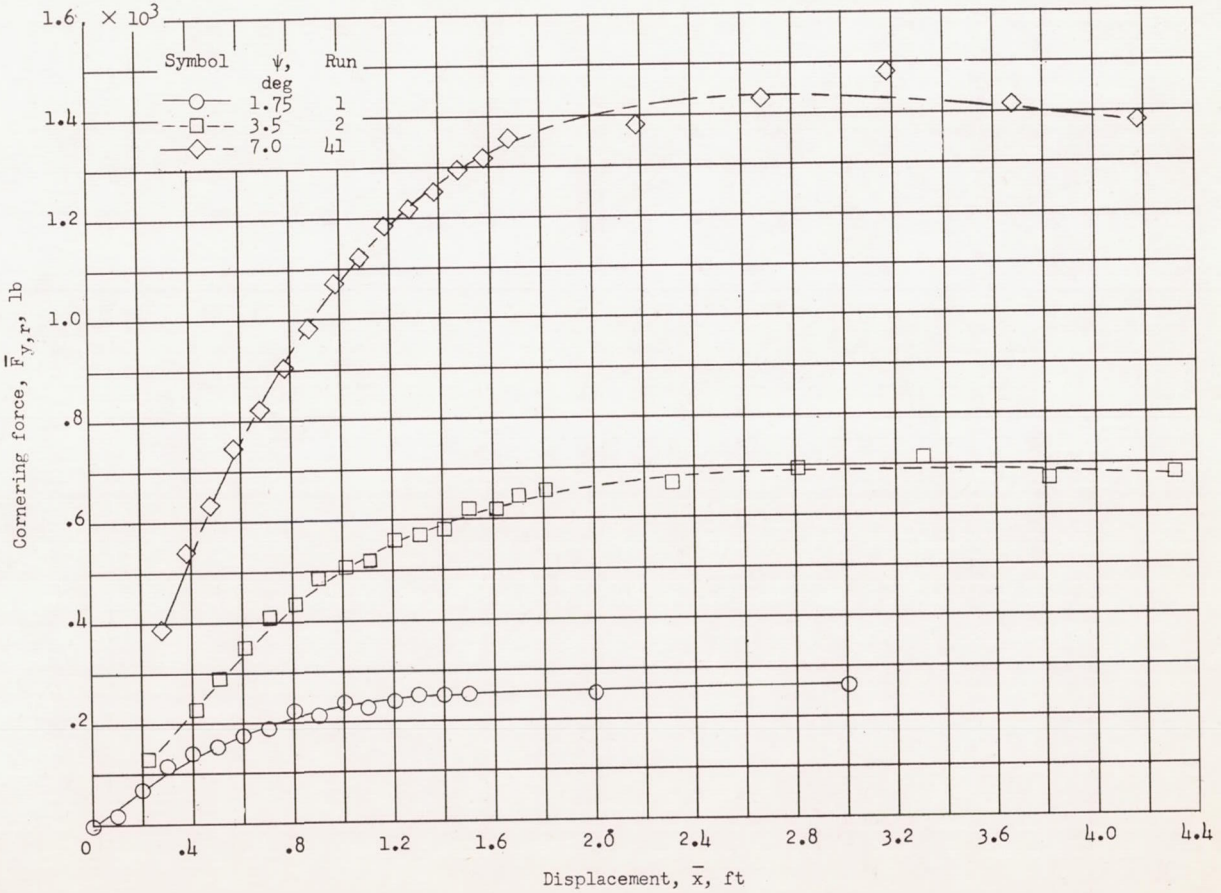

(a) Test series A and B: $\bar{F}_Z \approx 9{,}000$ pounds; $\bar{p} \approx 103$ pounds per square inch; $\bar{\delta}_o \approx 3.0$ inches.

Figure 12.- Buildup of cornering force with distance rolled for some typical runs at several pressures.

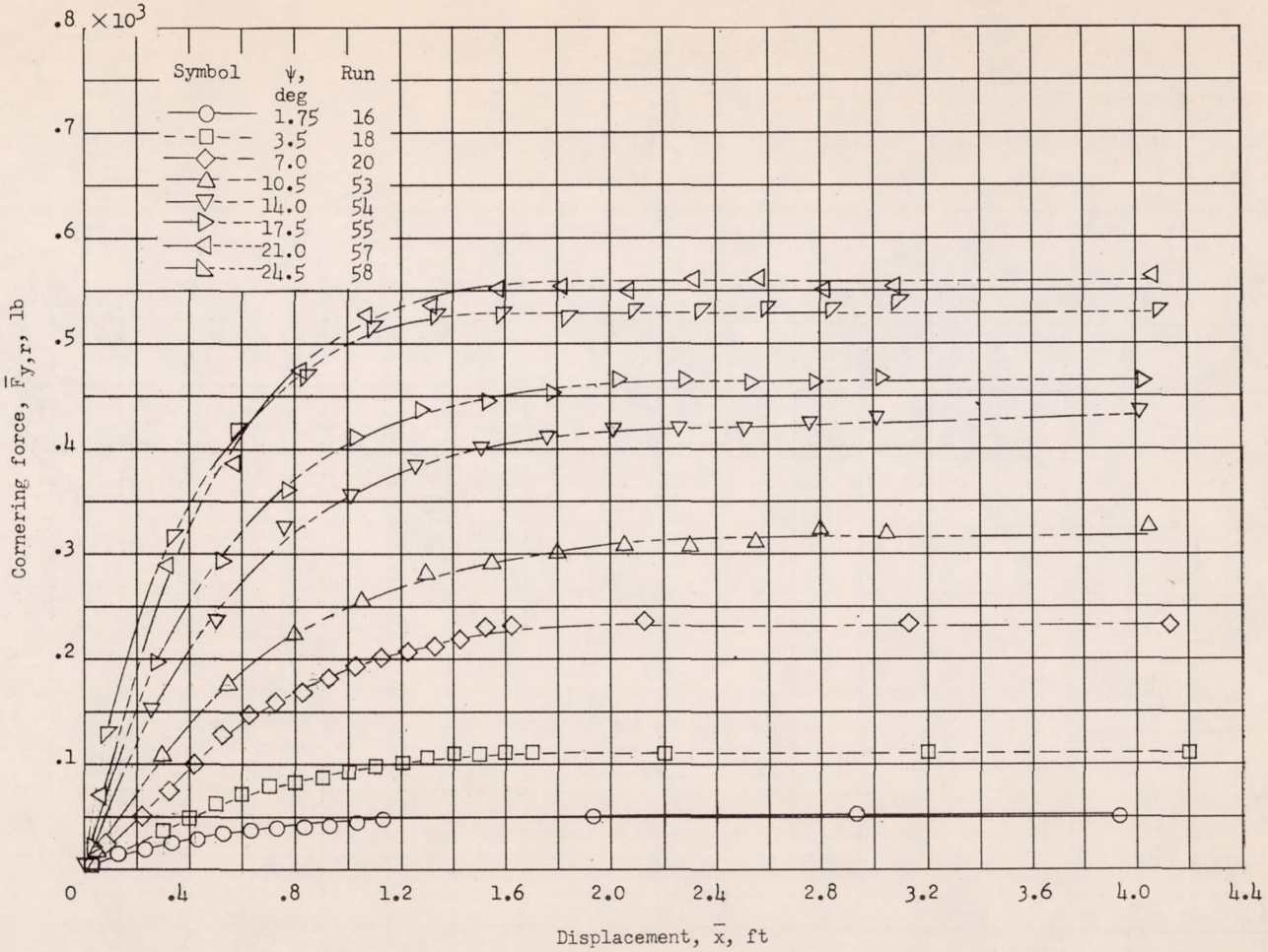

(b) Test series A and B: $\bar{F}_z \approx 9{,}000$ pounds; $\bar{p} \approx 163$ pounds per square inch; $\bar{\delta}_o \approx 2.1$ inches.

Figure 12.- Continued.

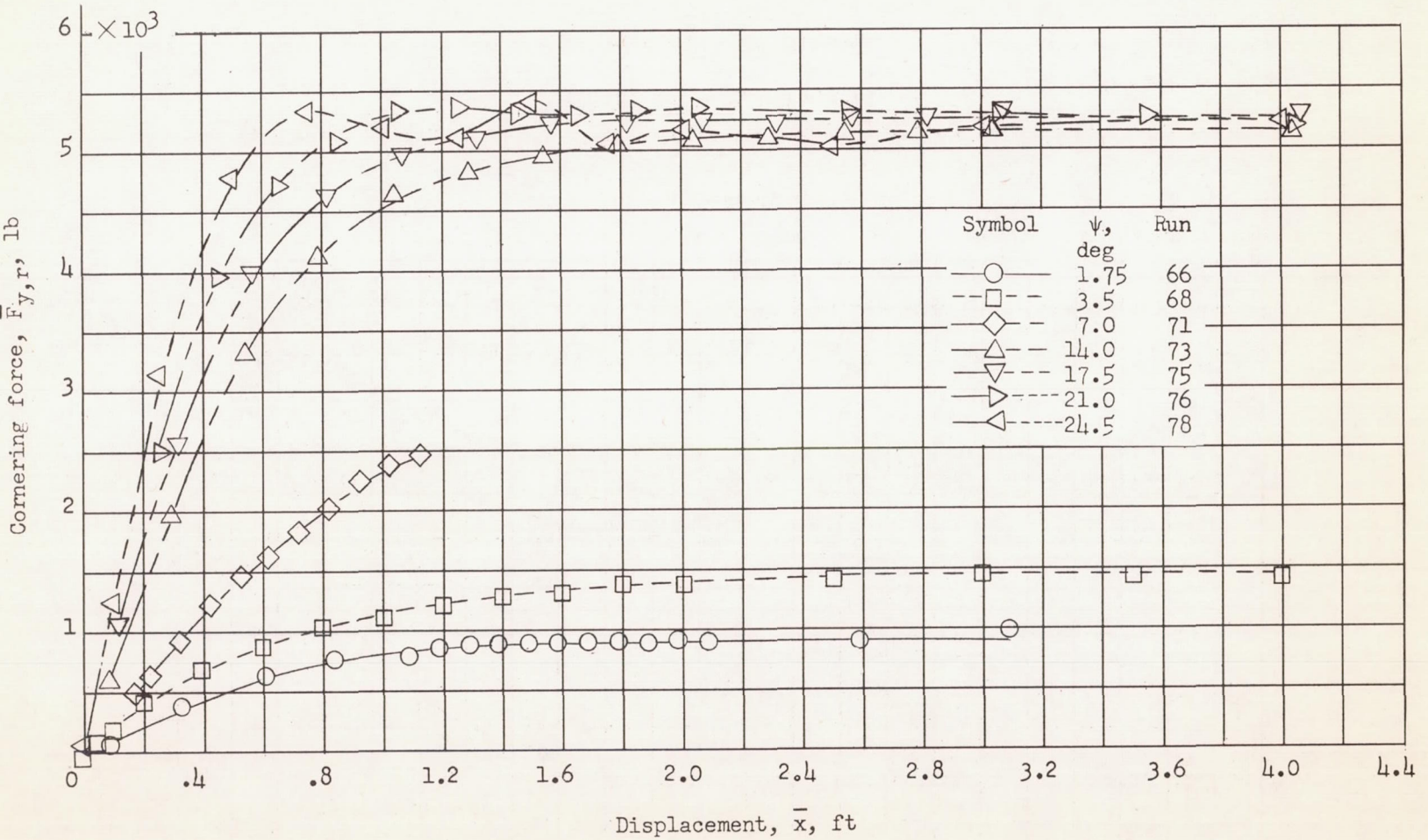

(c) Test series B: $\bar{F}_Z$ = 9,100 pounds; $\bar{p} \approx 226$ pounds per square inch; $\bar{\delta}_o \approx 1.7$ inches.

Figure 12.- Continued.

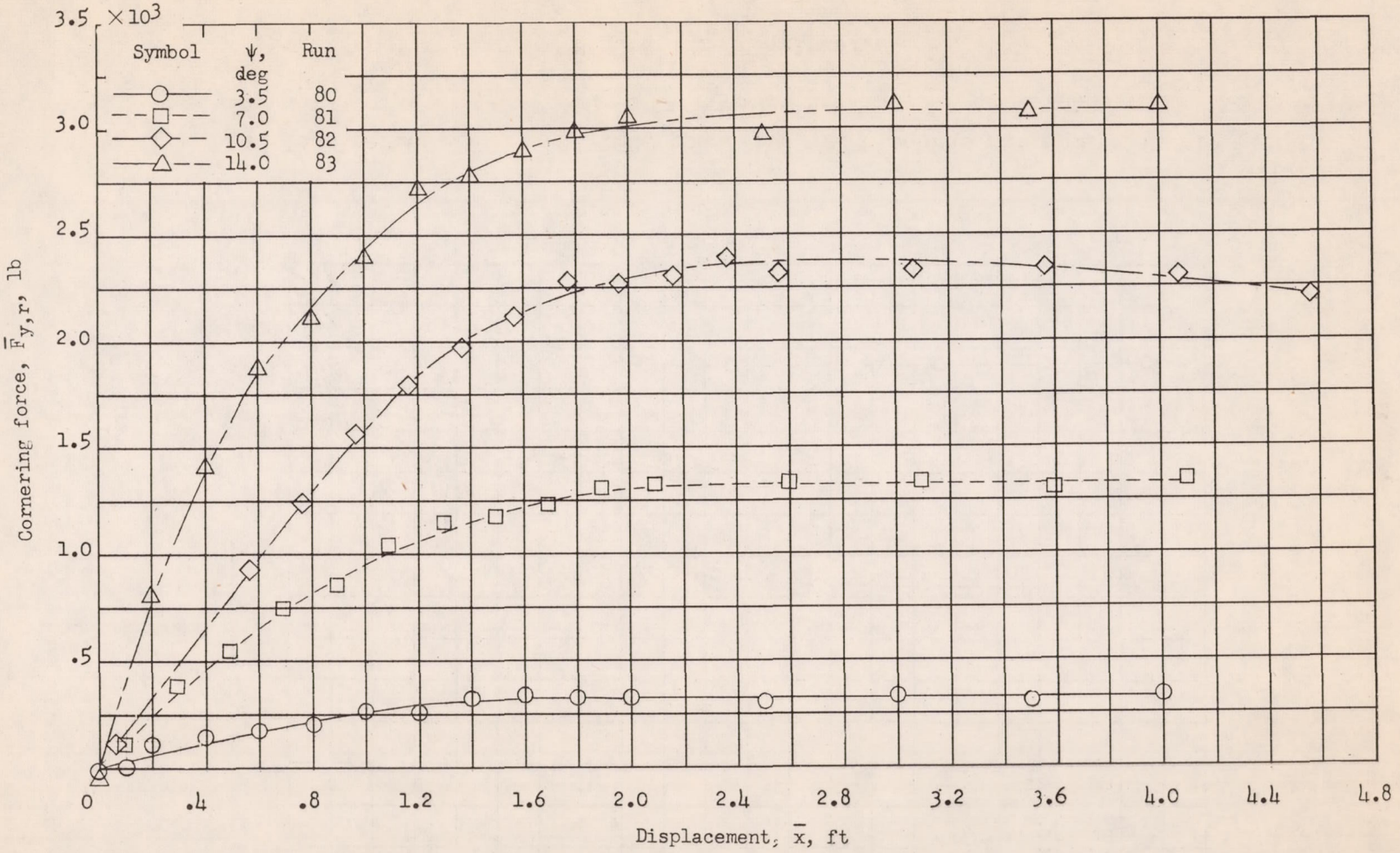

(d) Test series C: $\bar{F}_Z \approx 17{,}100$ pounds; $\bar{p} \approx 163$ pounds per square inch; $\bar{\delta}_o \approx 3.8$ inches.

Figure 12.- Continued.

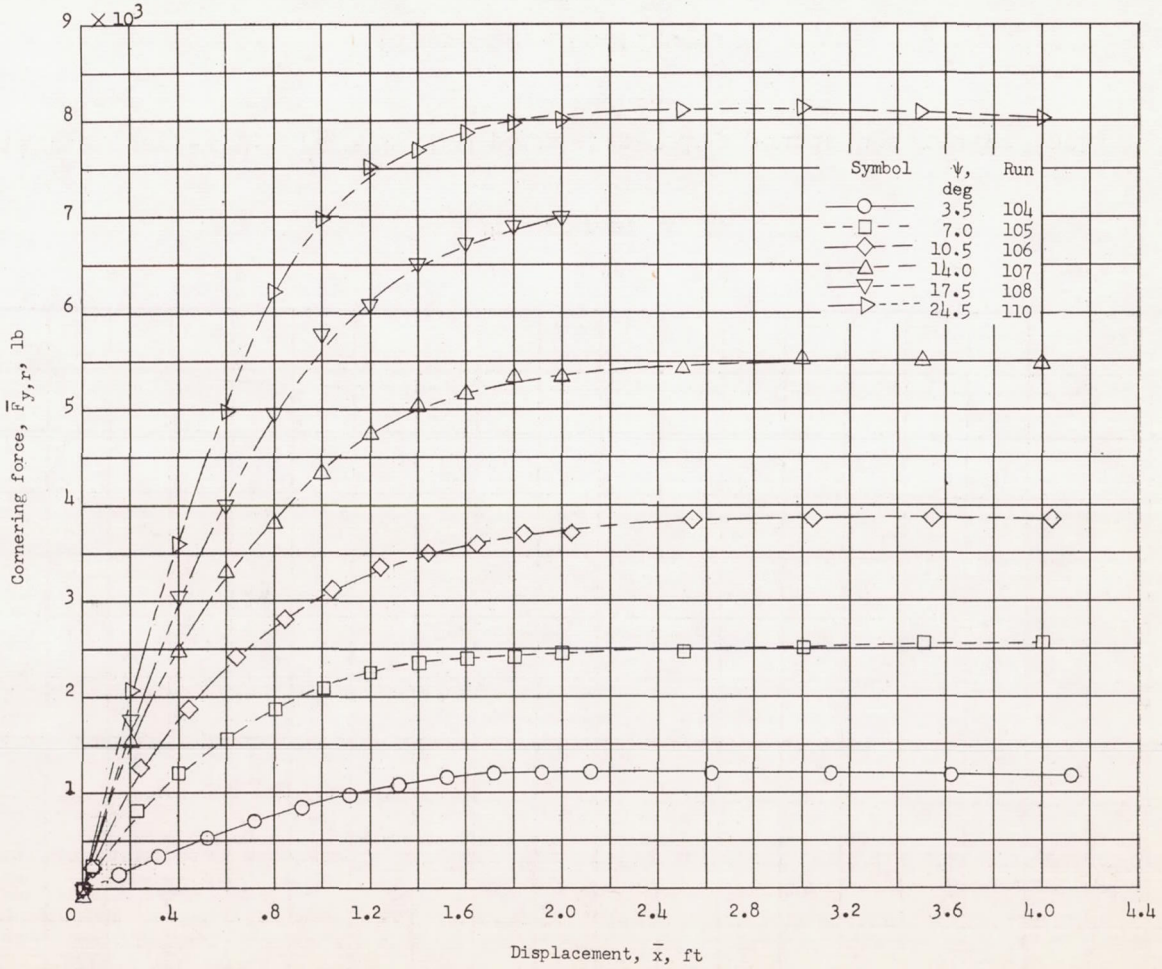

(e) Test series C: $\bar{F}_Z \approx 17{,}100$ pounds; $\bar{p} \approx 226$ pounds per square inch; $\bar{\delta}_o \approx 2.9$ inches.

Figure 12.- Concluded.

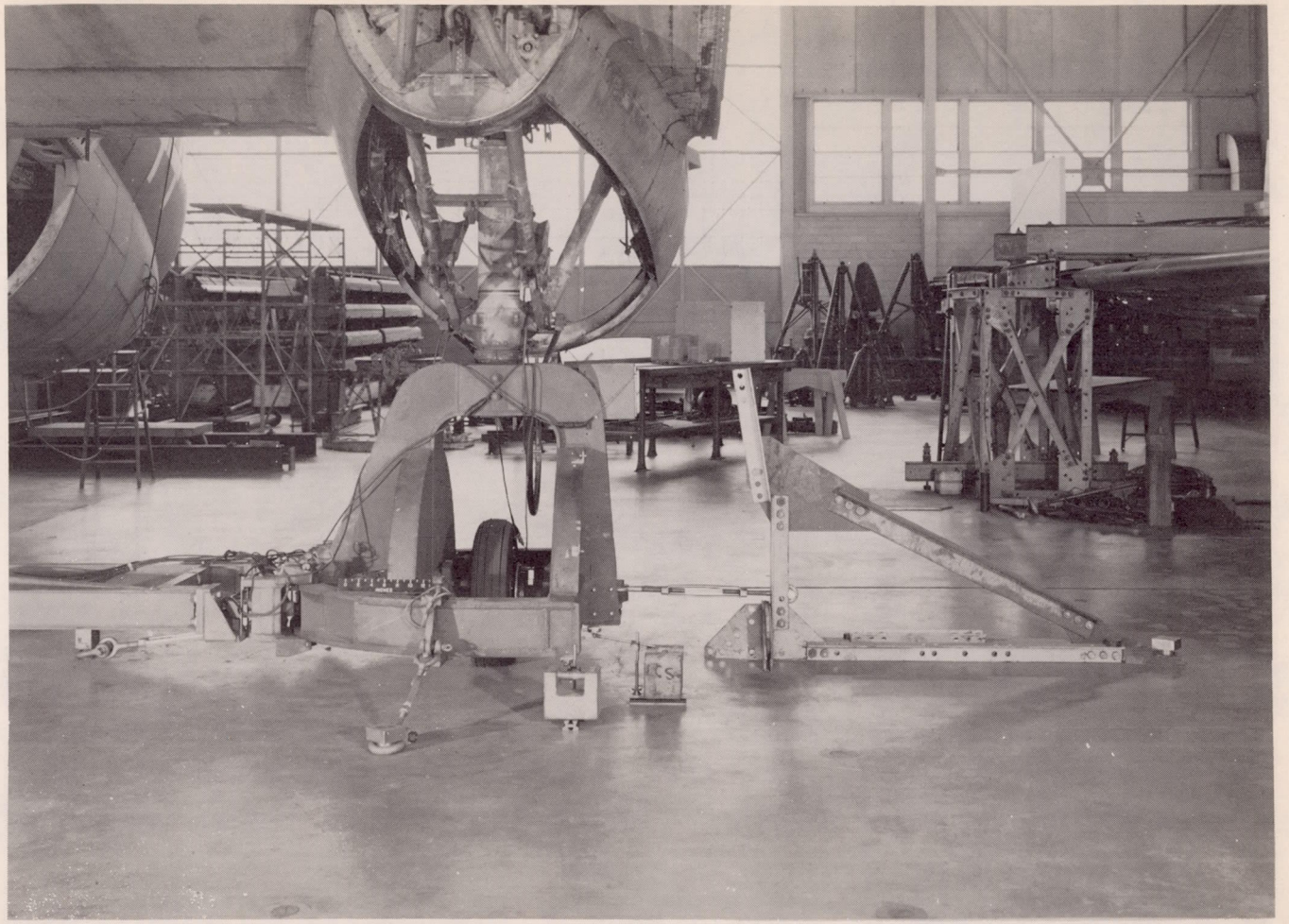

L-86825

(a) View of tie-down fittings anchoring right wheel frame to hanger floor.

Figure 13.- Yawed-curvilinear-rolling test setup.

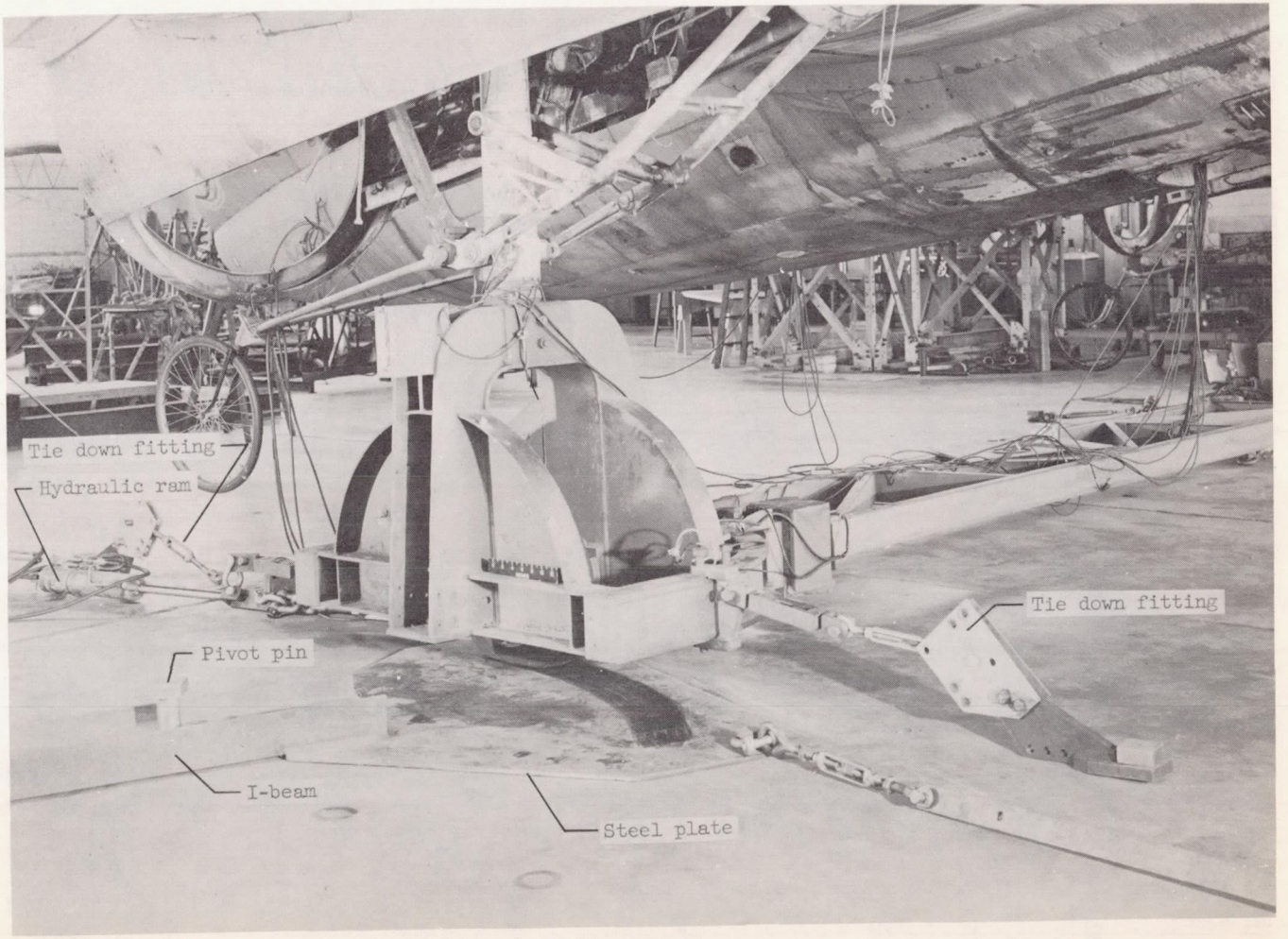

L-86826.1

(b) View of left wheel frame with tire A resting on the steel plate-beam combination used in the yawed-curvilinear rolling test.

Figure 13.- Continued.

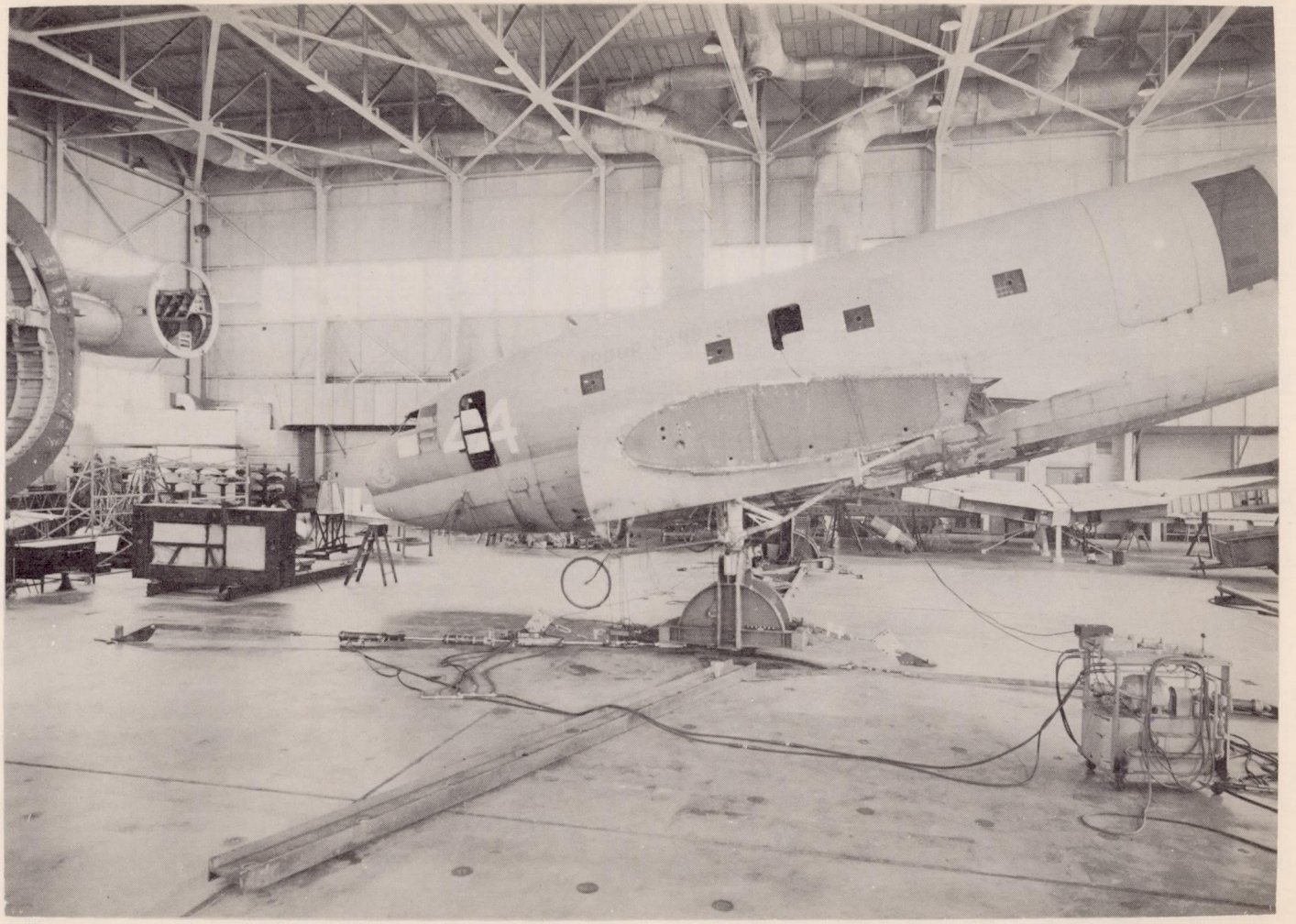

(c) Overall view of test setup. L-86827

Figure 13.- Concluded.

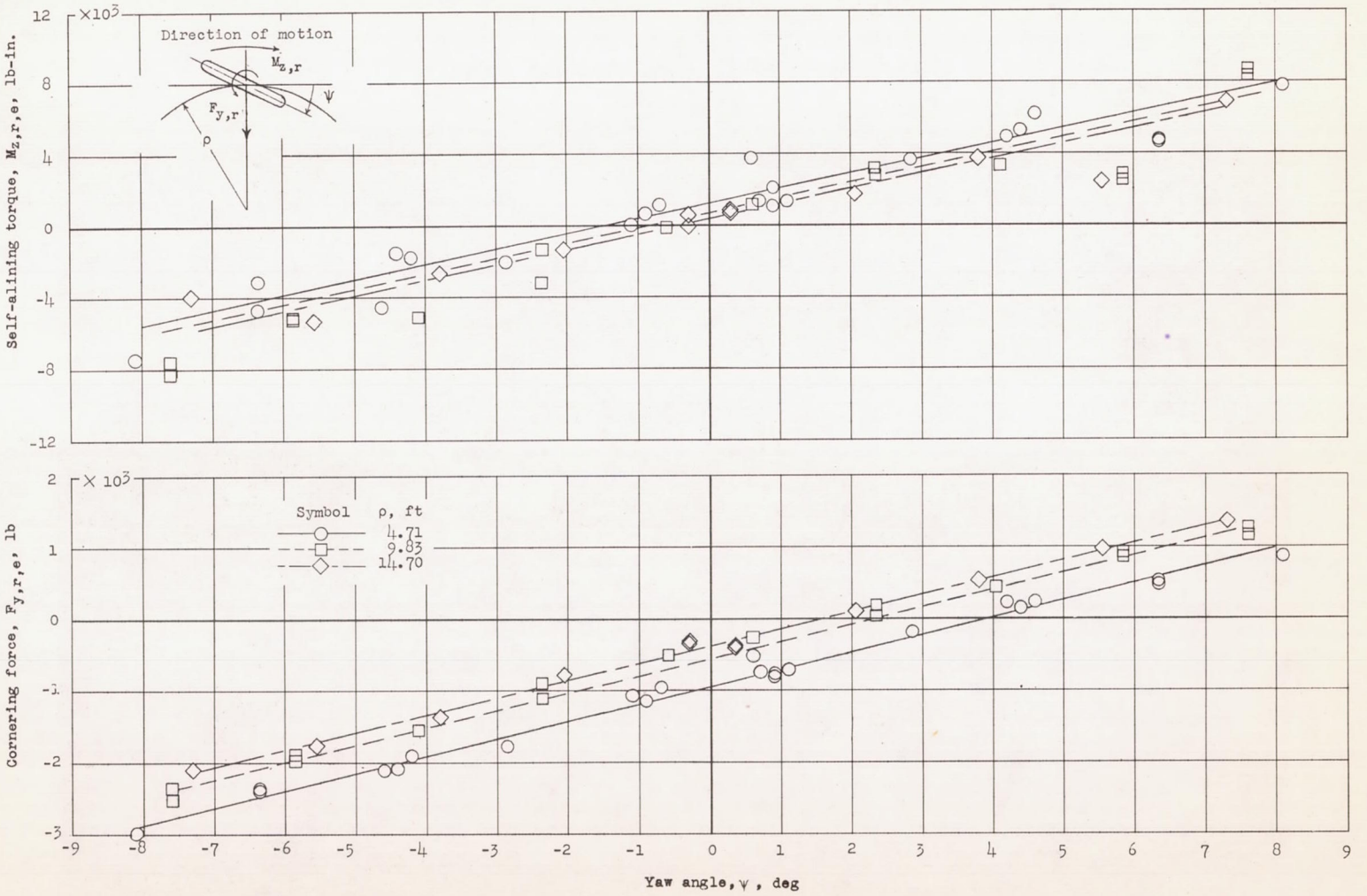

Figure 14.- Variation of cornering force and self-alining torque with yaw angle for three turning radii for tire A at F_Z = 9,000 pounds, p = 134 pounds per square inch, and $\delta_o \approx 2.3$ inches. Test series D.

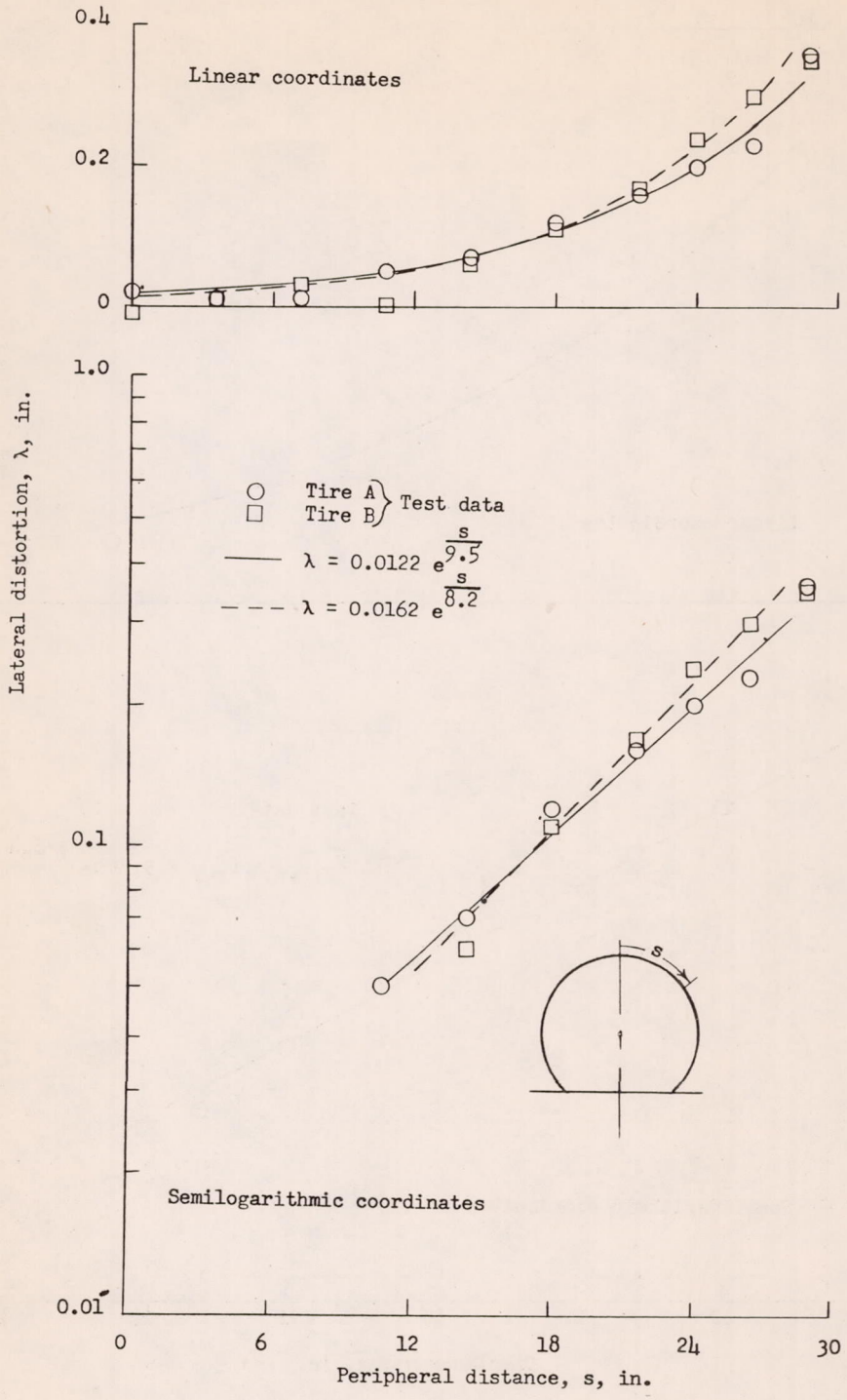

(a) Experimental data used for determining static relaxation length for run 115.

Figure 15.- Sample data obtained from the two methods used to determine relaxation length.

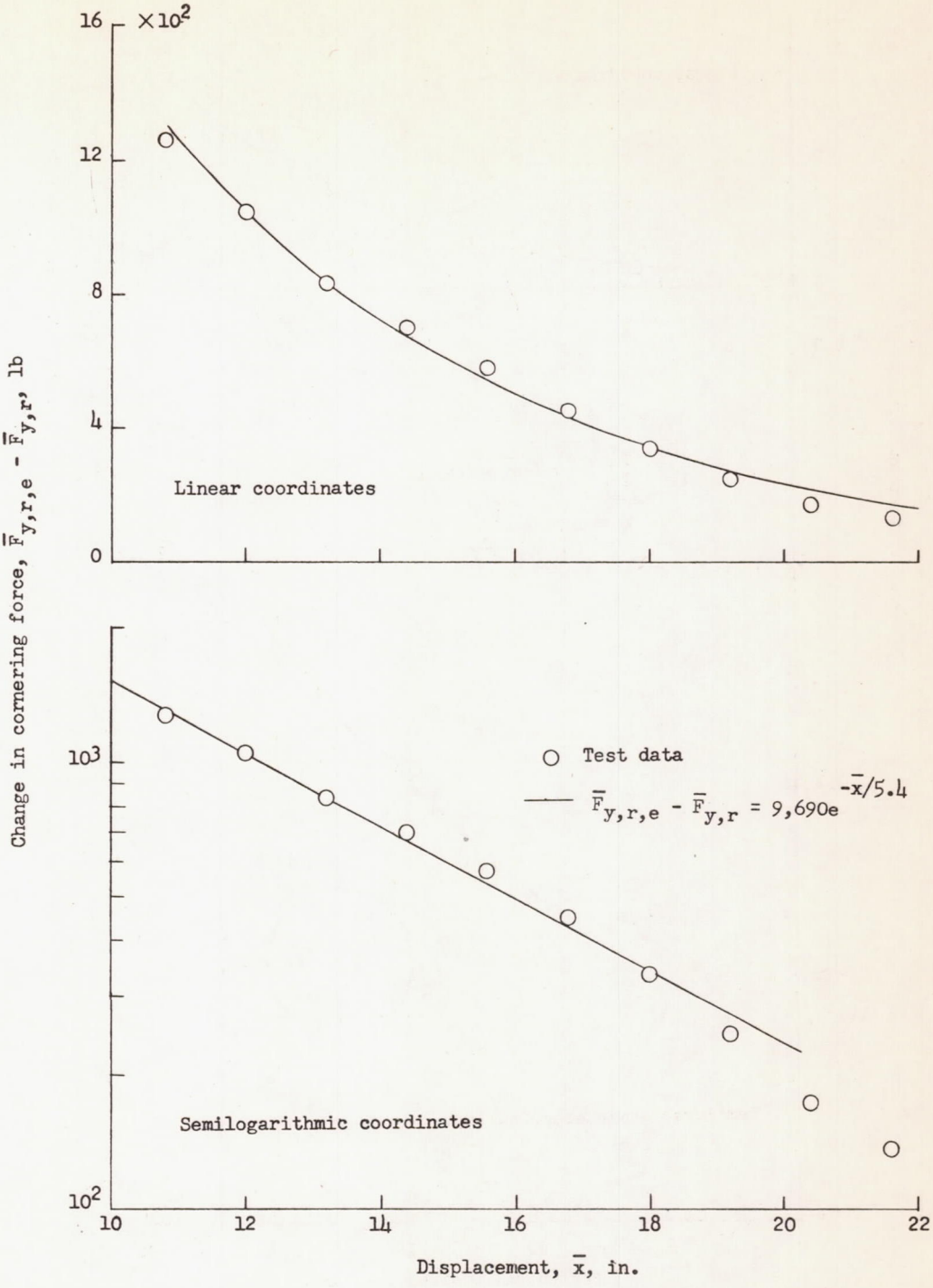

(b) Experimental data used for determining yawed-rolling relaxation length for run 33.

Figure 15.- Concluded.

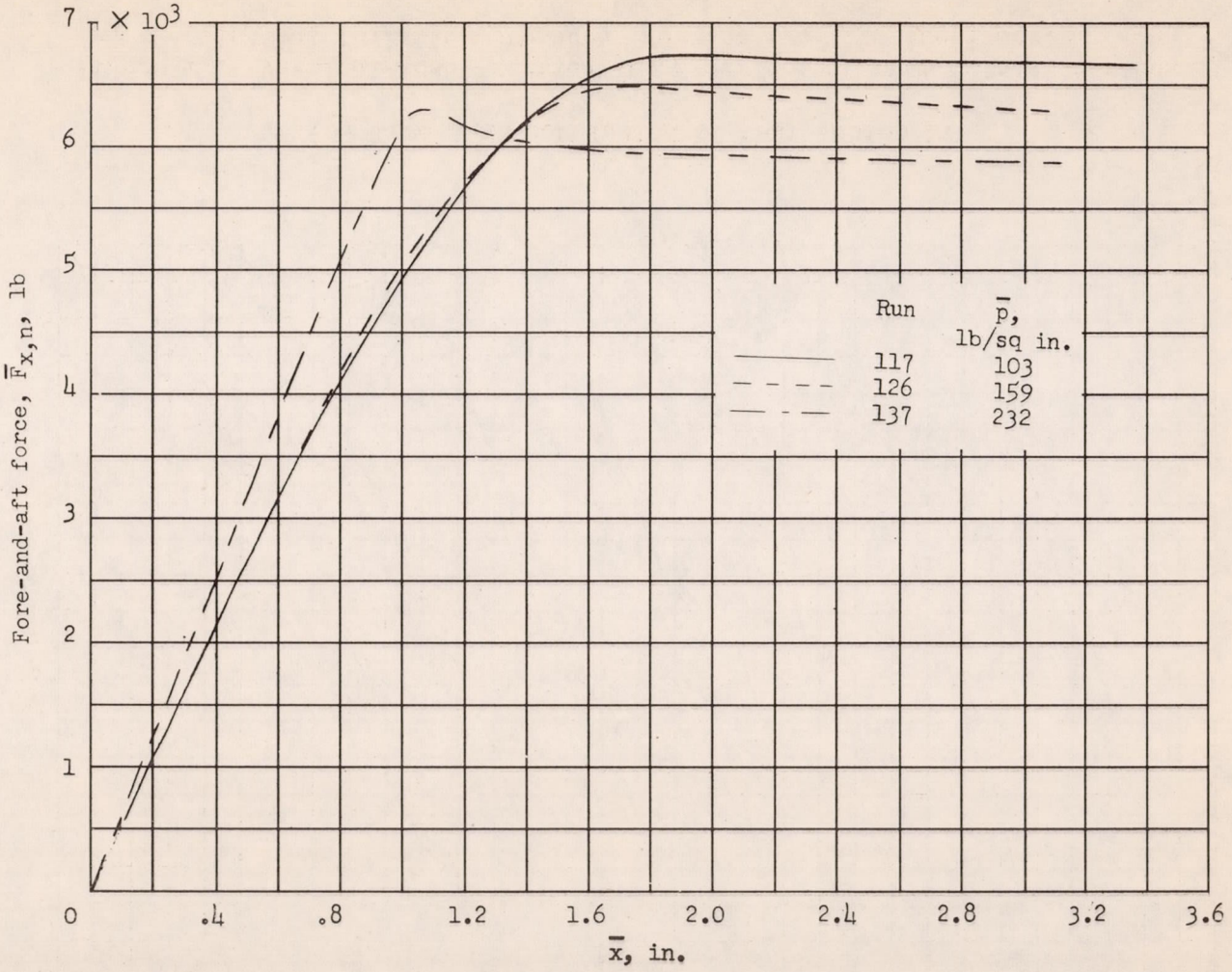

Figure 16.- Drag force buildup with horizontal distance pulled for several typical runs. $\bar{F}_z$ = 9,090 pounds for $\bar{F}_{x,n}$ = 0; $\bar{F}_z \approx$ 8,930 pounds at $\bar{F}_{x,n,m}$ (from locked-wheel drag tests).

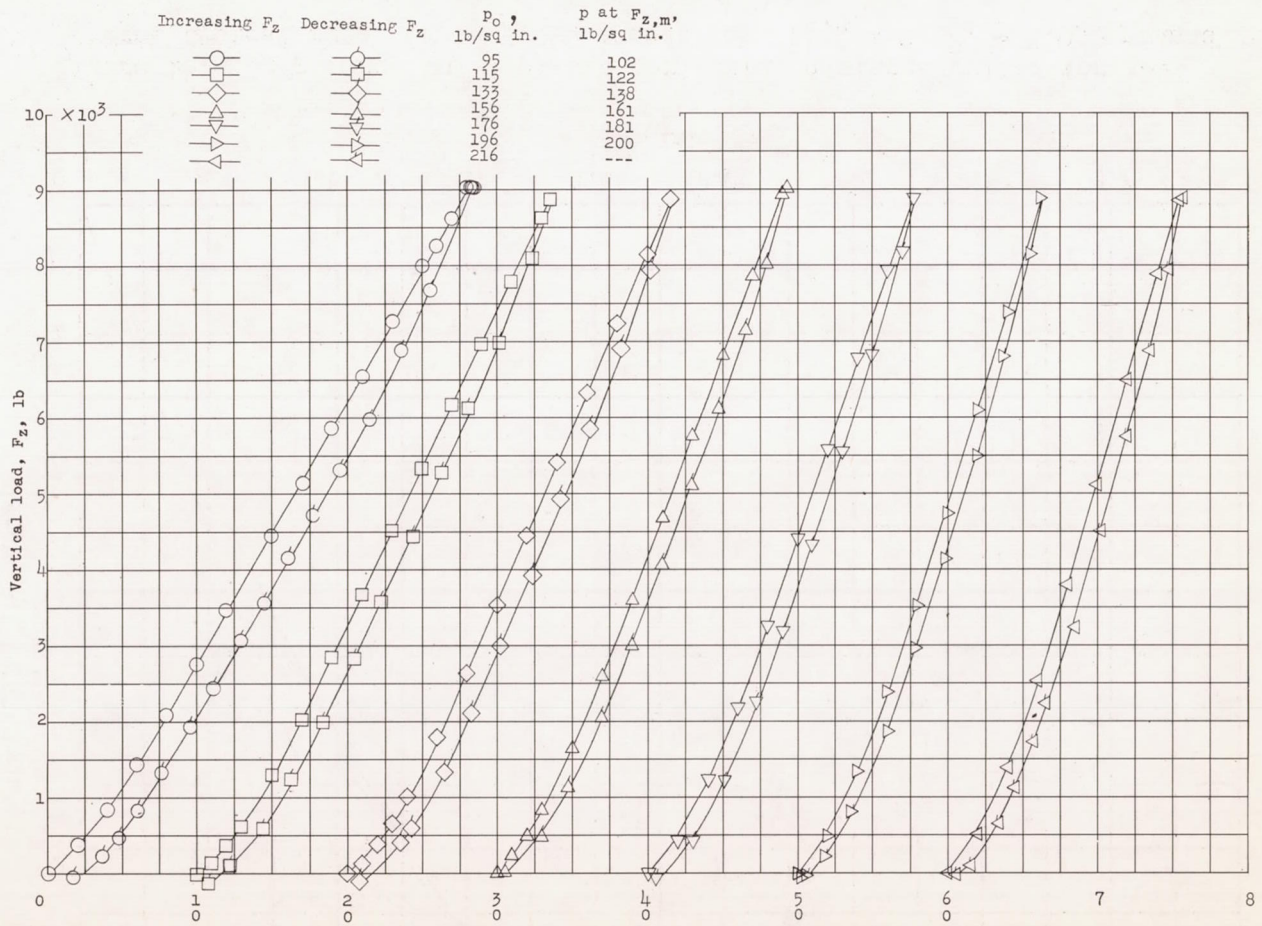

(a) Tire A at conclusion of test series D.

Figure 17.- Vertical-load—vertical-tire-deflection test data at various initial inflation pressures for the two tire specimens.

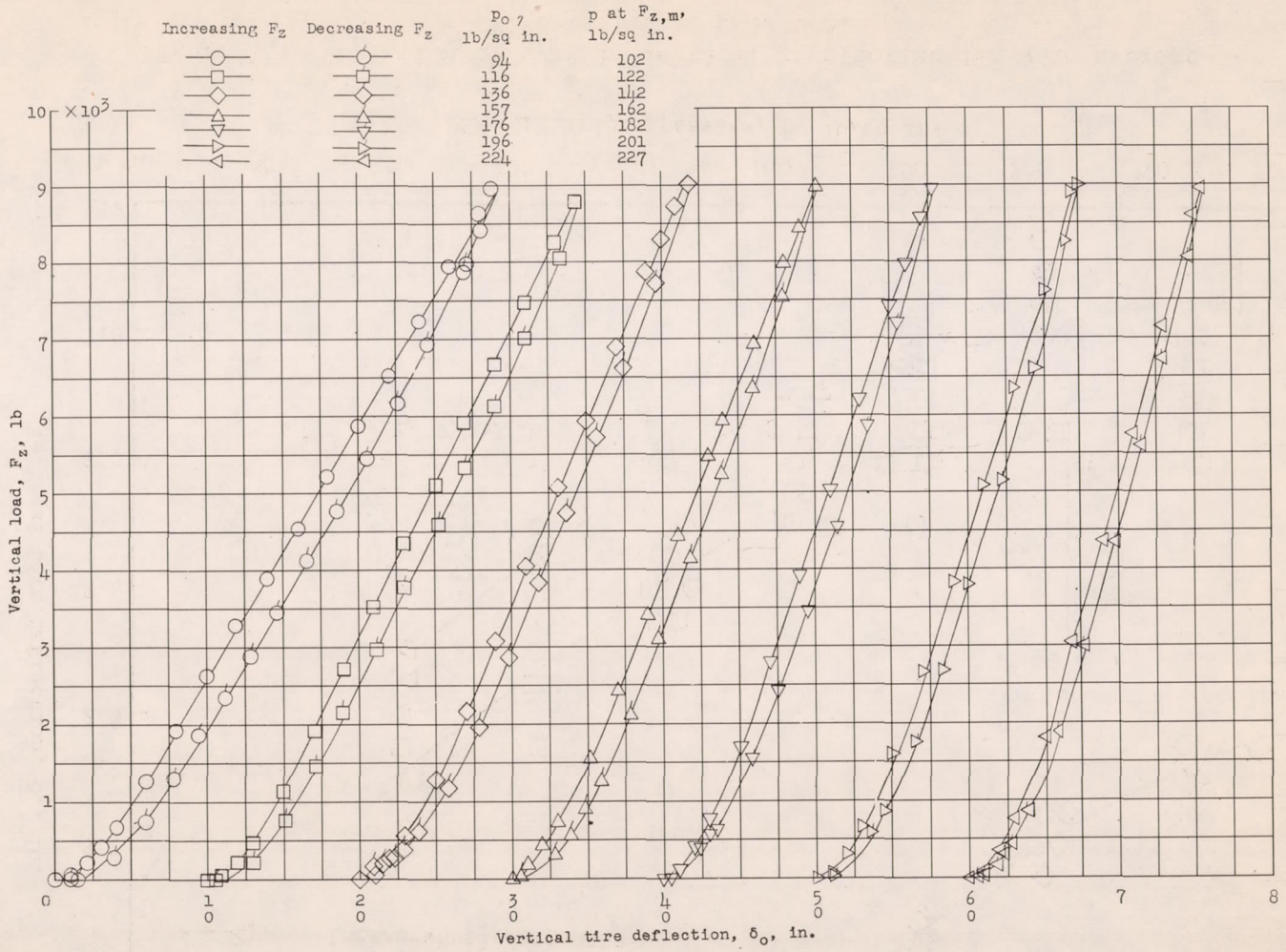

(b) Tire B at conclusion of test series C.

Figure 17.- Concluded.

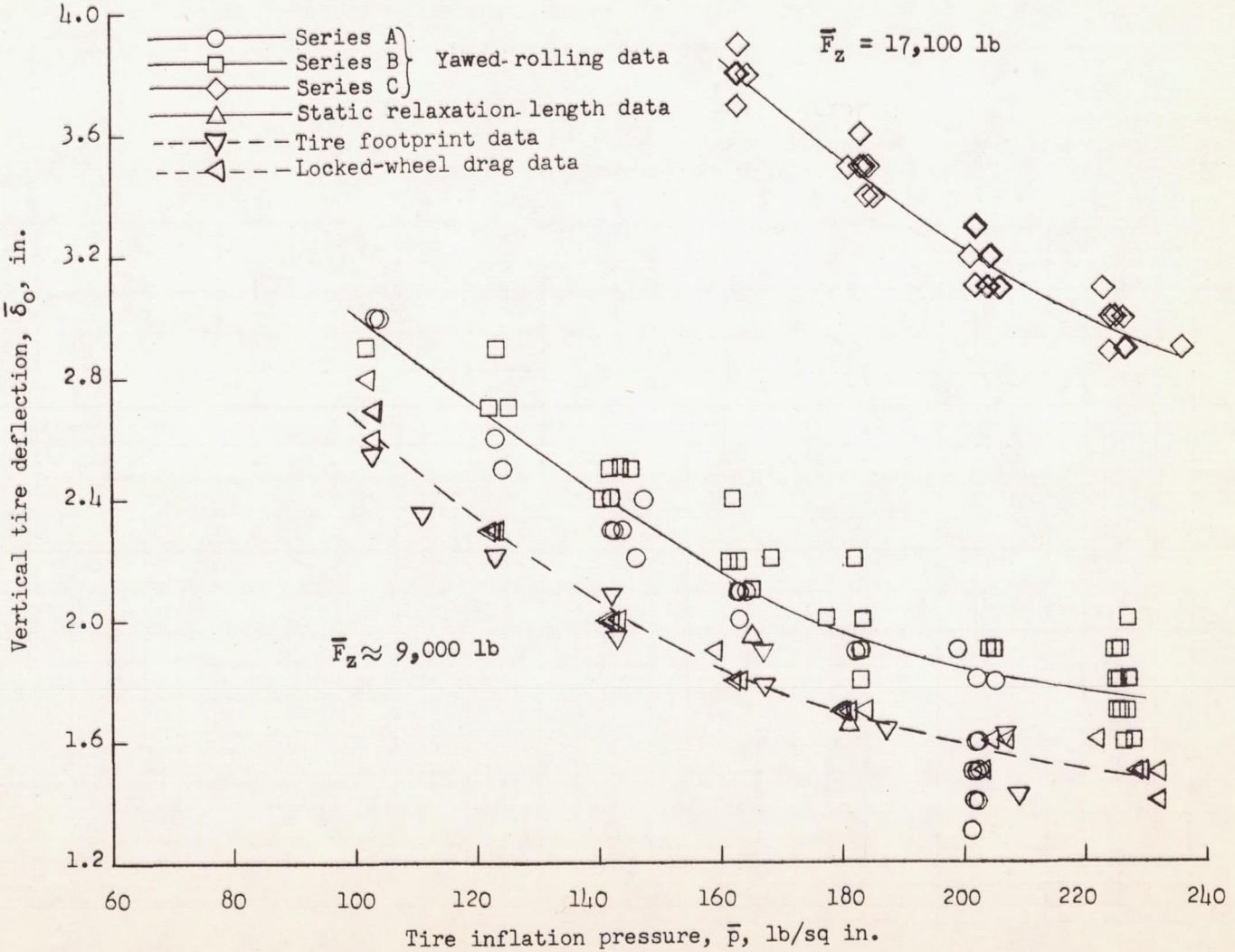

Figure 18.- Variation of average vertical tire deflection with average tire inflation pressure.

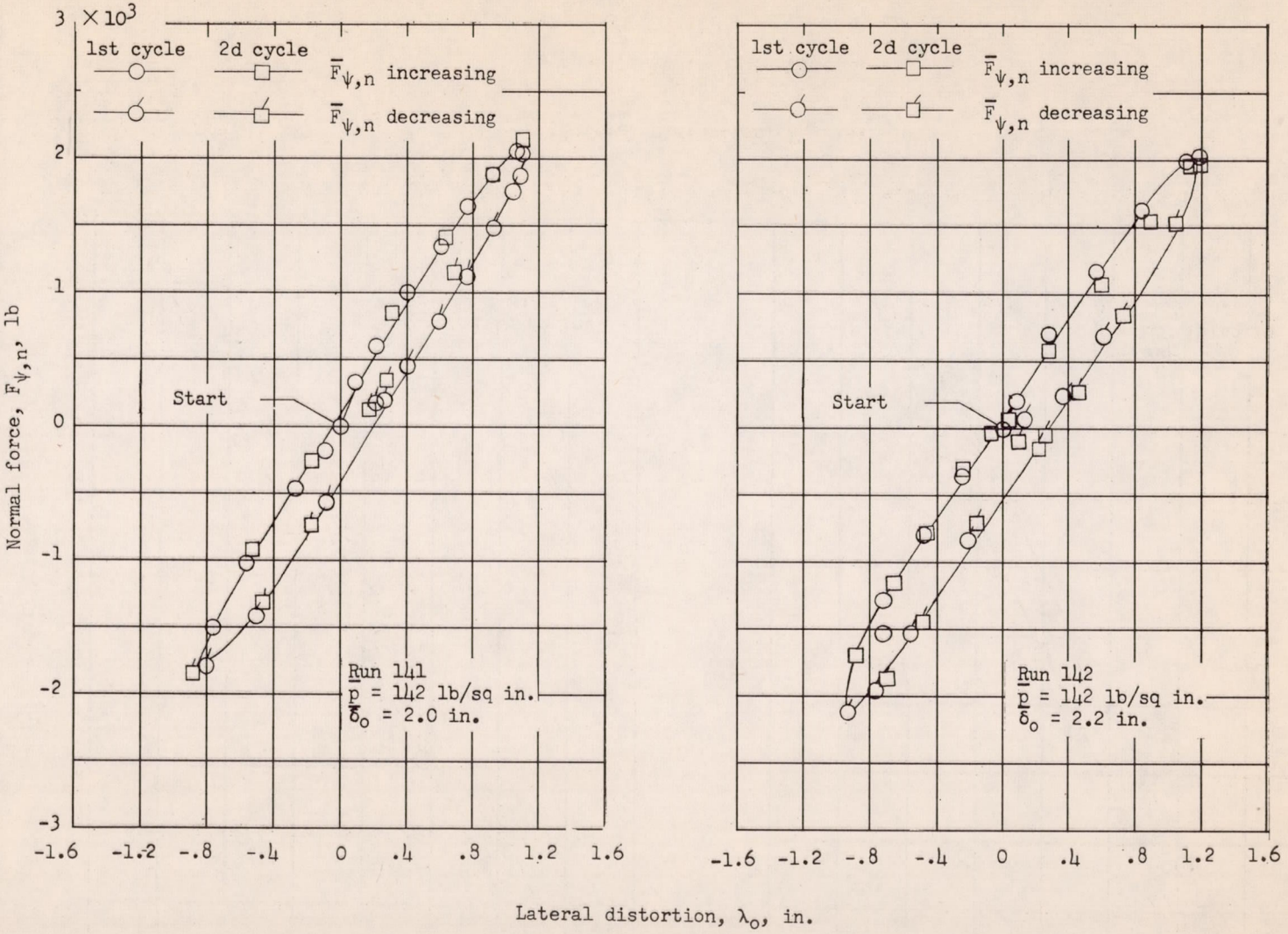

Figure 19.- Variation of side force with side tire deflection for test series A for a vertical load of 9,000 pounds on each tire.

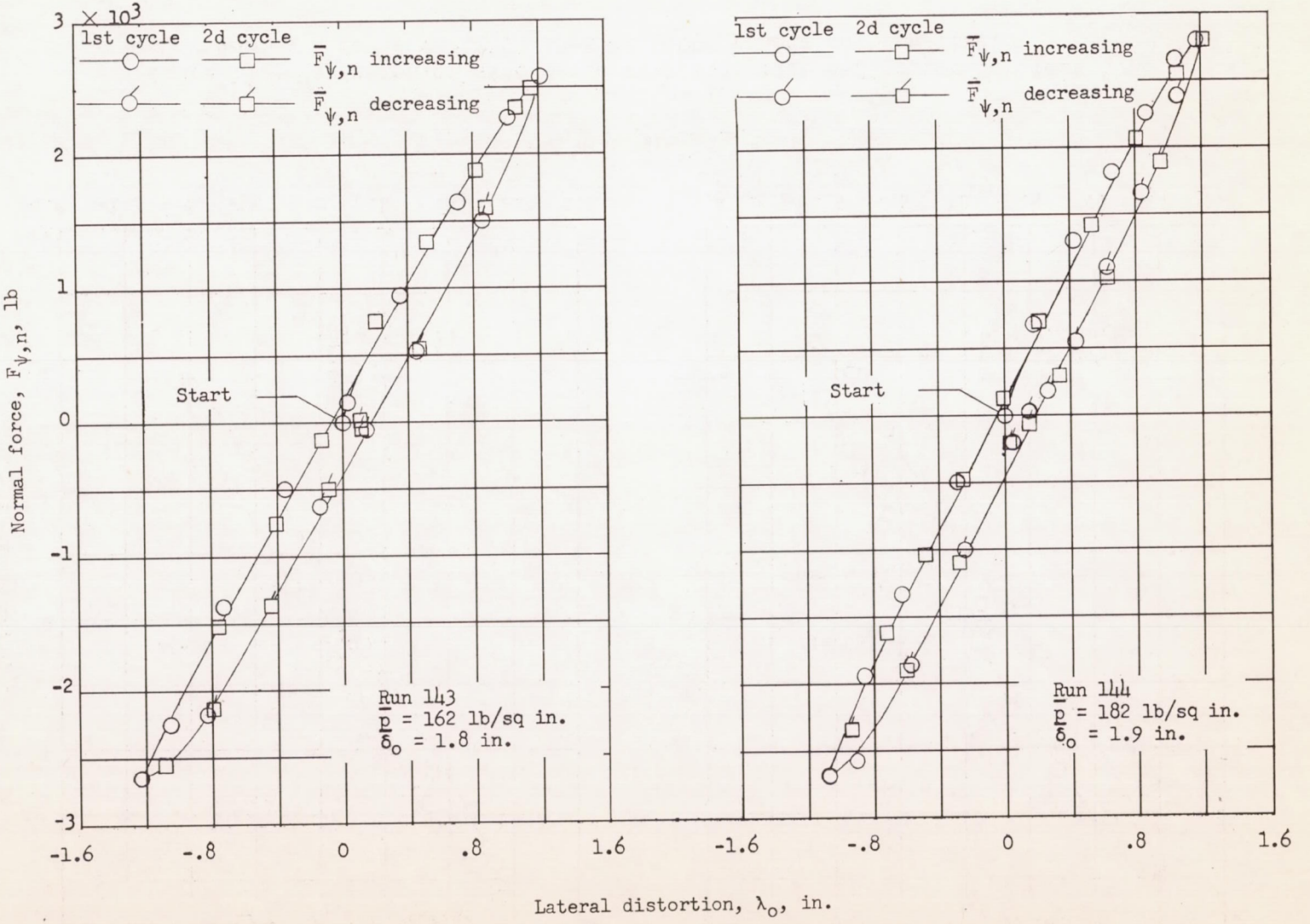

Figure 19.- Continued.

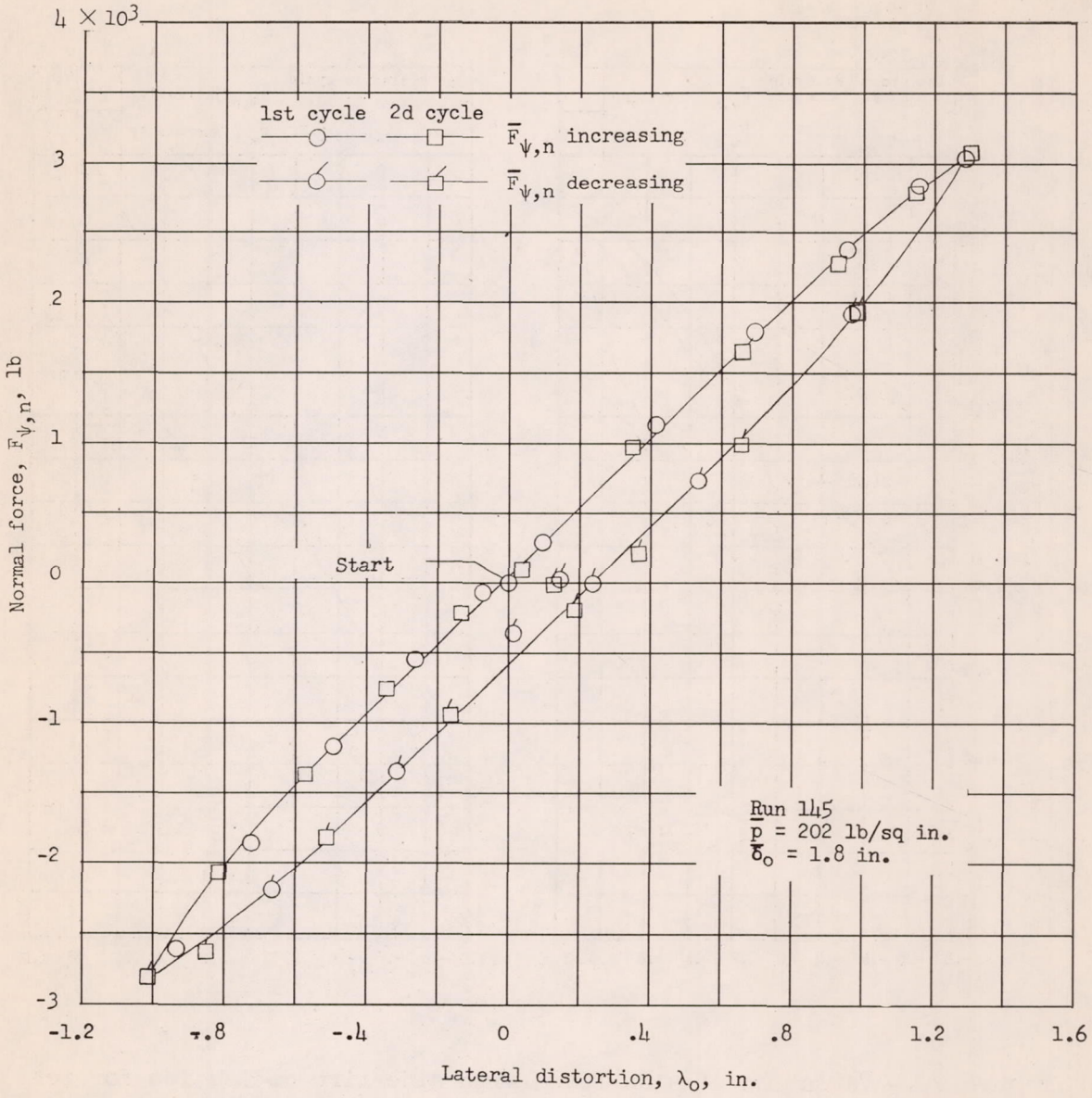

Figure 19.- Concluded.

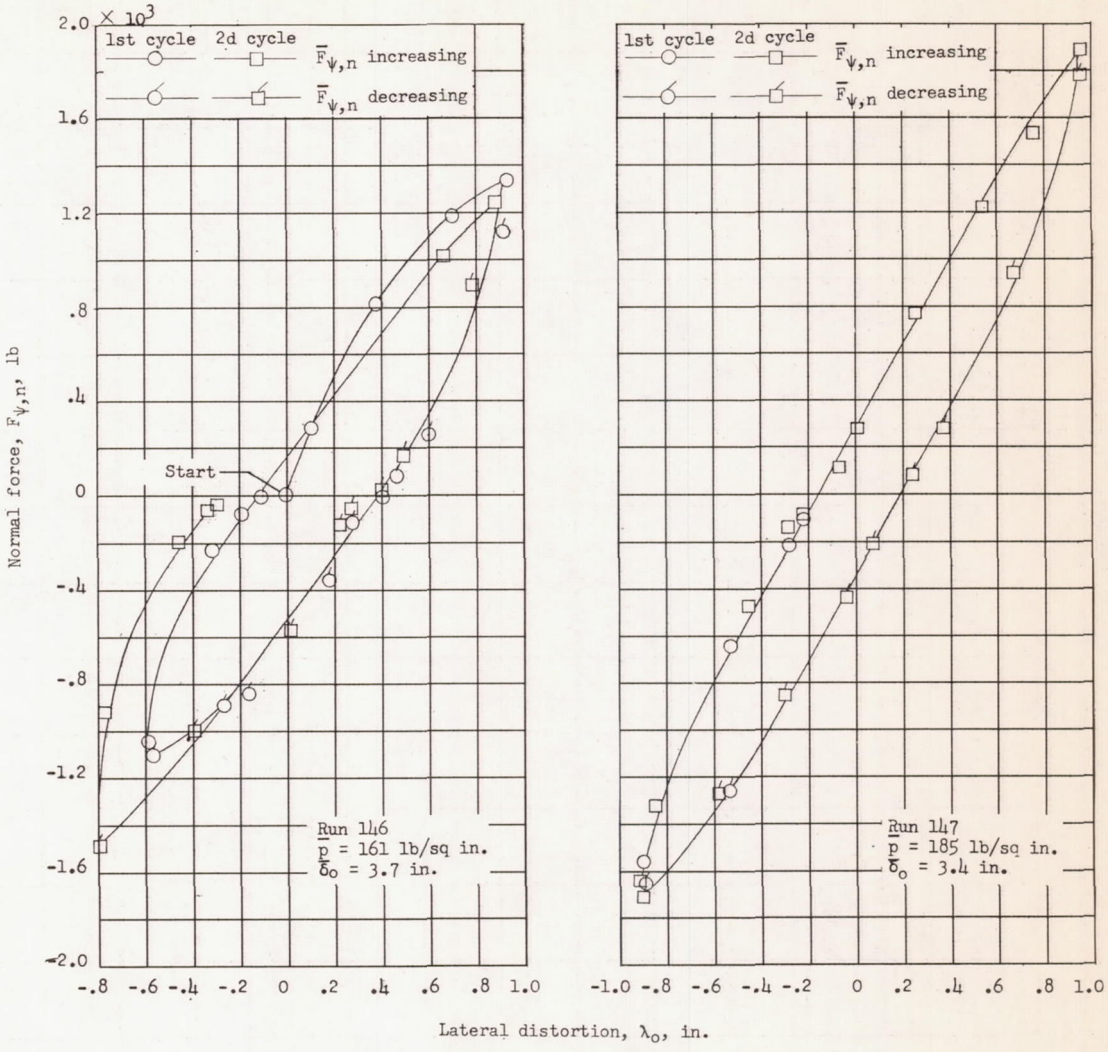

Figure 20.- Variation of side force with side tire deflection for test series C for a vertical load of 17,100 pounds on each tire.

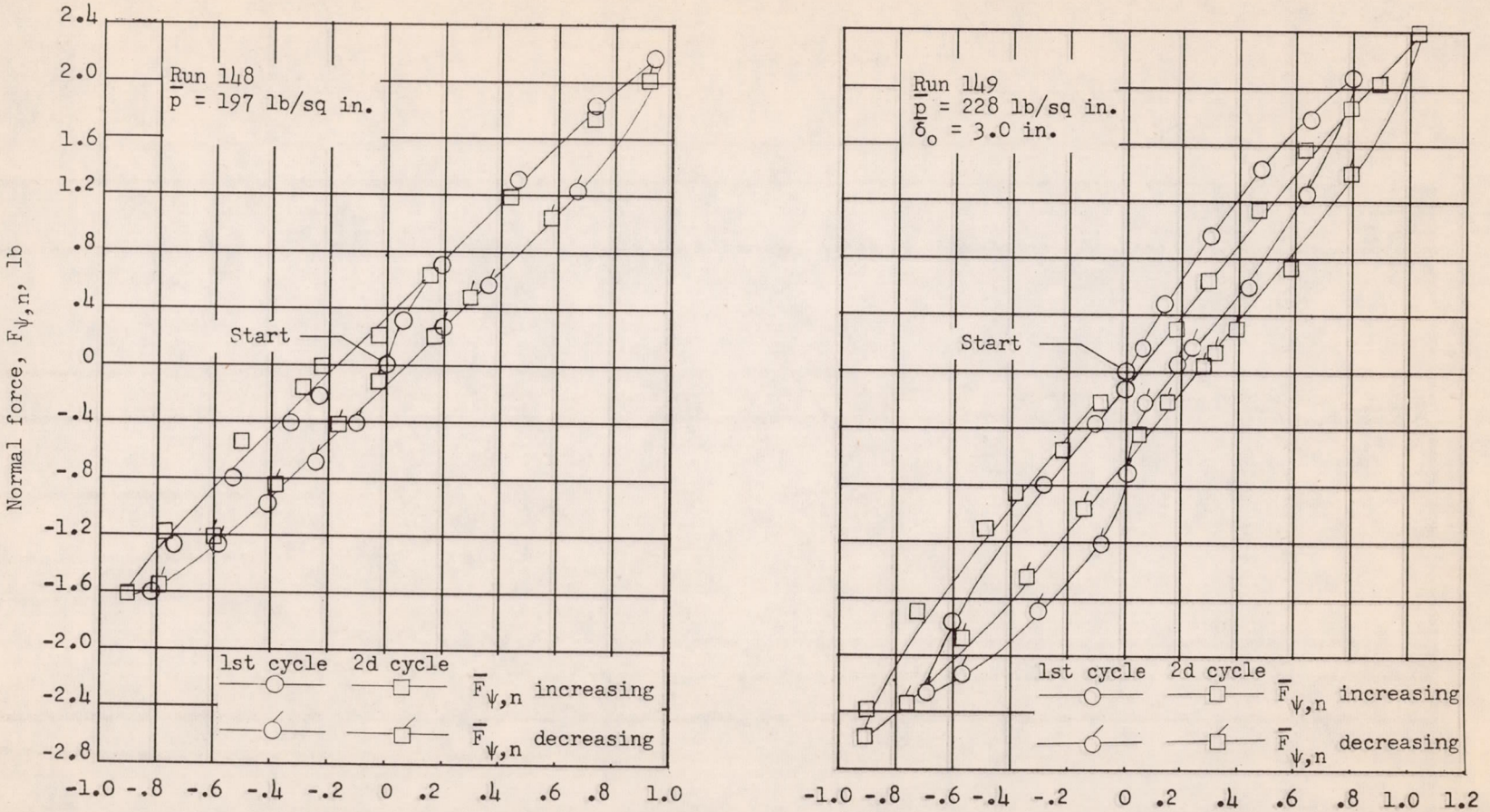

Figure 20.- Concluded.

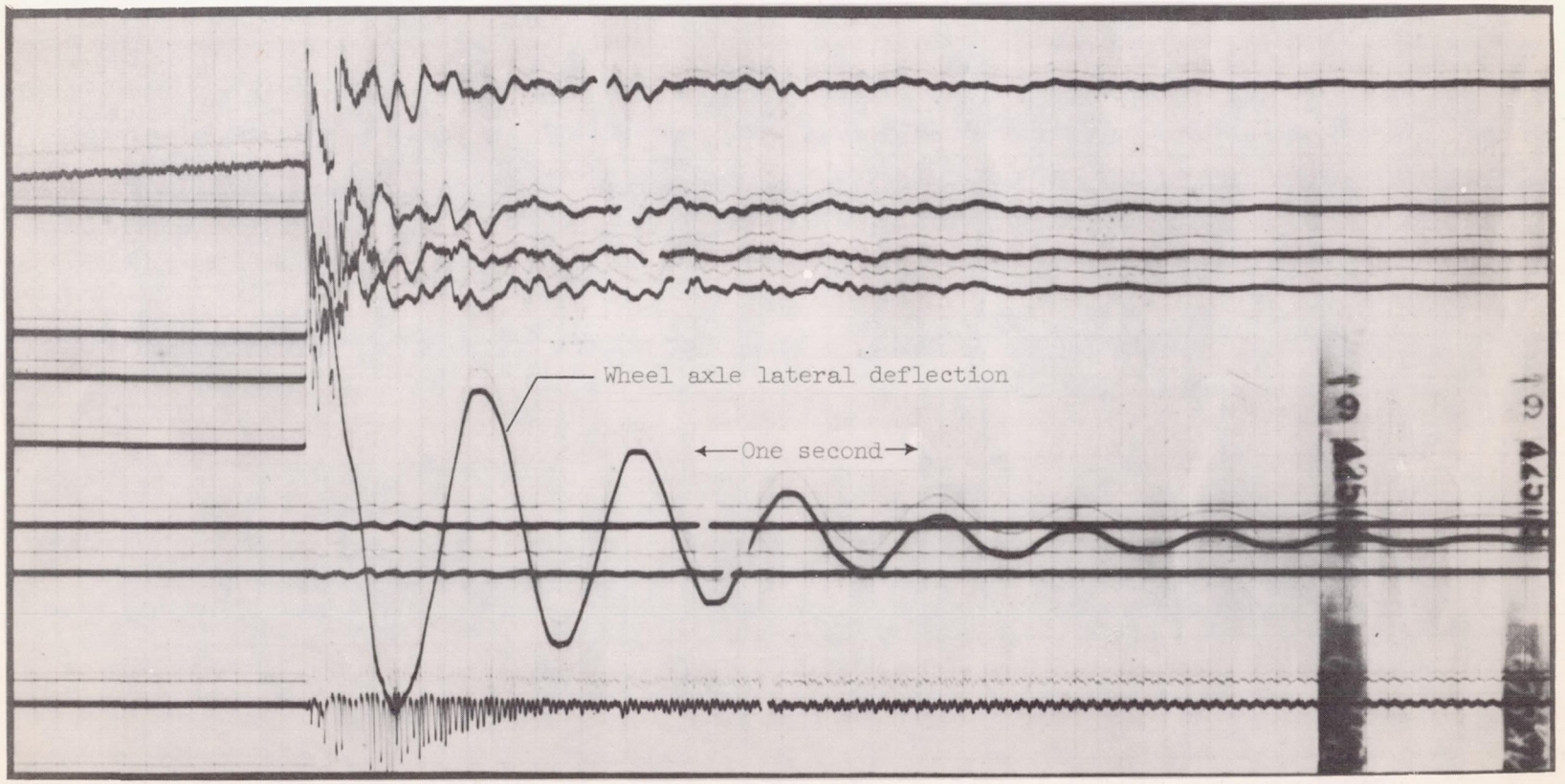

L-90527

Figure 21.- Sample oscillograph record from dynamic lateral-elasticity test. Run 153.

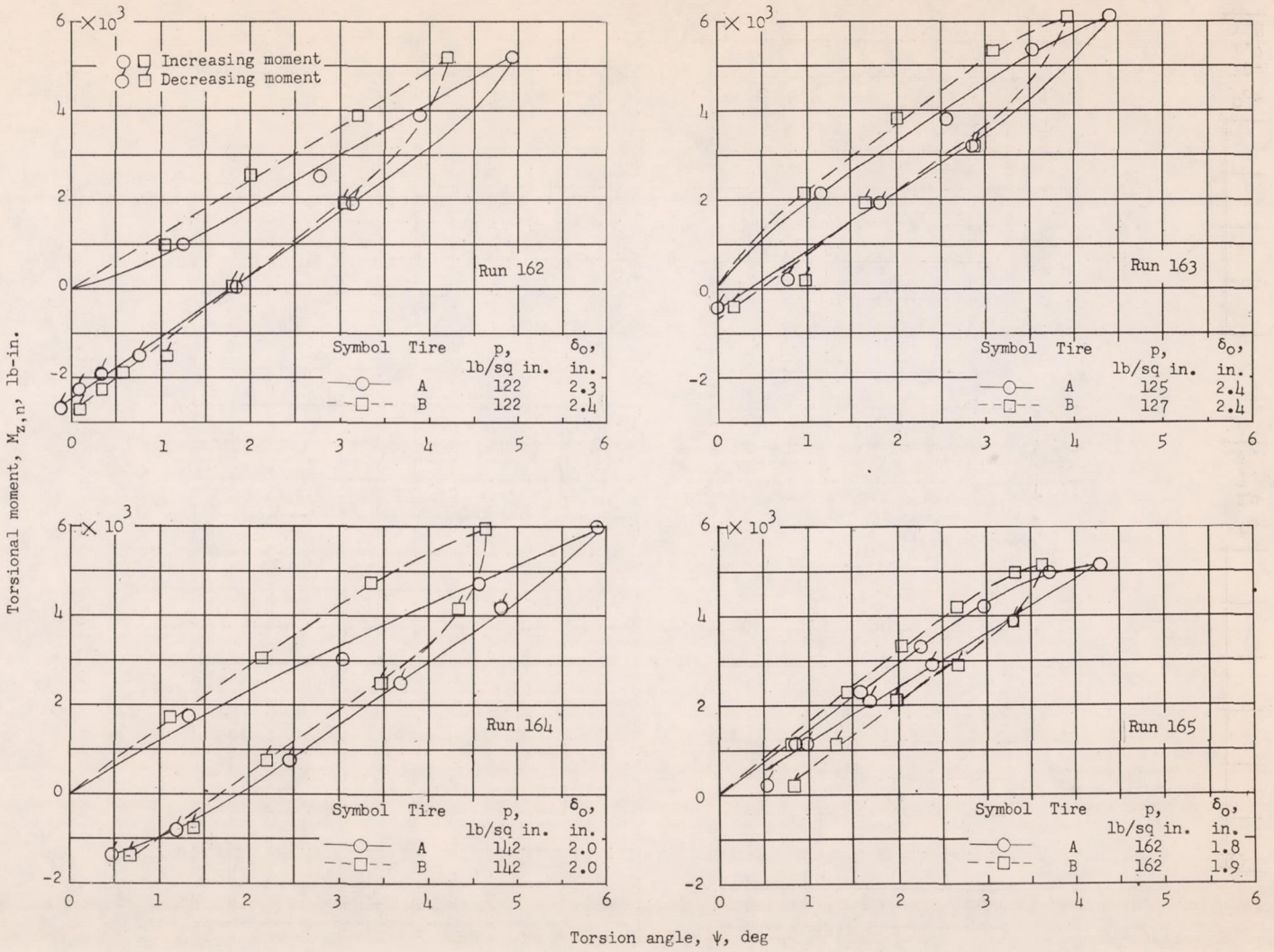

Figure 22.- Variation of torsional moment with torsion angle for test series A for a vertical load of 9,000 pounds on each tire.

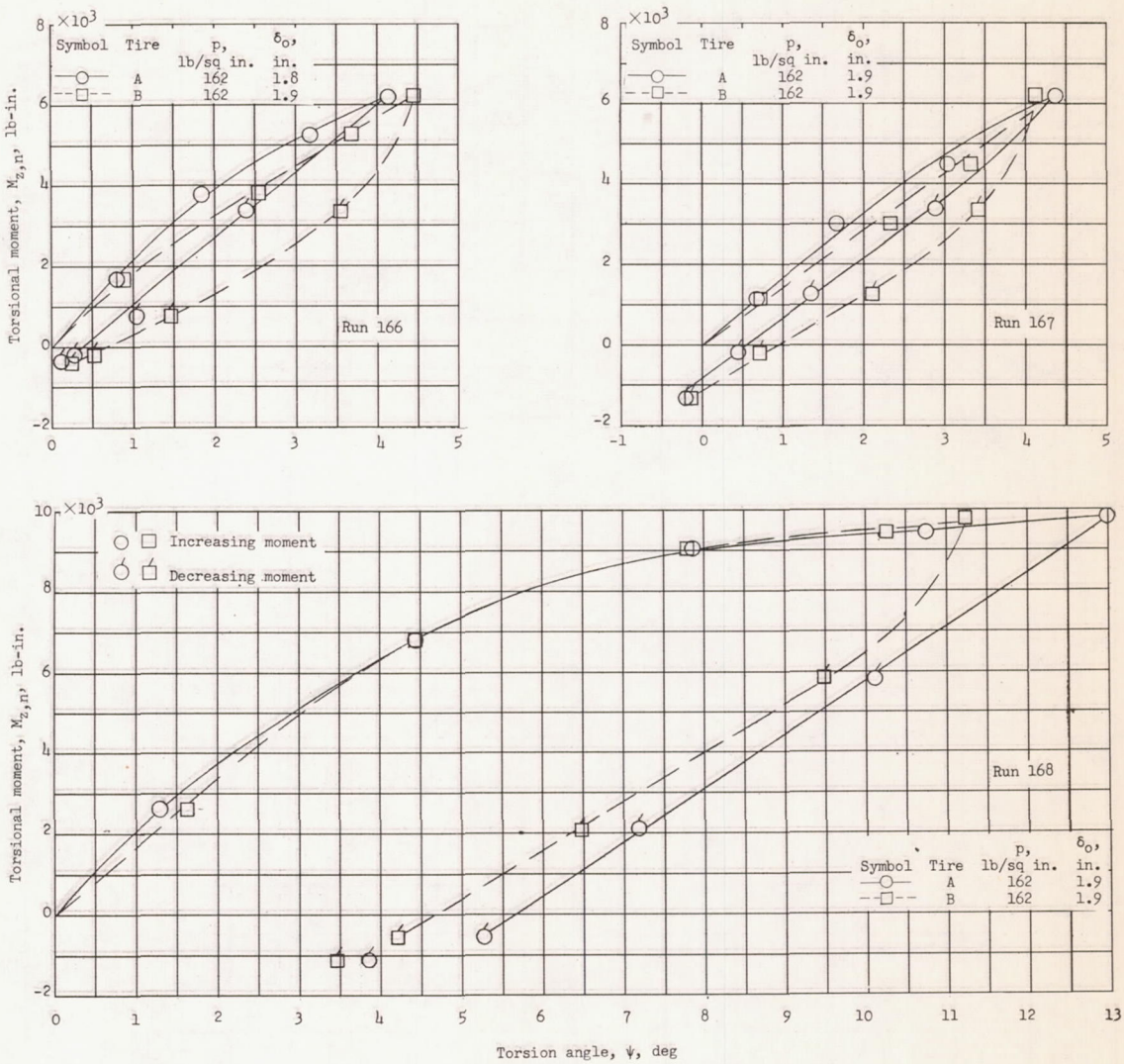

Figure 22.- Continued.

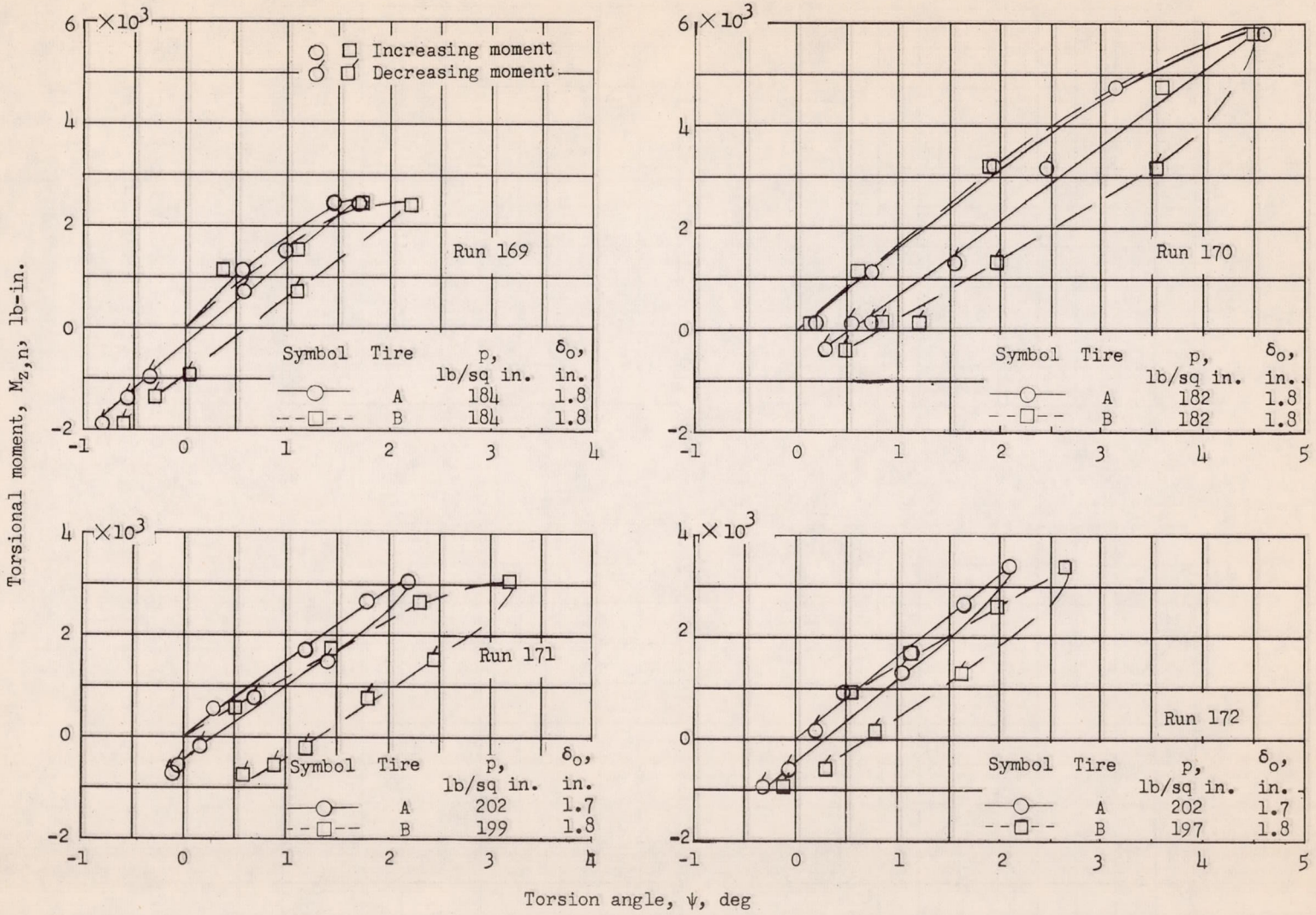

Figure 22.- Concluded.

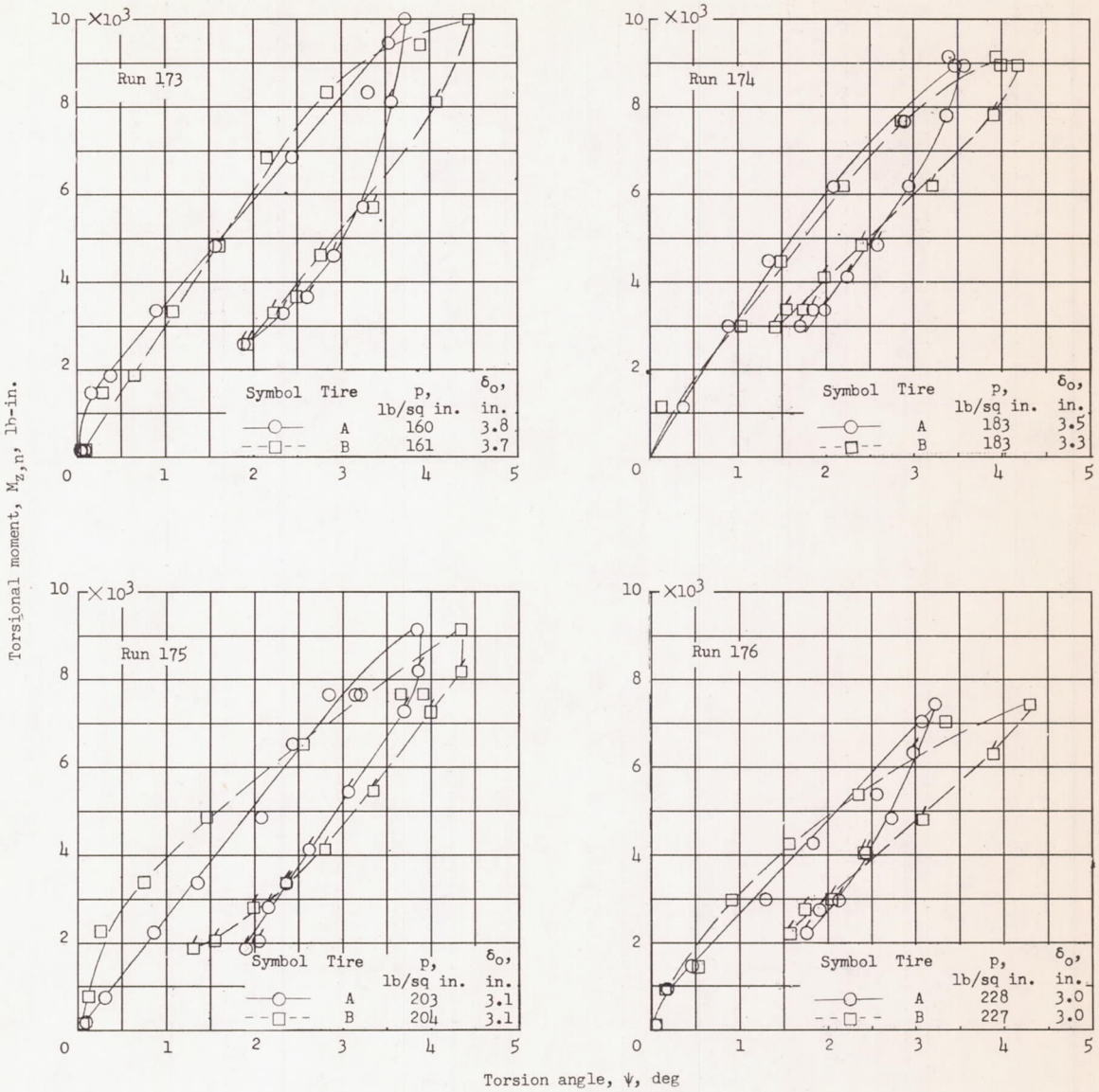

Figure 23.- Variation of torsion angle with torsional moment for test series C for a vertical load of 17,100 pounds on each tire.

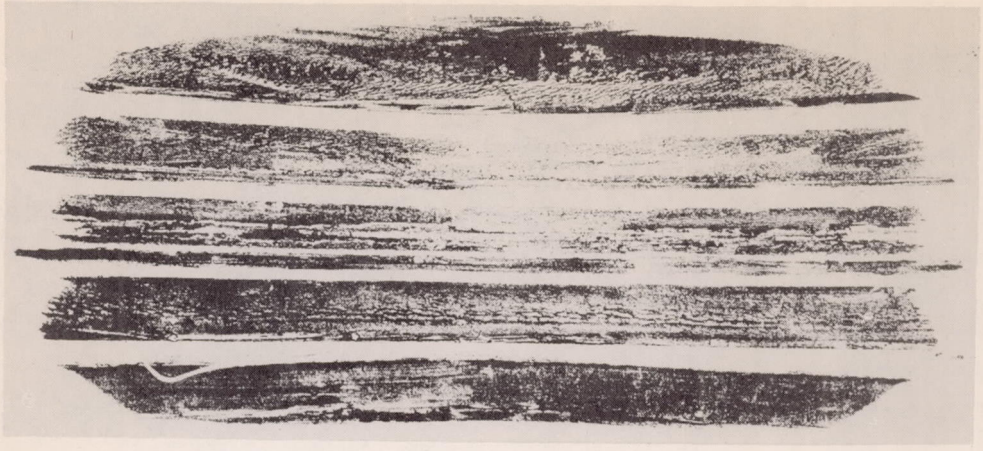

(a) Run 193; δ_o = 3.60 inches; p = 162 pounds per square inch; F_z = 17,200 pounds.

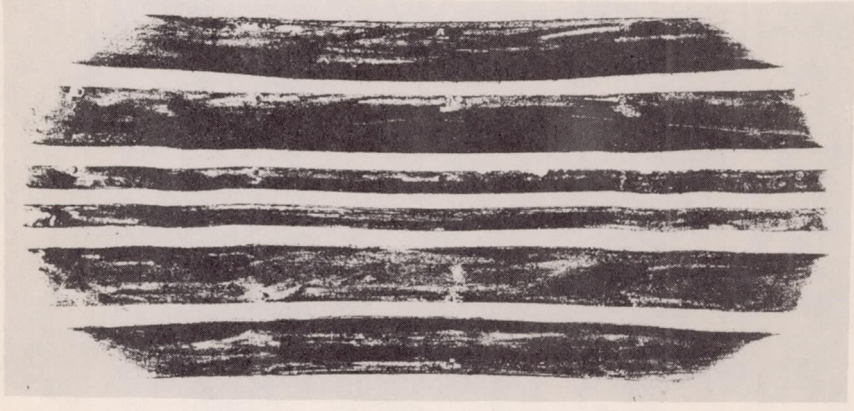

(b) Run 180; δ_o = 2.55 inches; p = 103 pounds per square inch; F_z = 9,000 pounds.

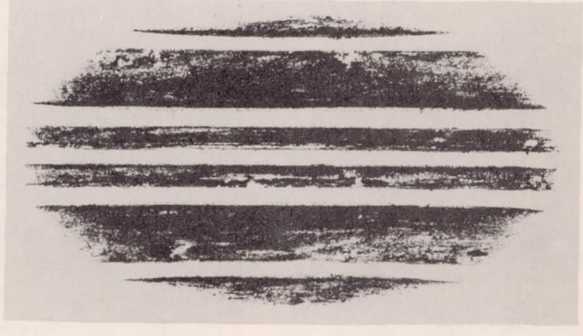

L-90528

(c) Run 187; δ_o = 1.20 inches; p_o = 159 pounds per square inch.

Figure 24.- Typical tire footprints for tire B.

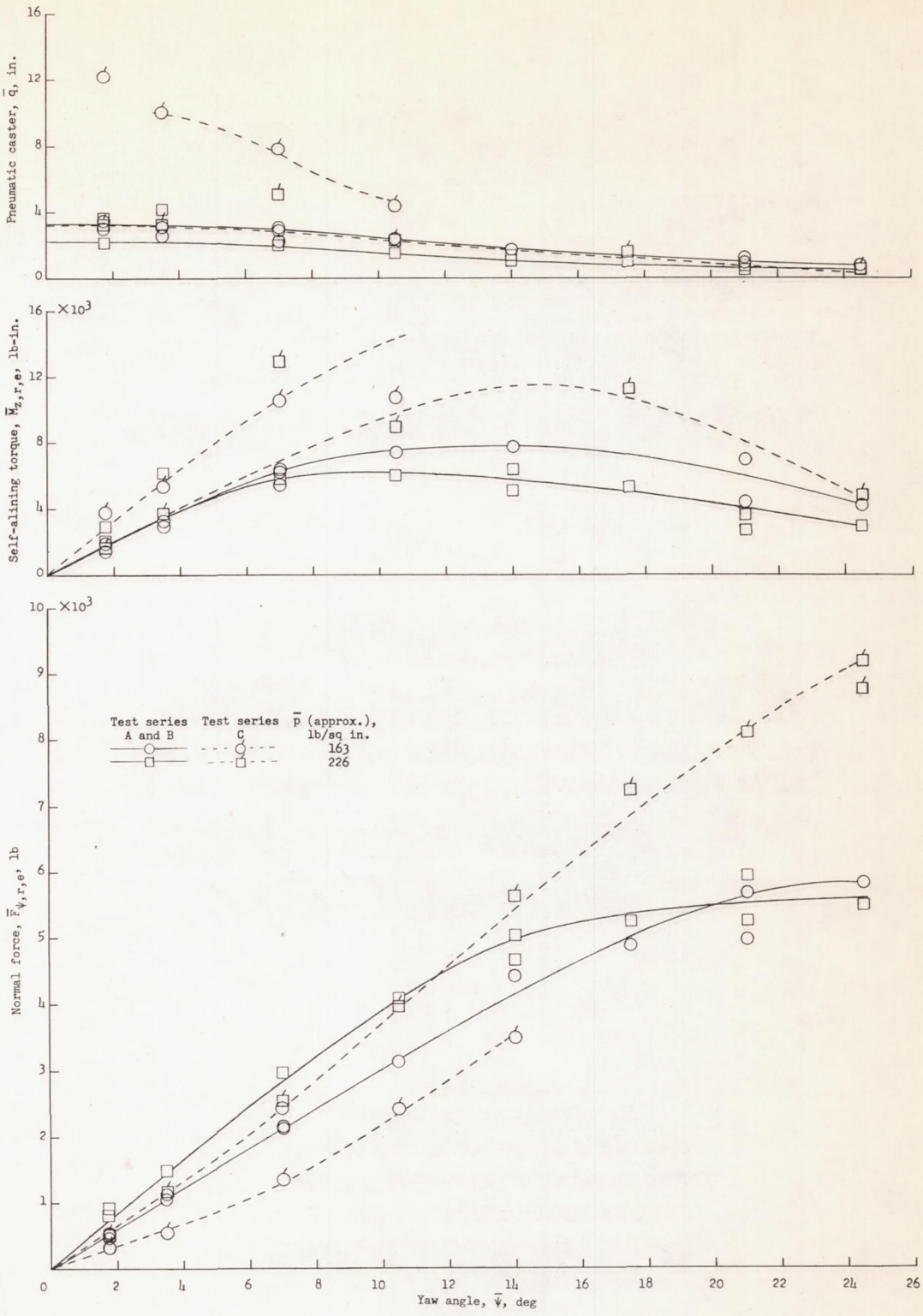

Figure 25.- Comparison of variation of normal force, self-alining torque, and pneumatic caster with yaw angle at two pressures for $\bar{F}_Z \approx 9{,}000$ pounds (test series A and B) $\bar{F}_Z = 17{,}100$ pounds (test series C).

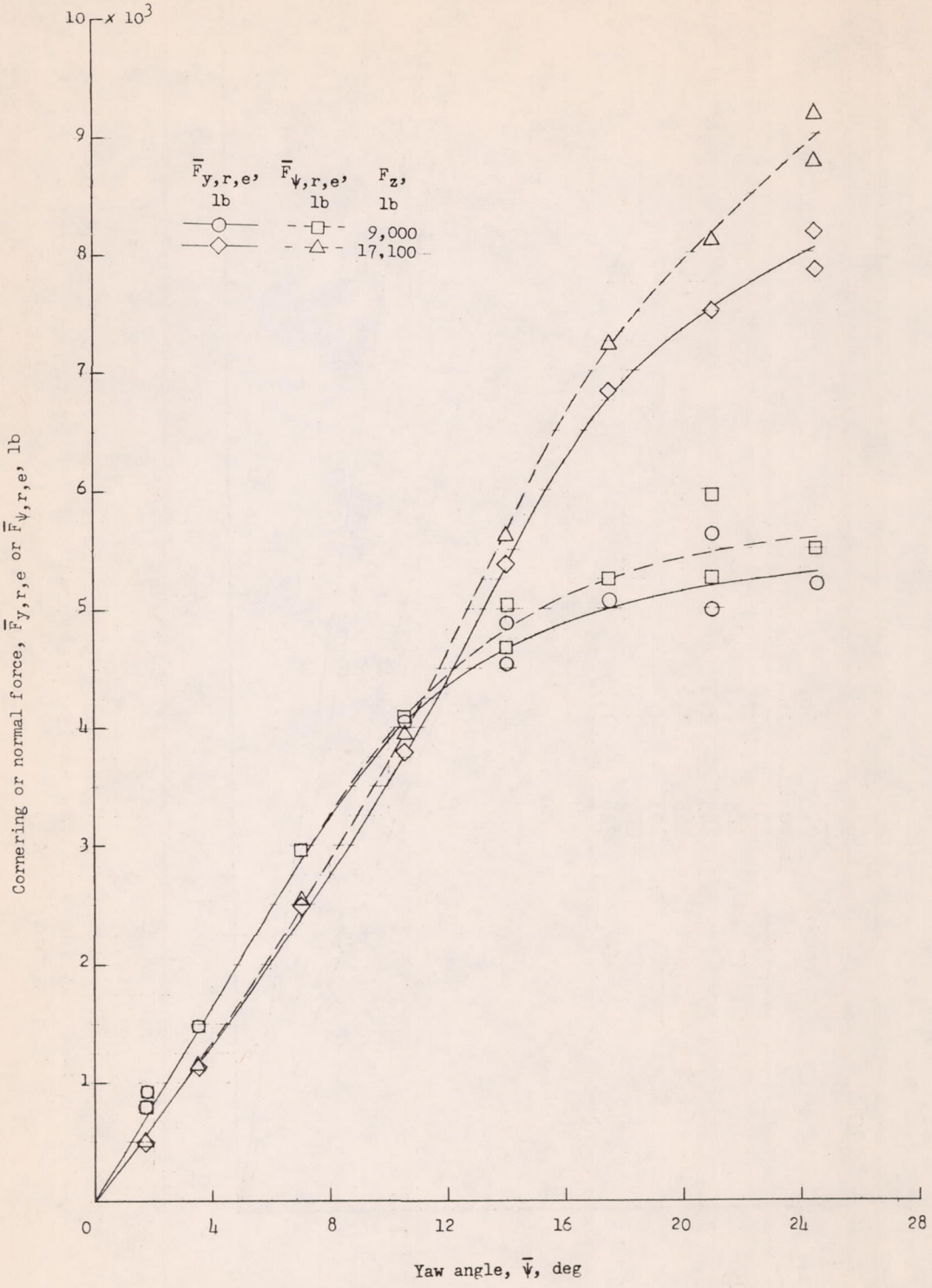

Figure 26.- Comparison of cornering-force and normal-force variations with yaw angle at $p \approx 226$ pounds per square inch for the two vertical load conditions tested.

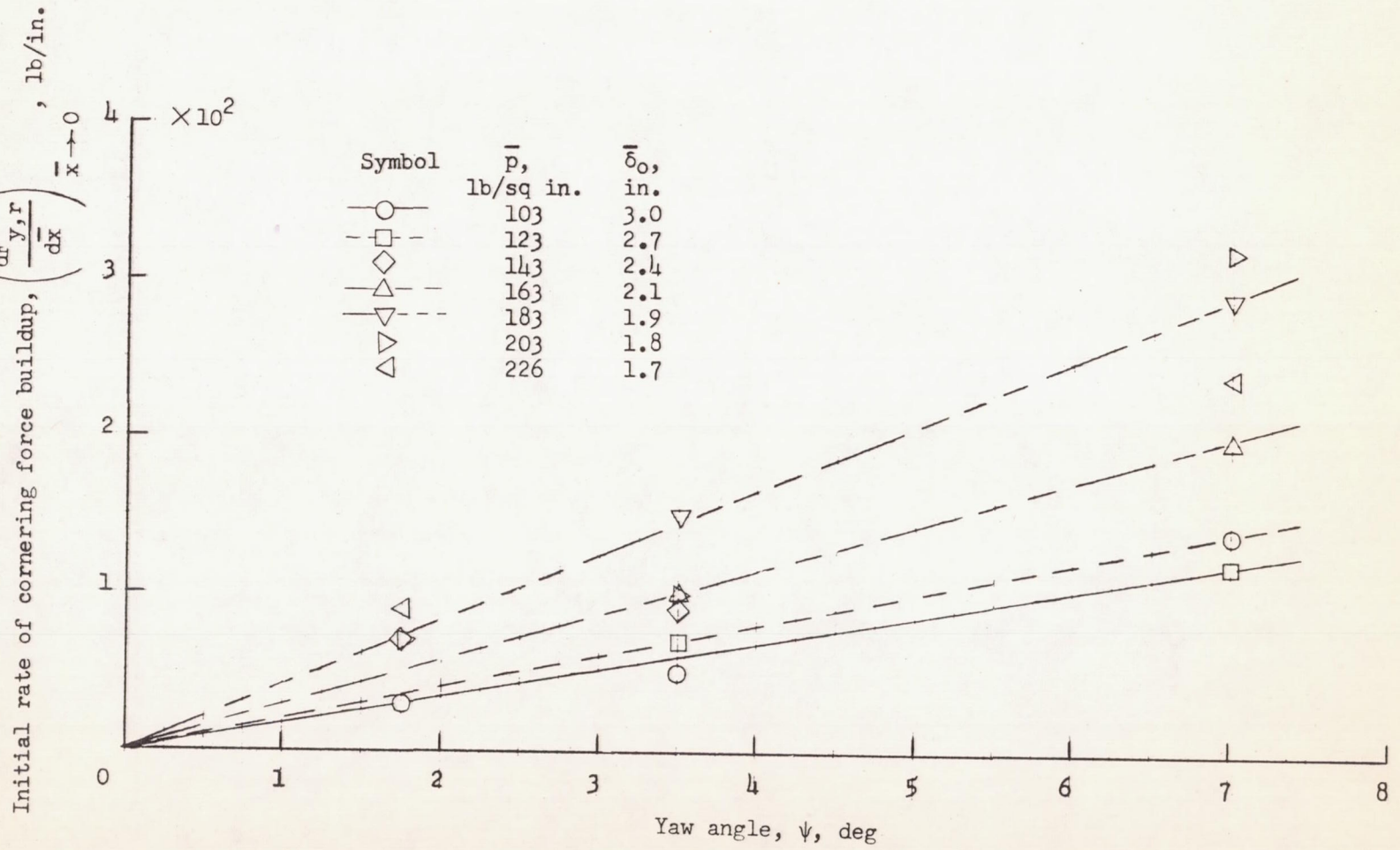

Figure 27.- Variation of initial rate of cornering-force buildup during yawed rolling with yaw angle, pressure, and deflection at a vertical load of approximately 9,000 pounds per tire (test series A and B).

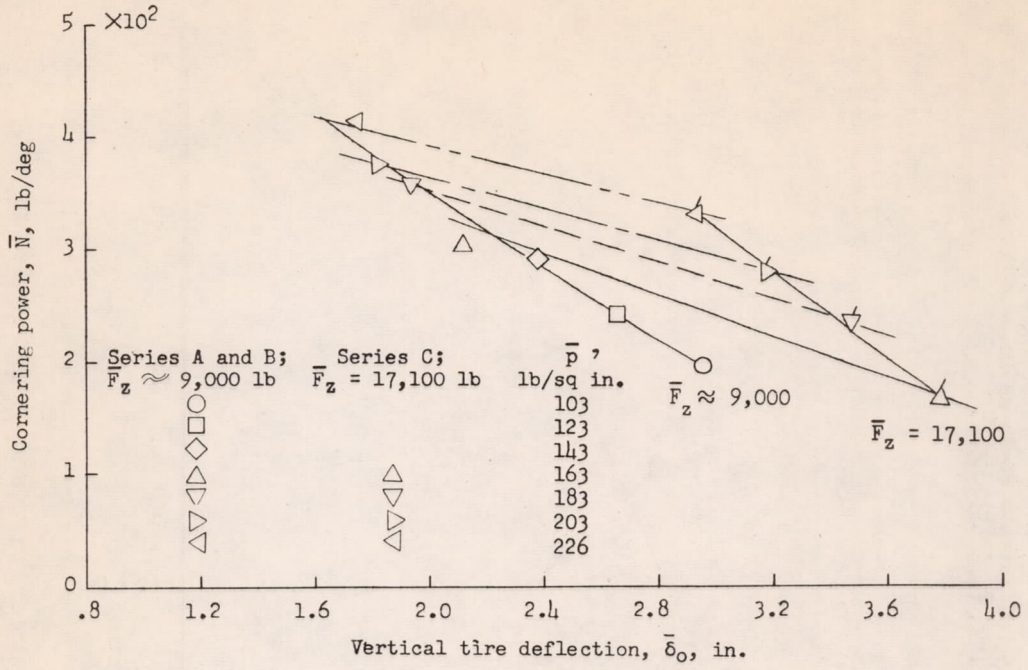

(a) Variation of cornering power with vertical tire deflection.

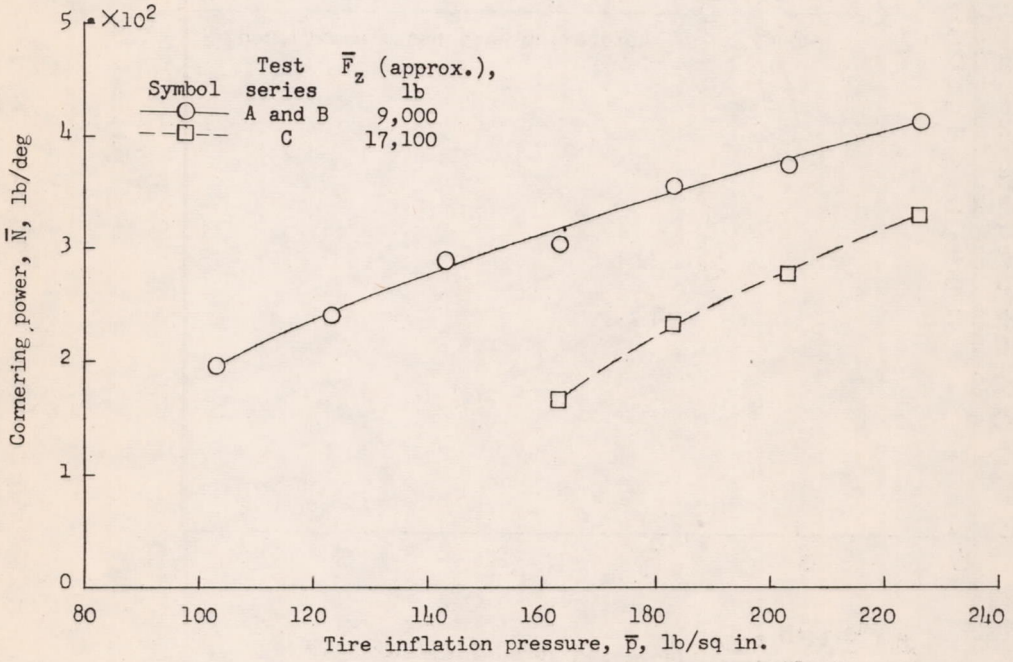

(b) Variation of cornering power with inflation pressure.

Figure 28.- Variation of cornering power with vertical tire deflection and inflation pressure.

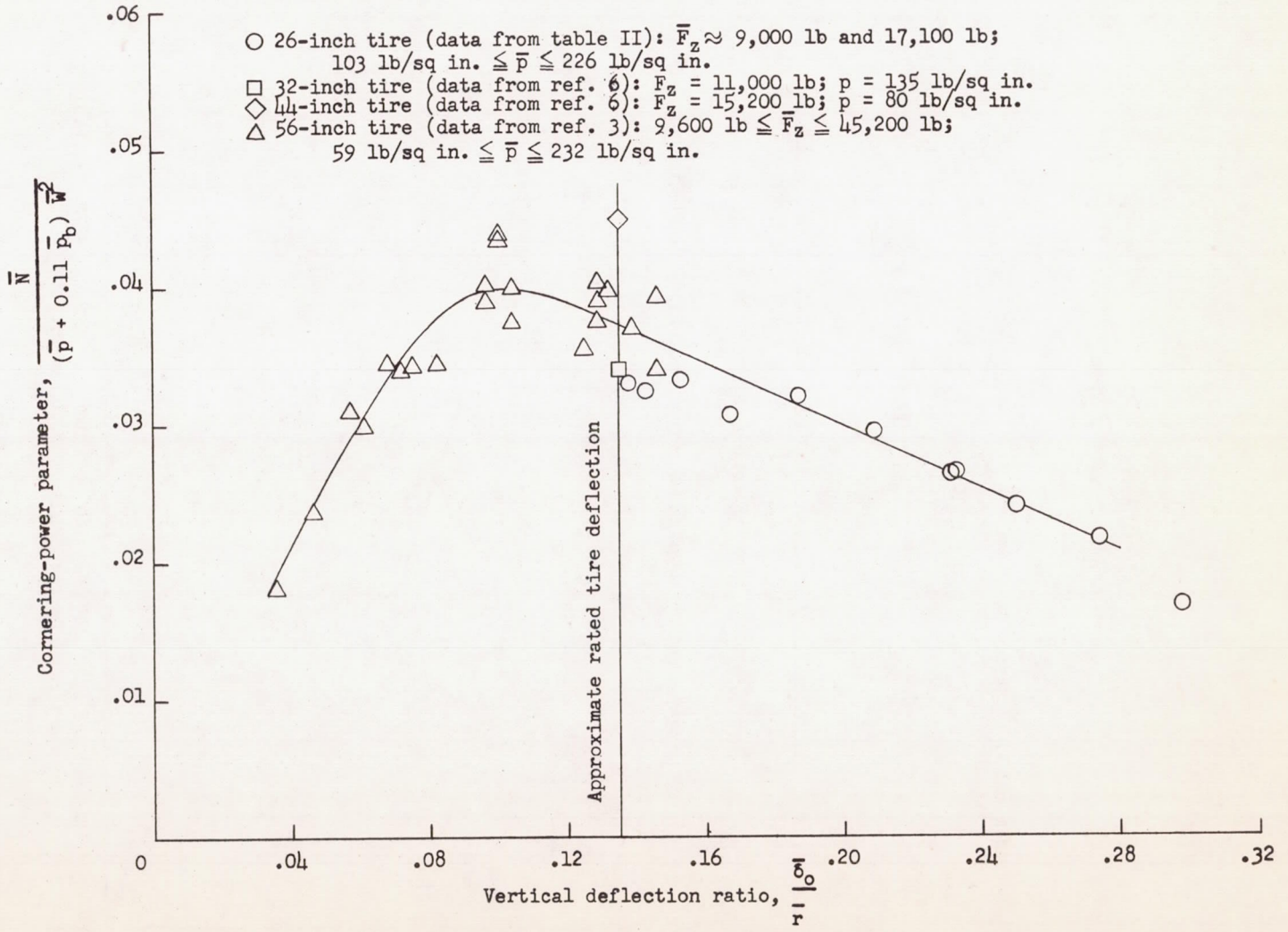

Figure 29.- Comparison of variation of cornering power with vertical deflection for four tires of different sizes.

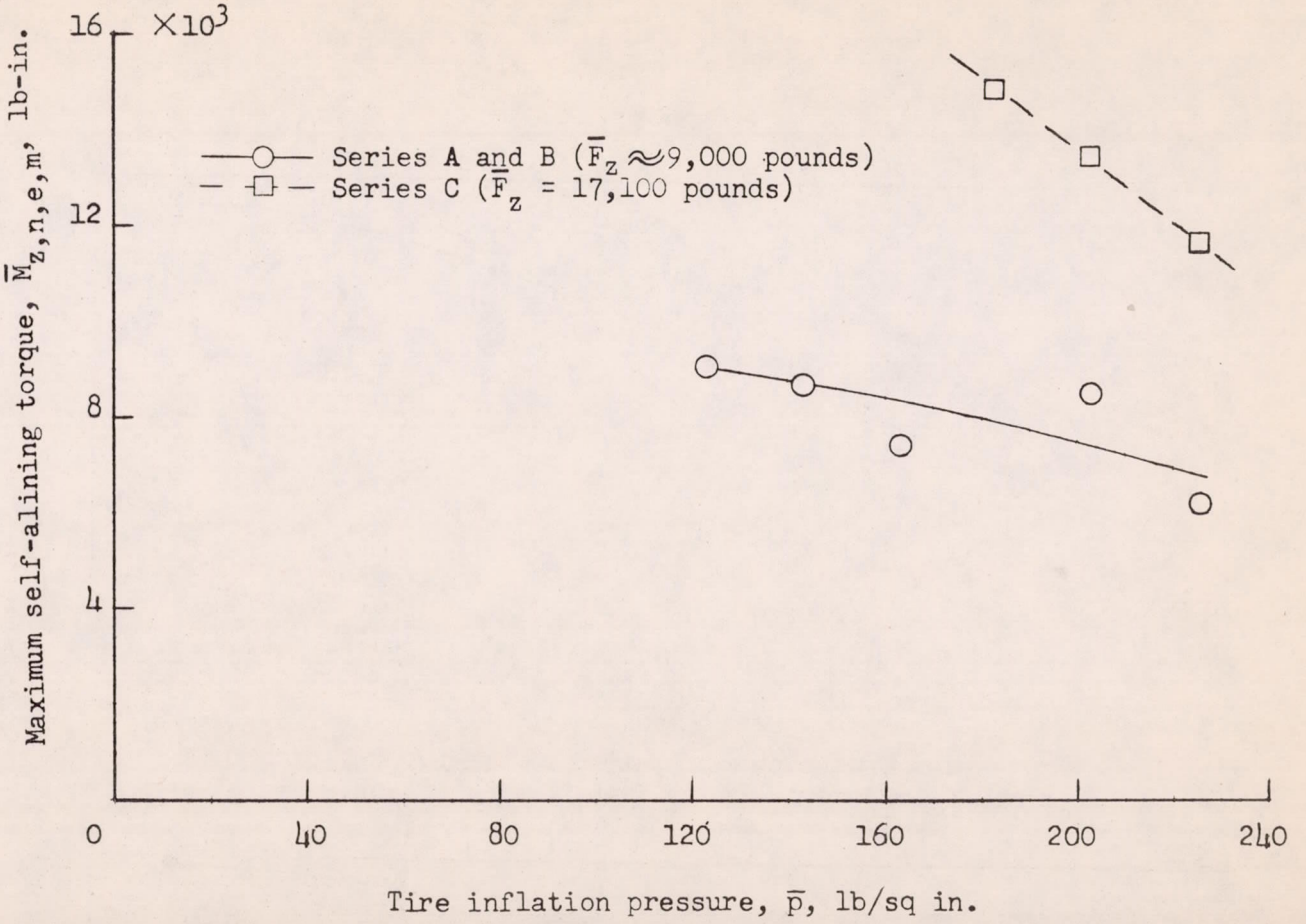

Figure 30.- Variation of maximum self-alining torque with inflation pressure for the two vertical loadings tested.

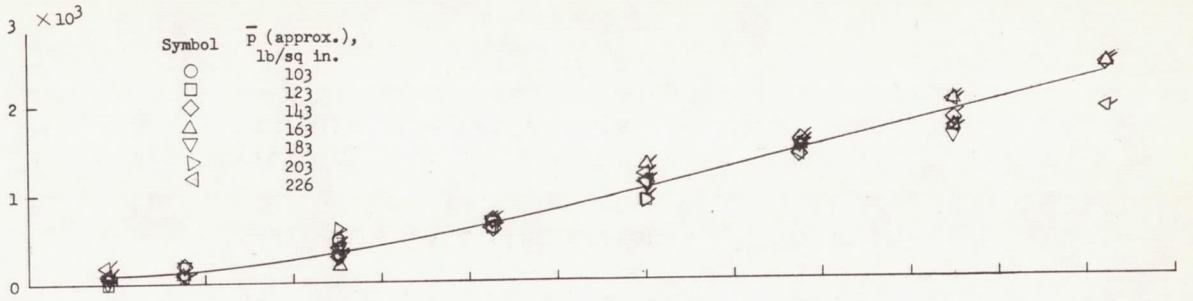

(a) Test series A and B; $\overline{F}_Z \approx 9{,}000$ pounds. Unflagged symbols denote test series A and flagged symbols denote test series B.

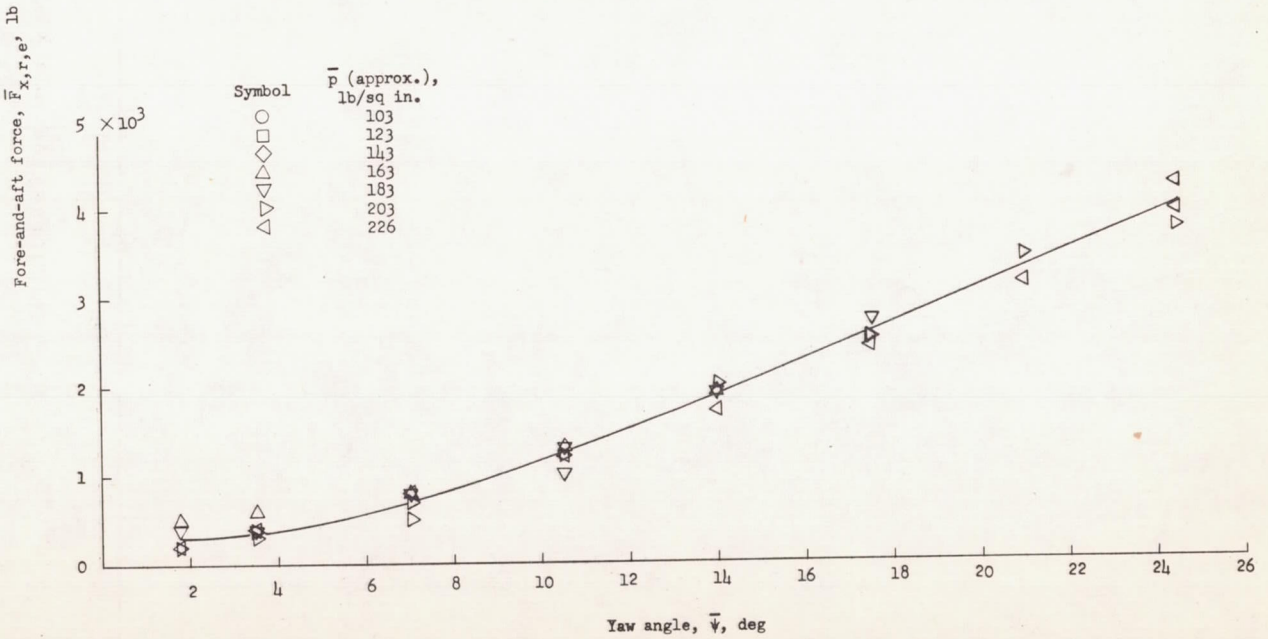

(b) Test series C; $\overline{F}_Z = 17{,}100$ pounds.

Figure 31.- Variation of drag force with yaw angle for the vertical-load and pressure ranges tested.

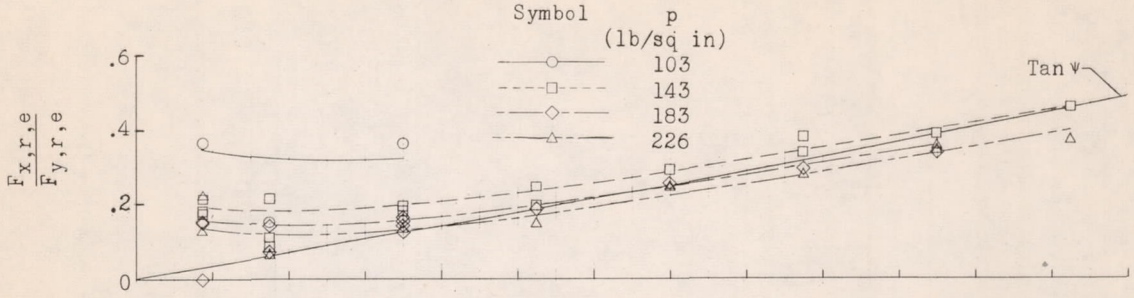

(a) Test series A and B; $\overline{F}_Z \approx 9{,}000$ pounds.

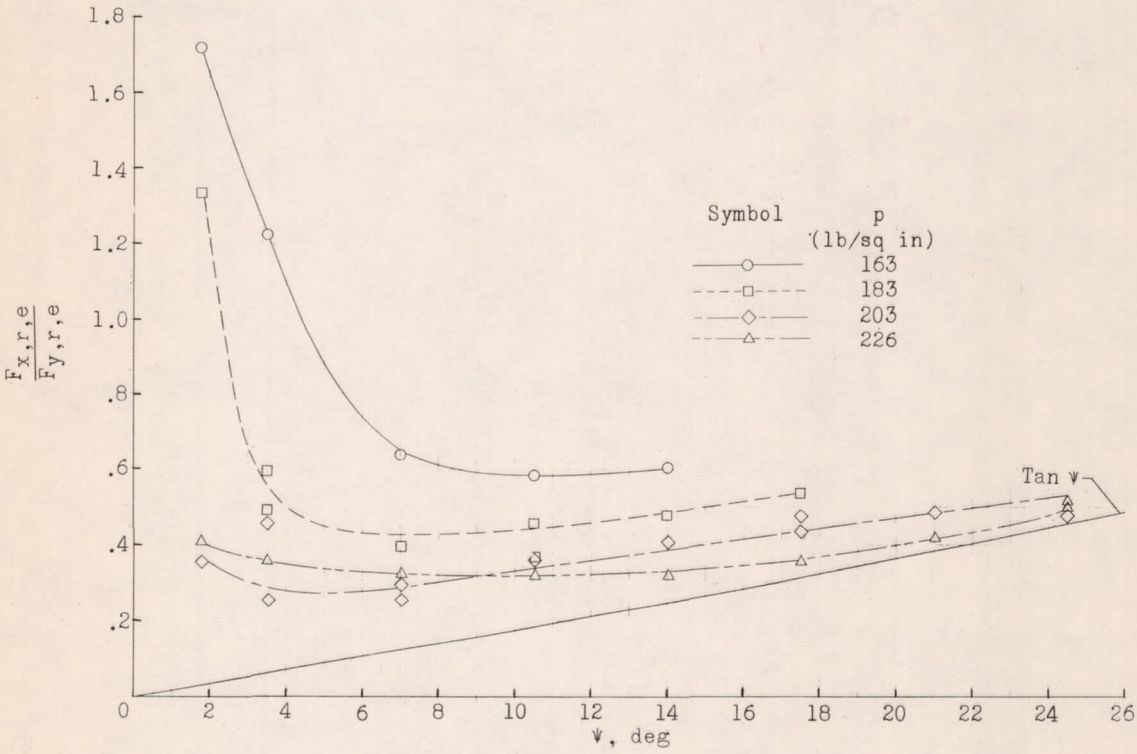

(b) Test series C; $\overline{F}_Z = 17{,}100$ pounds.

Figure 32.- Variation of the ratio of drag force to cornering force with yaw angle.

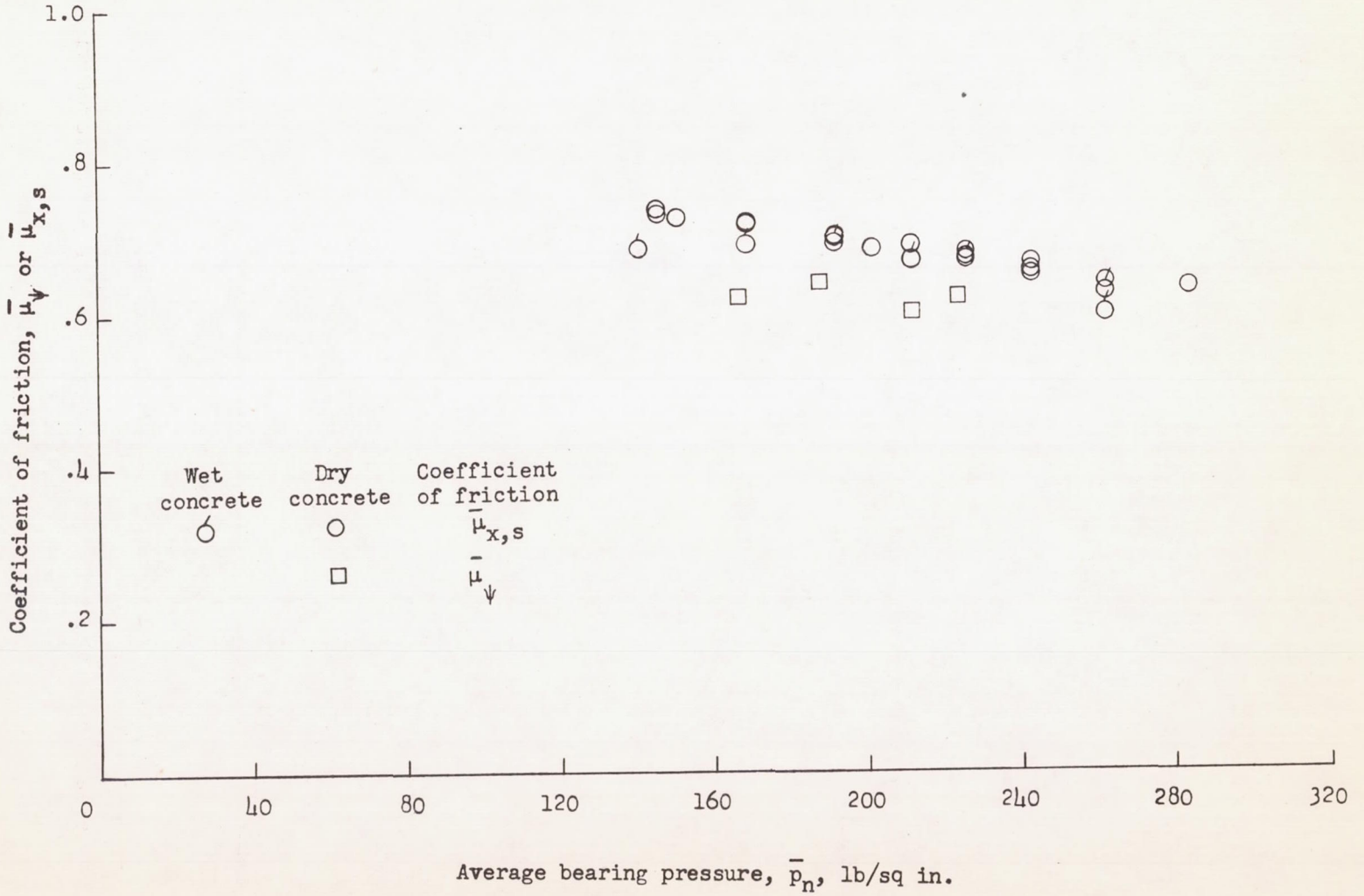

Figure 33.- Variation of sliding-drag and yawed-rolling coefficients of friction with average bearing pressure.

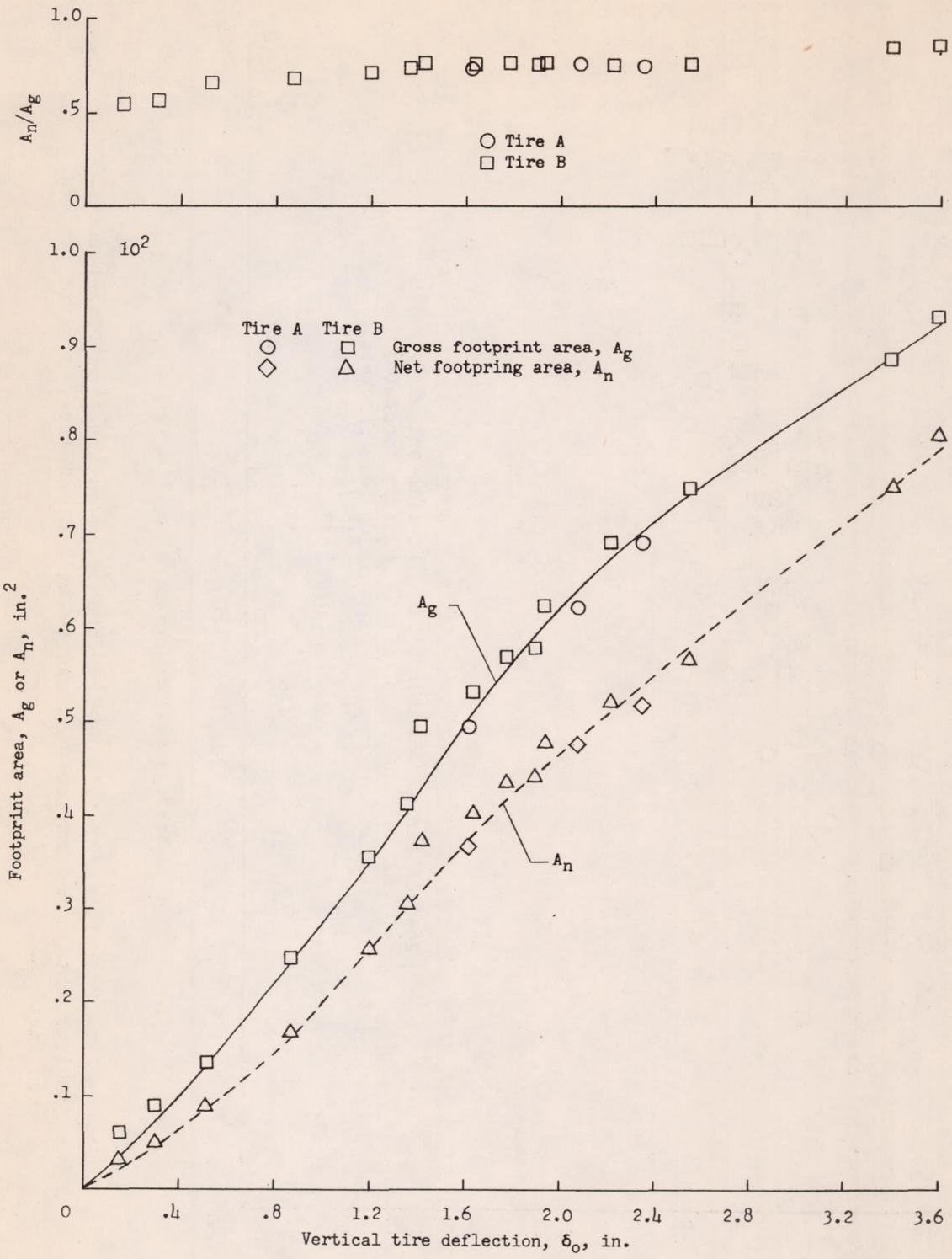

Figure 34.- Variation of gross footprint area, net footprint area, and the ratio of net footprint area to gross footprint area with vertical tire deflection for tires A and B.

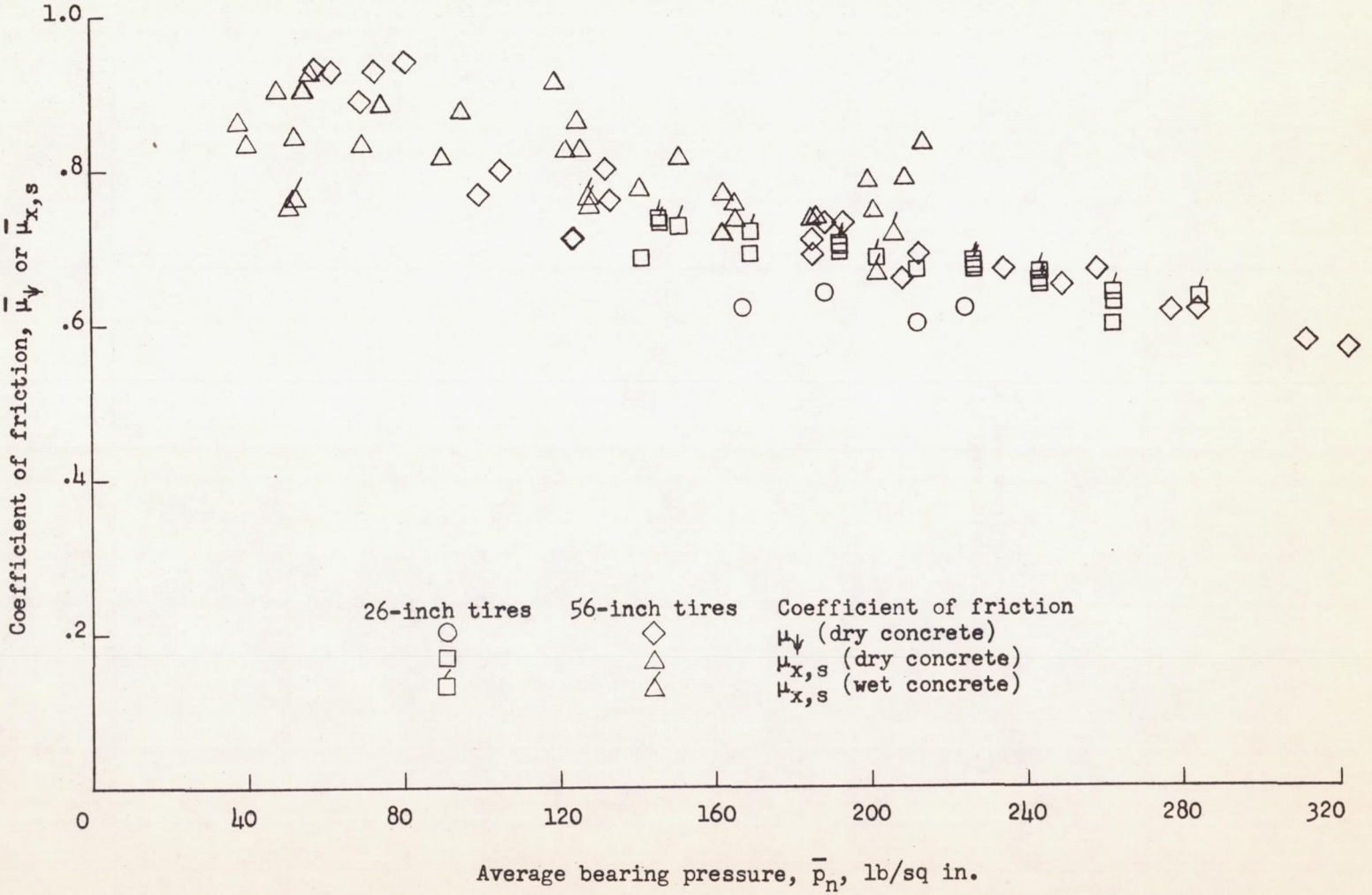

Figure 35.- Comparison of sliding-drag and yawed-rolling coefficients of friction obtained from tests on two 56-inch tires (ref. 3) with present test results.

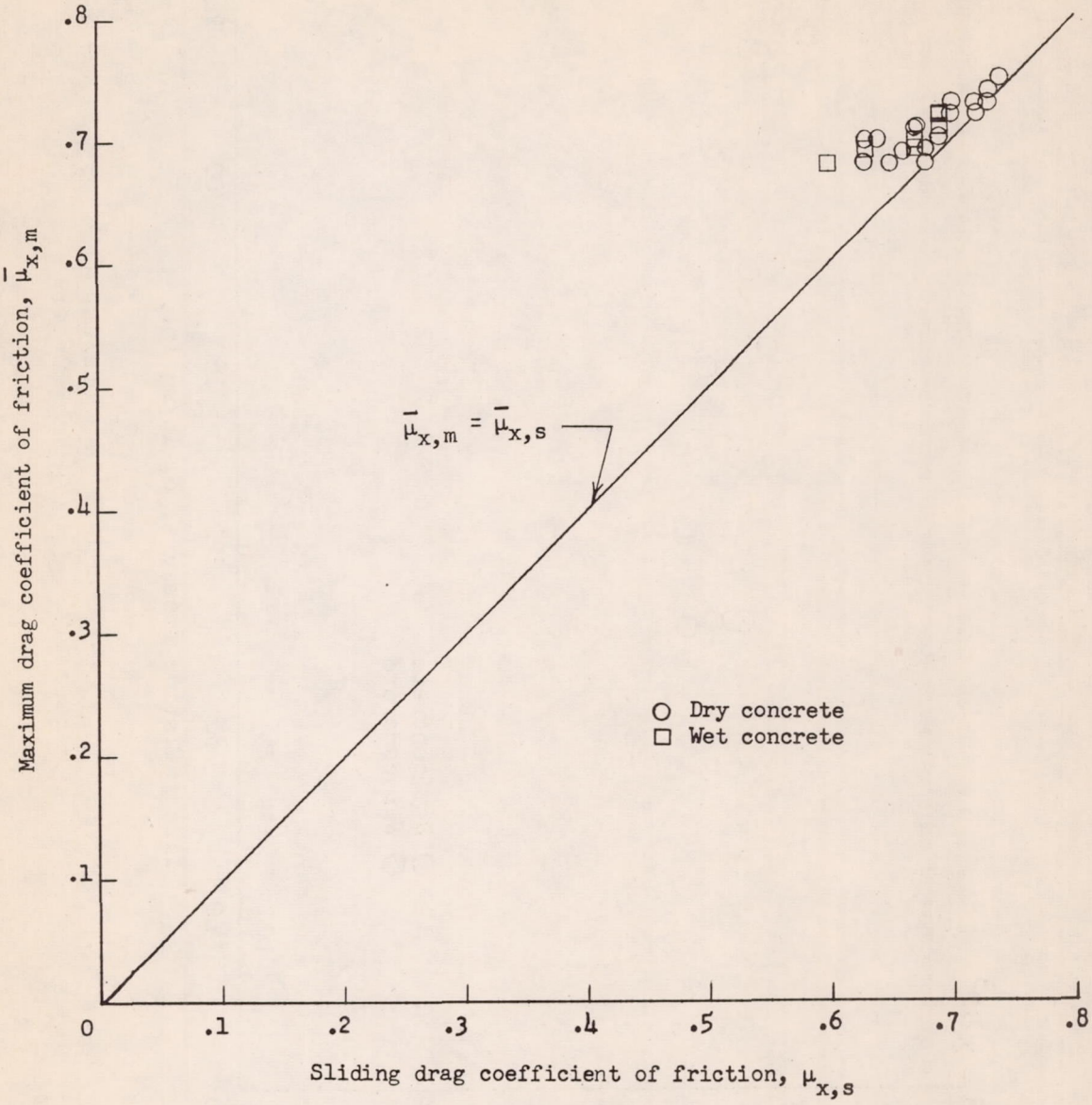

Figure 36.- Comparison of maximum and sliding-drag coefficients of friction.

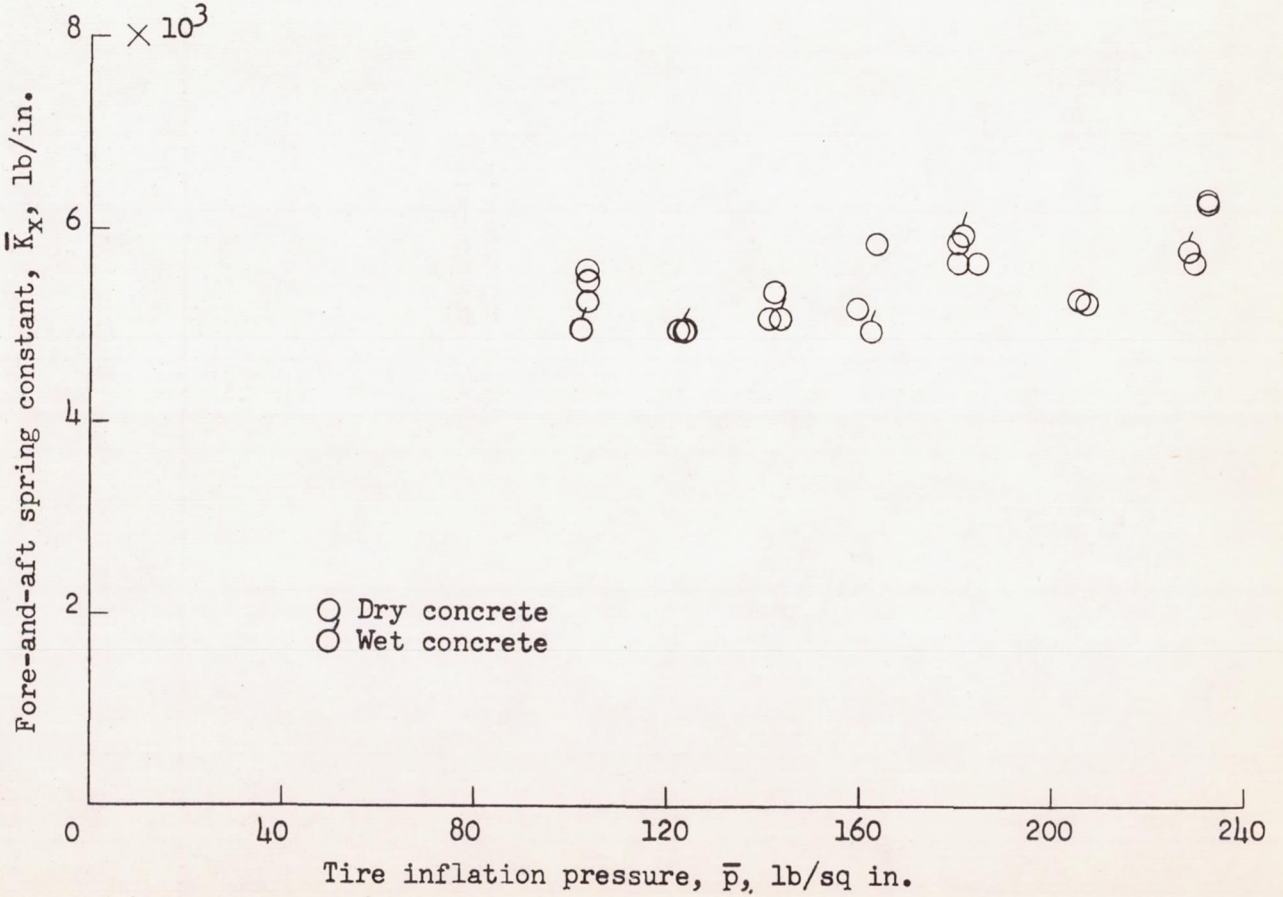

Figure 37.- Variation of fore-and-aft spring constant with tire inflation pressure. $\bar{F}_z \approx 9{,}000$ pounds.

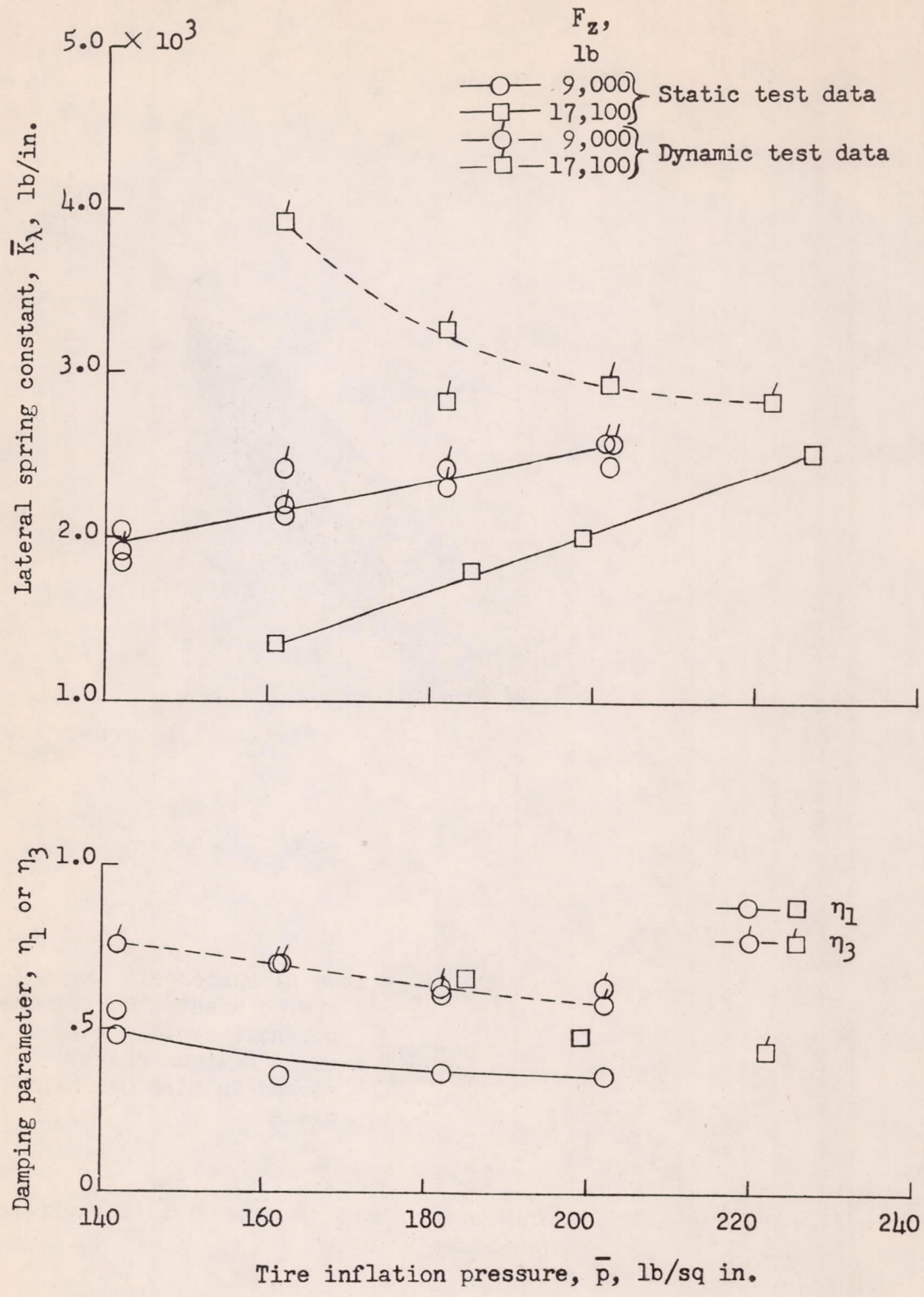

Figure 38.- Variation of lateral spring constants and damping parameters with tire inflation pressure.

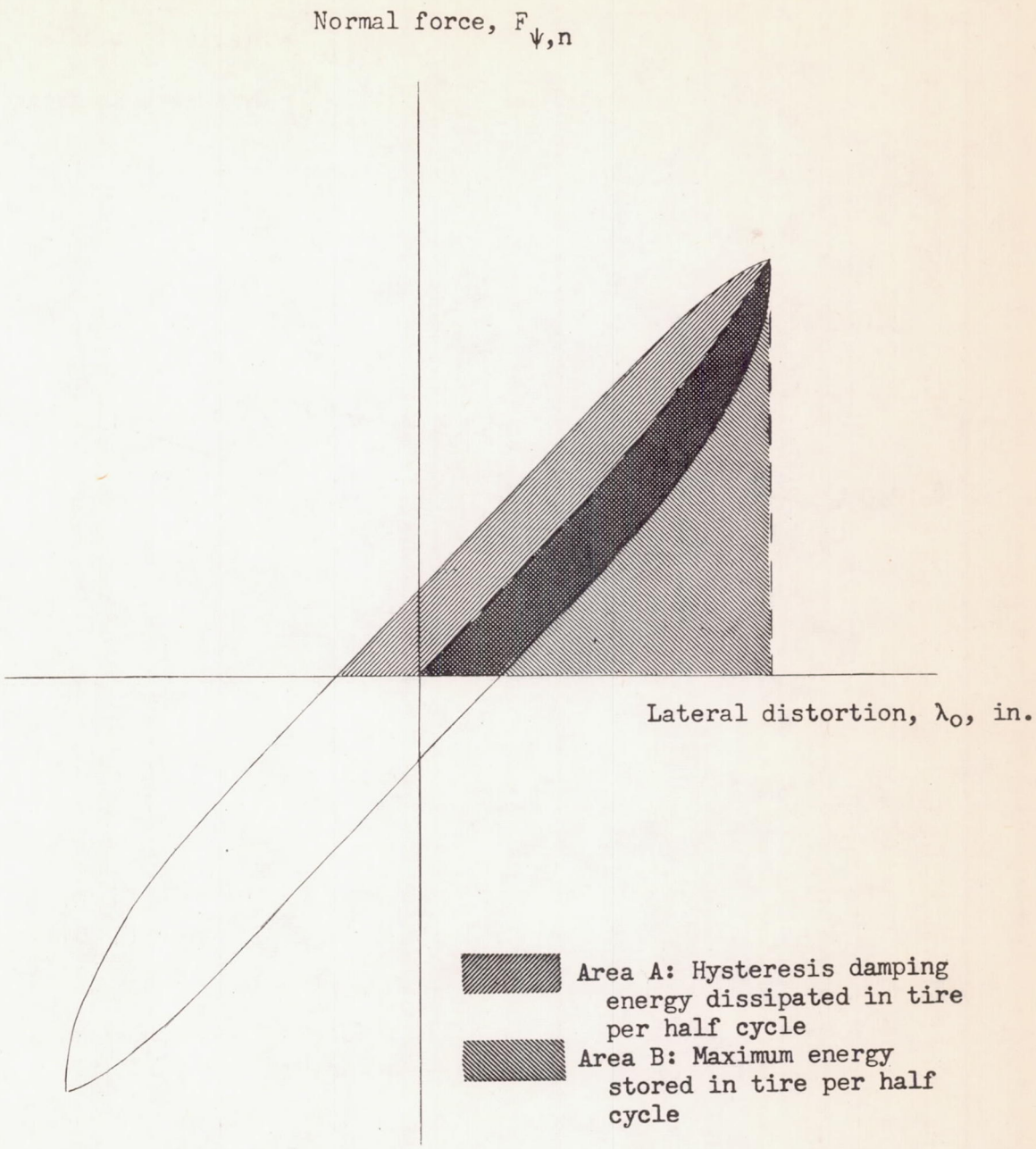

Figure 39.- Diagram illustrating factors used to determine the hysteresis parameter η_1.

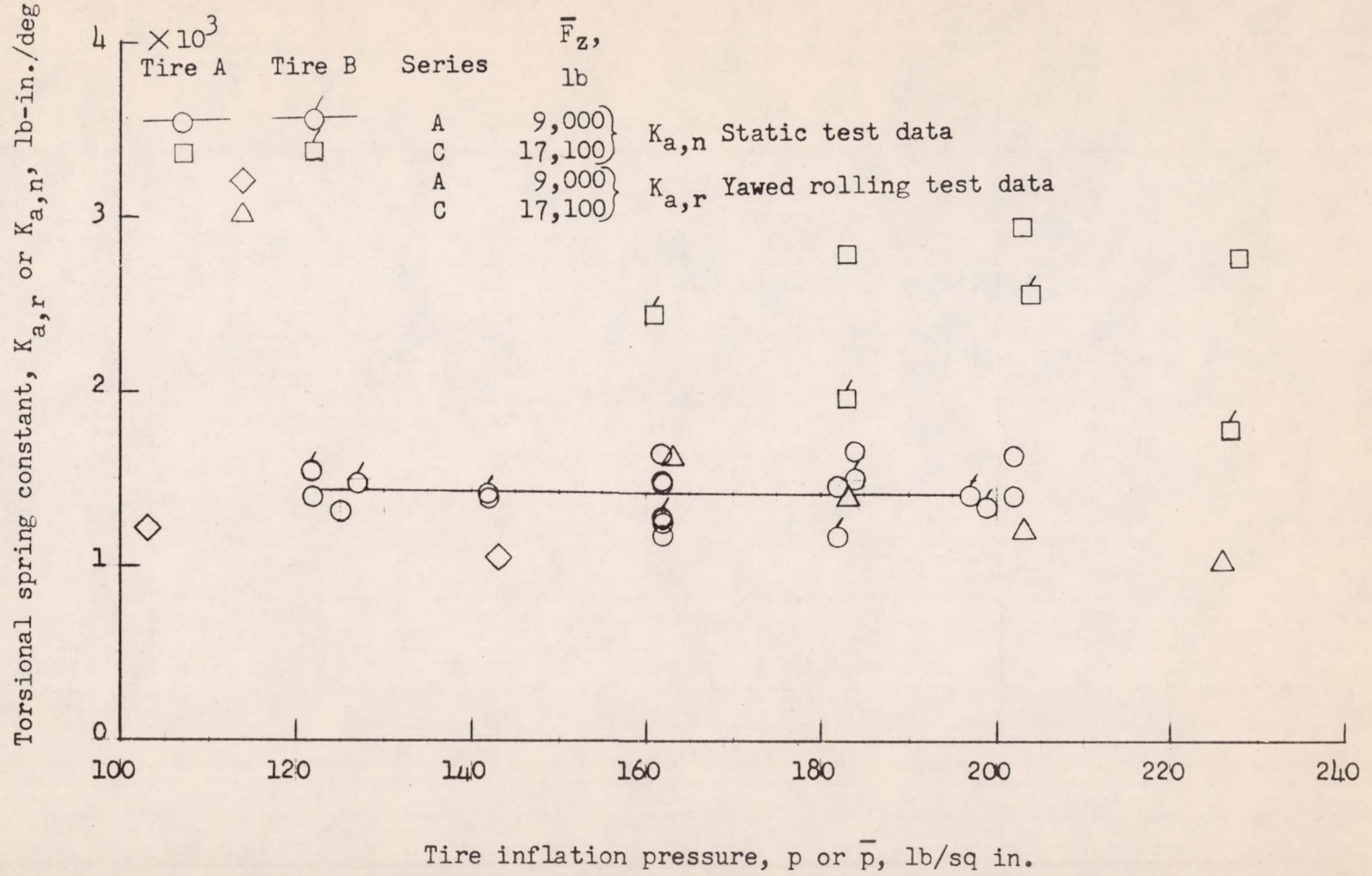

Figure 40.- Variation of tire torsional spring constants with inflation pressure.

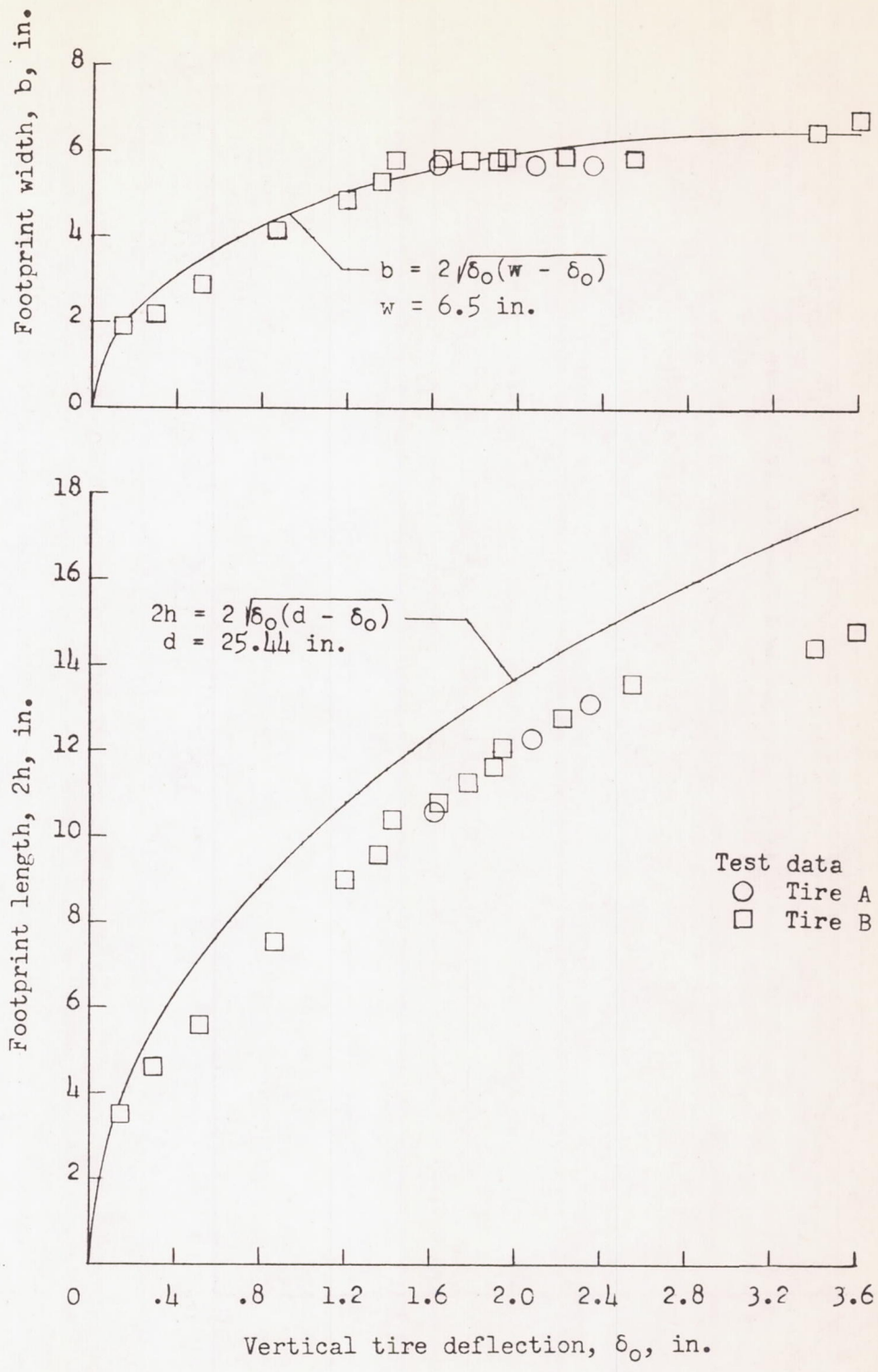

Figure 41.- Variation of footprint length and width with vertical deflection. Solid lines represent chord lengths of circles having diameters equal to the diameter and width at rated inflation pressure.

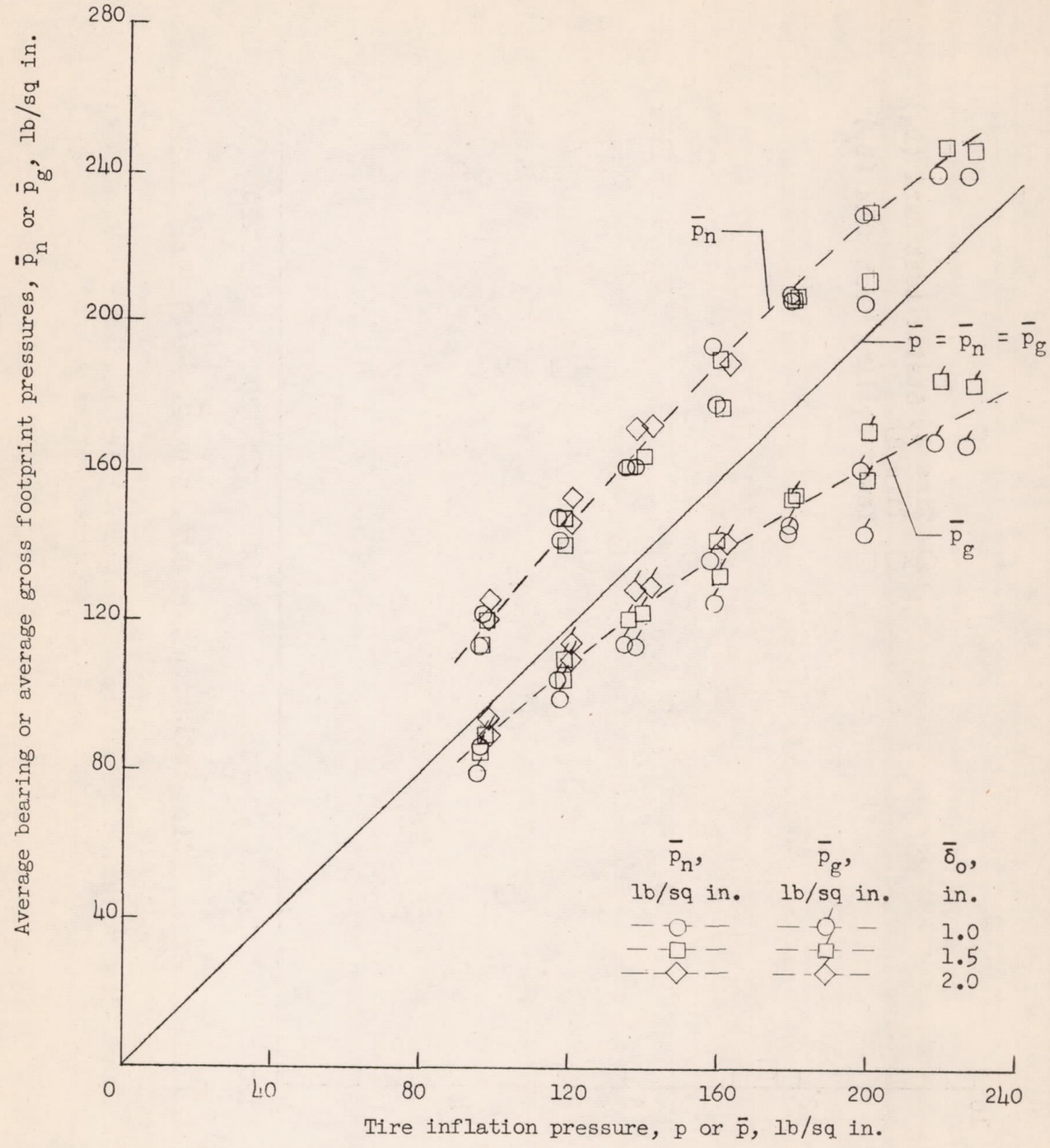

Figure 42.- Variation of average bearing and average gross footprint pressures with tire inflation pressure for several constant vertical tire deflections.

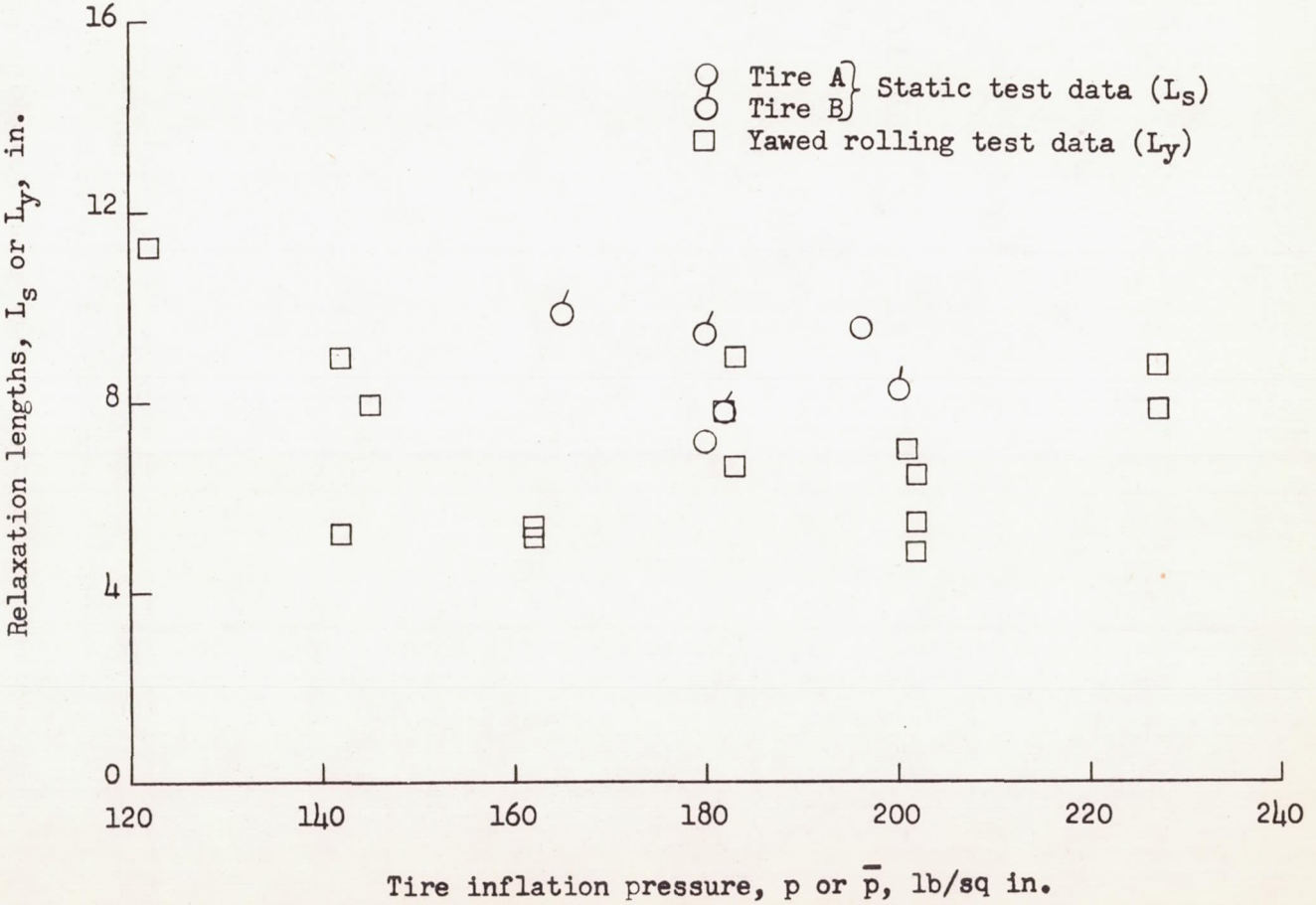

Figure 43.- Variation of static and yawed-rolling relaxation lengths with tire inflation pressure for test series A and B.

NACA - Langley Field, Va.